Chapter 1 Introduction

Since the late 1990s, the explosive growth of using email and the World Wide Web has driven the widespread deployment of computer networks. The popularity of the Internet has dramatically increased the amount of interchange and the sharing of information of graphical, audio data, video data and so on. This drastic advance has outgrown the communication infrastructure beyond its current bandwidth capacities (i.e. using LEDs as transmitters). Therefore, the use of high-speed vertical-cavity surface-emitting lasers (VCSELs) as the replacement for LEDs is the key technology to enable the next generation of low-cost, reliable, and high-speed optical interconnection [1]. Furthermore, there are other various applications of VCSELs in our daily lives, such as high-density optical storage, printing, scanner, optical sensing, display systems and so on. This chapter will briefly review the history of VCSELs and introduce the epitaxial structure of VCSEL from the structure of VCSELs. Then we will compare VCSELs with conventional edge emitting lasers (EELs). Finally, we will discuss the common process techniques of fabricating VCSEL devices and the commonly used structures of VCSEL devices.

1-1 A Brief History of Vertical Cavity Surface Emitting Laser (VCSEL)

Semiconductor Lasers have advanced a long way since the first semiconductor laser diode was demonstrated stimulating emission in 1962 [2-6]. Progress in material purify and epitaxial growth techniques enable the wavelength of semiconductor lasers covering a wide range from 0.3 to 100 μm. Compared to gas or solid state lasers of the He-Ne or Nd^{+} YAG types, respectively, the semiconductor laser diodes possess particular properties, such as considerably smaller size, potentially lower cost, high efficiency and unique ability to modulate the optical output up to gigahertz (GHz) rates

by simply changing the current through the device. The unique properties of the laser diodes make them as a source for optical fiber systems, which form the backbone of modern terrestrial telecommunications systems; they enable data to be read from compact discs (CDs) and from barcode labels. Laser diodes also act as a compact light source for lighting or display.

There are two main types of semiconductor laser diodes. One is edge-emitting laser (EEL), whose structure consists of active region and two cleaved facets perpendicular to the junction plane provided the optical feedback and the stimulated emission light was coming out from the cleaved edge (Figure 1-1(a)). The other one is vertical-cavity surface-emitting laser (VCSEL). This structure was first proposed by Dr. Iga *et al.* at Tokyo Institute of Technology, Japan, in 1979 [7], demonstrated under pulsed conditions at room temperature (RT) by the same group in 1984 [8], and continuous wave (CW) operation at room temperature was achieved in 1989 [9]. VCSELs are made by sandwiching an active region between two highly reflective mirrors. (Figure 1-1(b)). The highly reflective mirrors can be dielectric or epitaxial growth mirrors of distributed Bragg reflectors (DBR) with reflectivity grater than 99.9%. Light is emitted from the surface DBR paralleling to the epitaxial direction of the VCSELs structure. Consequently, simple testing procedure is one of the virtues of VCSELs. This is due to VCSELs allow manufactures to accomplish on-wafer testing prior to dicing and packaging. Consequently, production cost could be much lower than that of the EELs. In addition, the compact size of VCSELs (typically 400×400 μm^2) yields more devices per wafer than do EEL [10]. Hence, these unique characteristics of VCSEL allow manufacturing of low-cost semiconductor lasers in large quantities. Furthermore, narrow divergence circular laser beam, low threshold current for its small cavity volume, low power consumption, high modulation bandwidth, easy polarization control and capability of fabricating dense two-dimensional laser arrays are the other advantages of

VCSEL over EEL. Therefore, VCSELs are ideal candidates for the light sources of optical fiber communication networks such as local area networks (LANs) and metropolitan networks. VCSELs also can be applied in optical storage, print heads, optical sensors, barcode scanners, digital displays, spatial light modulators, backplanes and smart pixels, and microscopes [11-14].

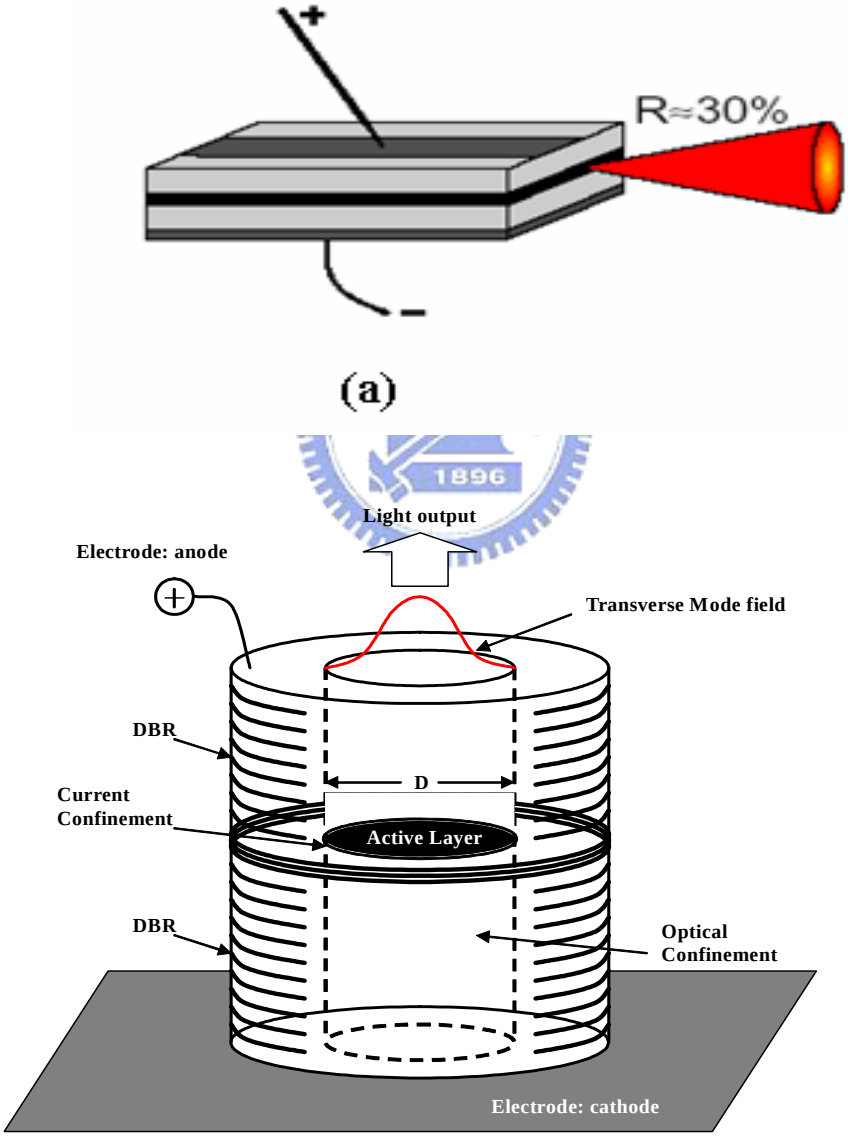

Figure 1-1 Schematic structure of (a) edge emitting laser, (b) vertical-cavity surface-emitting laser.

1-2 Fabricating Processes of VCSEL Devices

For VCSEL designers, the first issue to consider in the design of VCSELs is defining the operating wavelength. The choice of the material systems for the active region, and DBRs define the lasing wavelength of VCSELs under construction. Figure 1-2 shows various choices of the active region materials for VCSEL [15]. For example, the implementation of 850nm VCSELs requires the use of a GaAs-based materials system as the active region. In addition, the longitudinal cavity mode should match with the gain peak of the active region in order to maximize the wallplug conversion efficiency. The mirrors should have a maximum reflectivity at the operating wavelength with the appropriate number of dielectric layers to generate reflectivity greater than 99.9%. It is noted that the mirrors can be dielectric multilayered mirrors or DBRs with material system lattice-matched to the active region (i.e. GaAlAs/AlAs DBRs are lattice-matched with the GaAs material system). It is preferred to grow devices directly using lattice-match active layer and DBRs as this approach will reduce fabrication cost and enhance the reliability of the devices. However, for some materials, it may be difficult to realize all-monolithic growth. For example, it is hard to monolithically grow hole epitaxial long-wavelength VCSEL using the InP-based system. Although InGaAsP/InP DBR is lattice-matched with InP based systems, the difference in refractive index between InGaAsP and InP [16] is small. Hence, requiring more than 40 pairs of such epitaxial layers to obtain high reflectivity would lead to impractical mass production and difficulty in quality control. In addition, the electrical and thermal resistivities will increase with the number of epitaxial layers [17-19], and this is not desired in VCSELs. Therefore, it is very important to select an appropriate material system of active region and DBRs, which can allow the commercialization of VCSELs more easily.

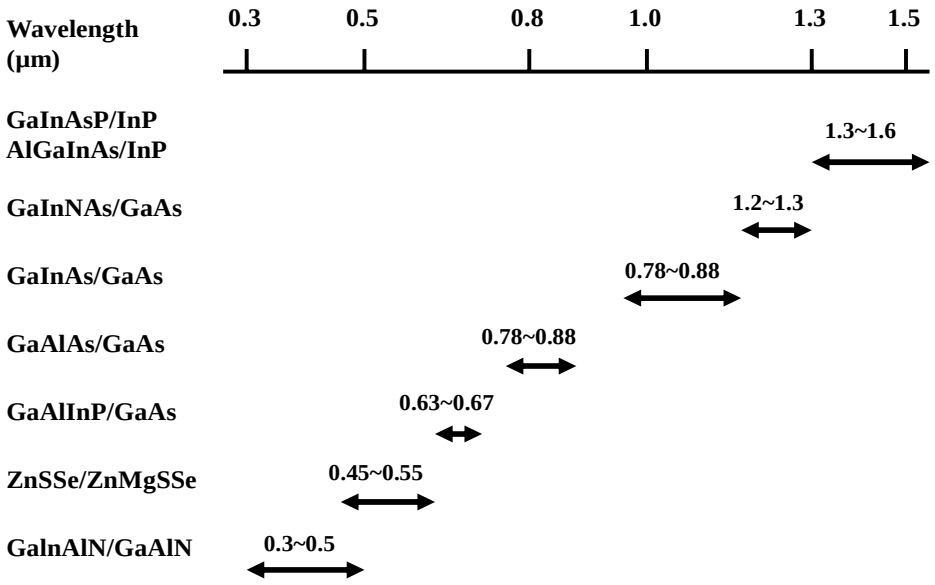

Figure 1-2 Various choices of the active region materials for VCSEL

After selecting an appropriate material system and accomplishing the growth of VCSEL wafers, following is the processes of fabricating the VCSEL devices. In the processes of fabricating VCSEL devices, there are several main techniques, including mesa etching, transverse confinement of electrical current or optical fields, ohmic contact metal deposition and dielectric film deposition. The mesa etching technique forms the shape of the VCSEL devices to isolate devices or to form air-post confinement. Ohmic contact metal deposition facilitates driving current poured well into the active region with the minimum of electric resistance. There are two purposes of dielectric film deposited during fabricating VCSEL devices. One is single or dual layers deposited on the surface of the VCSEL devices for protection. The other is to deposit dielectric DBR mirrors on the VCSEL wafer to form high reflectors of the VCSELs and the thickness of each dielectric layer is equal to one quarter of the wavelength of light in the medium. Transverse confinement technique, the most important of the processes of fabricating VCSEL device, which determines the active area where the current can funnel into, the size of output light aperture, the threshold current and the transverse

mode pattern. A well design of optical and electrical confinement will enhance the electrical-to-optical conversion efficiency or the wallplug efficiency of the devices. Basically, the transverse optical field can be confined inside the VCSELs using gain-guiding, index-guiding, or hybrid-guiding of gain-guiding and index-guiding mechanisms. This dissertation will focus on study of the process techniques of various transverse guiding methods of VCSEL devices. Therefore, the basically guiding mechanism will be first reviewed in the following paragraph.

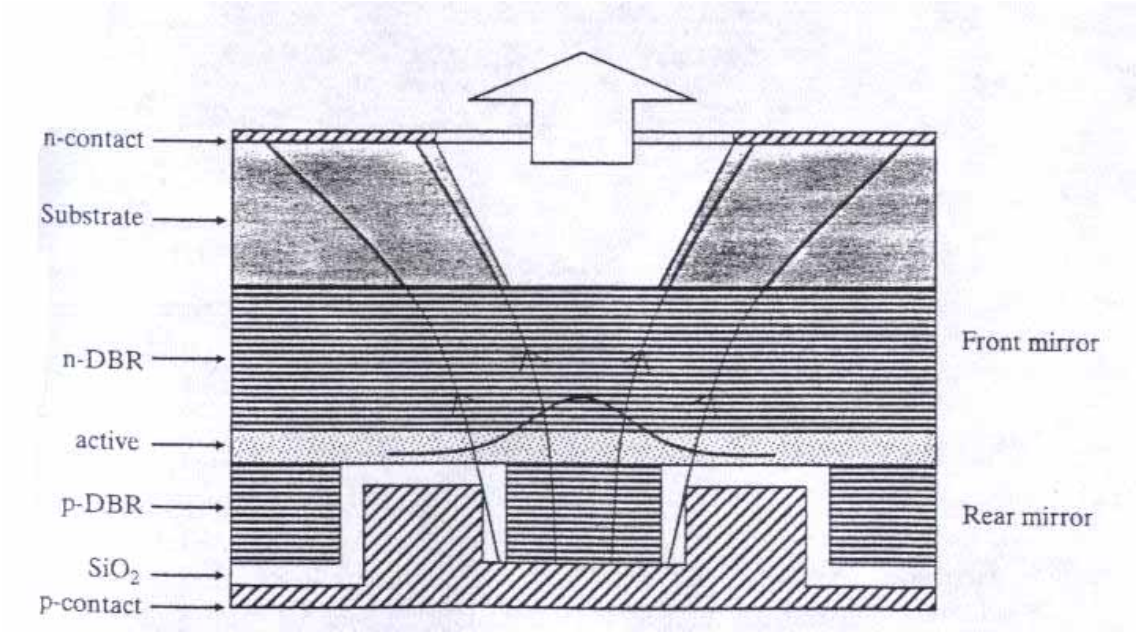

Figure 1-3 Schematic diagram of a gain-guiding VCSEL with circular electrode to confine injection carrier concentration into the active layer.

1-2-1 Gain-guiding mechanism

In the early development of a laser with a gain-guiding mechanism is based on a simple fabrication technique that is compatible with the existing technologies of facet emitting lasers [20]. A gain-guiding mechanism can be realized by forming a circular

metal contact close to the active layer. The injection carrier concentration defines the gain region to confine the transverse mode. Figure 1-3 shows the schematic of a gain-guided VCSEL. The major advantage of this structure is that it is easy to fabricate, but the transverse confinement of optical field and injection current density is weak so that the corresponding threshold current is high. The threshold current can be improved if the current leakage is minimized along the transverse direction. This can be easily achieved by ion implantation into the *p*-DBR (but should avoid damaging the active layer) to increase the electrical resistivity [21]. Figure 1-4 shows the schematic of an ion implanted VCSEL. As is shown, the ion-implanted region is defined selectively to control the flow of the injection current into the active layer. Unfortunately, this configuration of ion-implanted region has no control on the diffusion of carrier concentration along the transverse direction of the active layer. It is possible to apply ion implantation into the active layer, but this well increase the optical absorption loss (i.e., due to scattering of ions) of the device. Moreover, at high-power operation, higher-order transverse nodes can be excited because of the influence of thermal lensing and spatial hole burning of carrier concentration, which are the undesired characteristics of gain-guided VCSELs. The other problem is the electrical resistivity of the DBRs, which may increase the heat generation inside the laser cavity. Nonetheless, the attractions of this structure is its planar configuration, which guarantees the simplification in fabrication process and packaging so that low production costs can be maintained and the ion implantation can be executed in any semiconductor materials. Therefore, many manufacturers (Honeywell, etc.) manufactured products using ion implantation technology in their early-state development of VCSEL. The ion implantation technique has also been applied to fabricate long-wavelength VCSELs [22, 23].

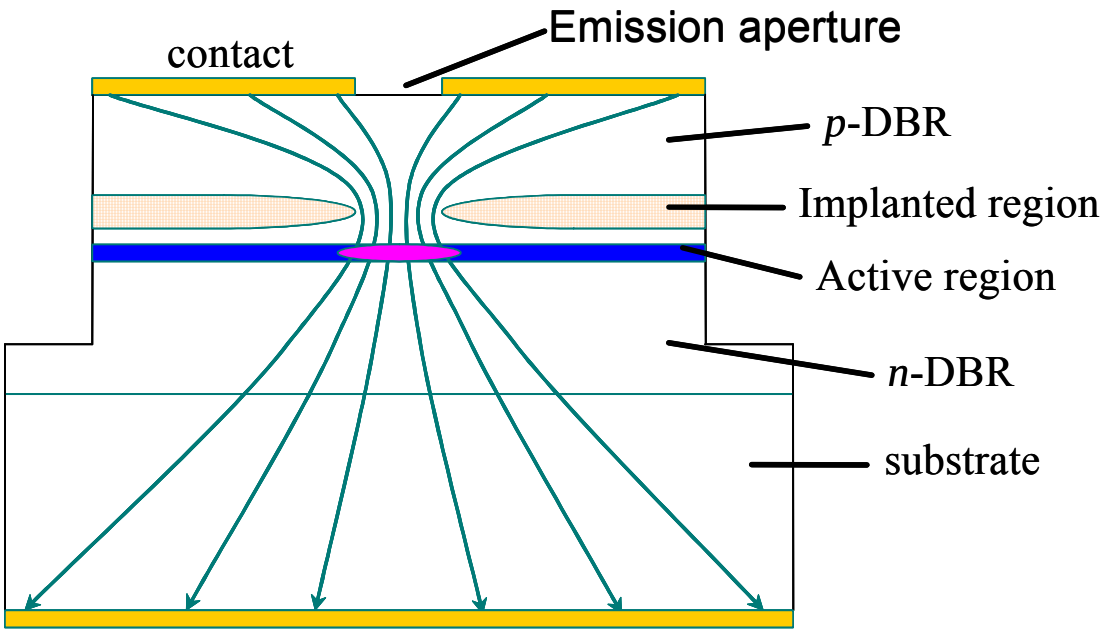

Figure 1-4 Schematic diagram of a gain-guided VCSEL ion implantation regions to confined injection carrier concentration into the active region.

1-2-2 Index-guiding mechanism

Index-guided VCSELs have better transverse confinement of optical field than do the gain-guided devices. Several types of index-guided VCSELs had been studied, such as (a) air-post, (b) intracavity, (c) regrowth buried heterostructure, (d) antiguiding and (e) selective oxidation etc., which have different mechanisms to confine the optical field and injection current as well as different fabrication procedure complexities.

(a) Air-post type:

Figure 1-5(a) and 1-5(b) show the two possible configurations of air-posted VCSELs [24, 25]. The edges of *p*-DBR section of air-posted VCSELs are directly contact with the air and stand alone on the base material and the active layer, which is sandwiched between the *n*- and *p*-type DBRs (*p*-DBR). The large difference of

refractive index between the semiconductor and the air provided strong transverse confinement of the optical field. However, diffraction and scattering losses increase with the decrease (increase) of the active layer's diameter (sidewall roughness). In addition, single-mode operation is not stable in this structure. The surface recombination of carrier concentration also can be enormous. Furthermore, low electrical and thermal conductivities of the air-posted VCSELs can have serious problems in highly biased voltage and insufficient heatsinking.

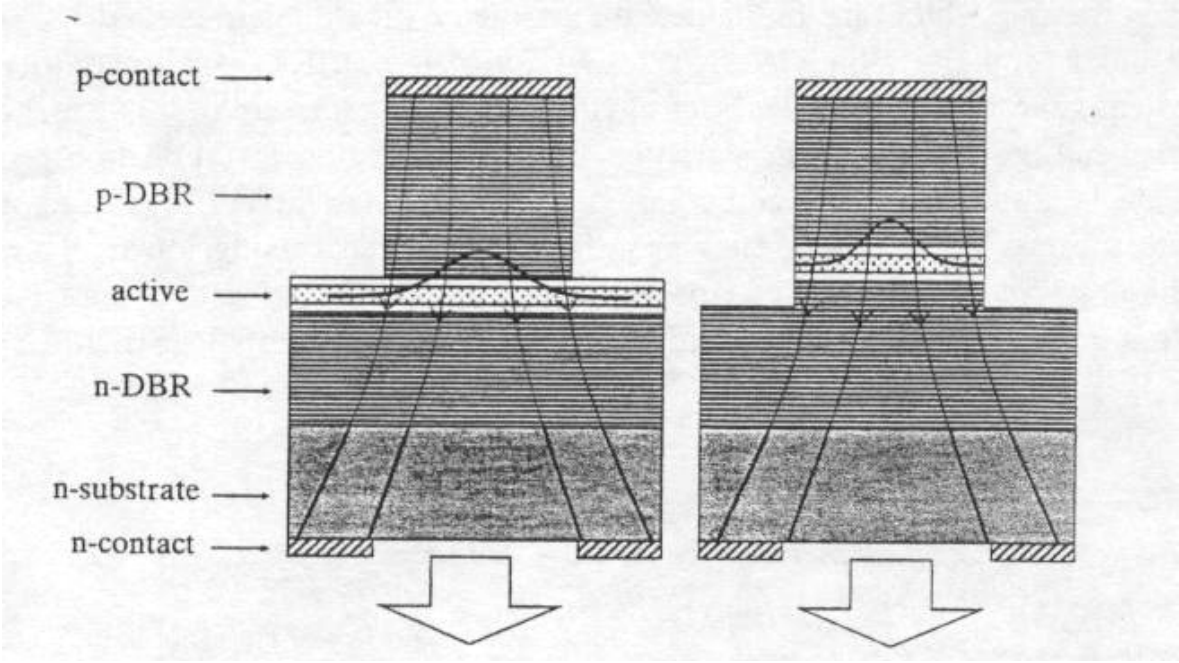

Figure 1-5 Schematic diagram of aorposted VCSEL (index-guided structure); active layer (a) below and (b) within the airposted column.

(b) Intracavity type:

A schematic structure of intracavity is shown as Figure 1-6 [26]. Additional layers, the *p*- and *n*-type layers, are inserted between the *n*- and *p*-DBRs on either surface of the active region to provide an electrical path for the injection current to

reach the active region. A current constriction is also formed on top of the active layer to force the current flowing into the optical mode. This current blocking layer can be realized by ion implantation, diffusion, or a simple selective wet etch. Current crowding may occur near the periphery of the device where the optical mode is weak, so that the influence of spatial hole burning of carrier concentration can be multiplied. A resistive layer between the conductive current distribution layer and the active layer can be introduced to minimize the influence of crowding. This current layer limits the influence of current crowding by diffusion of the injected current from the center of the active layer. This device is expected to have low biasing voltage and high single-mode output power.

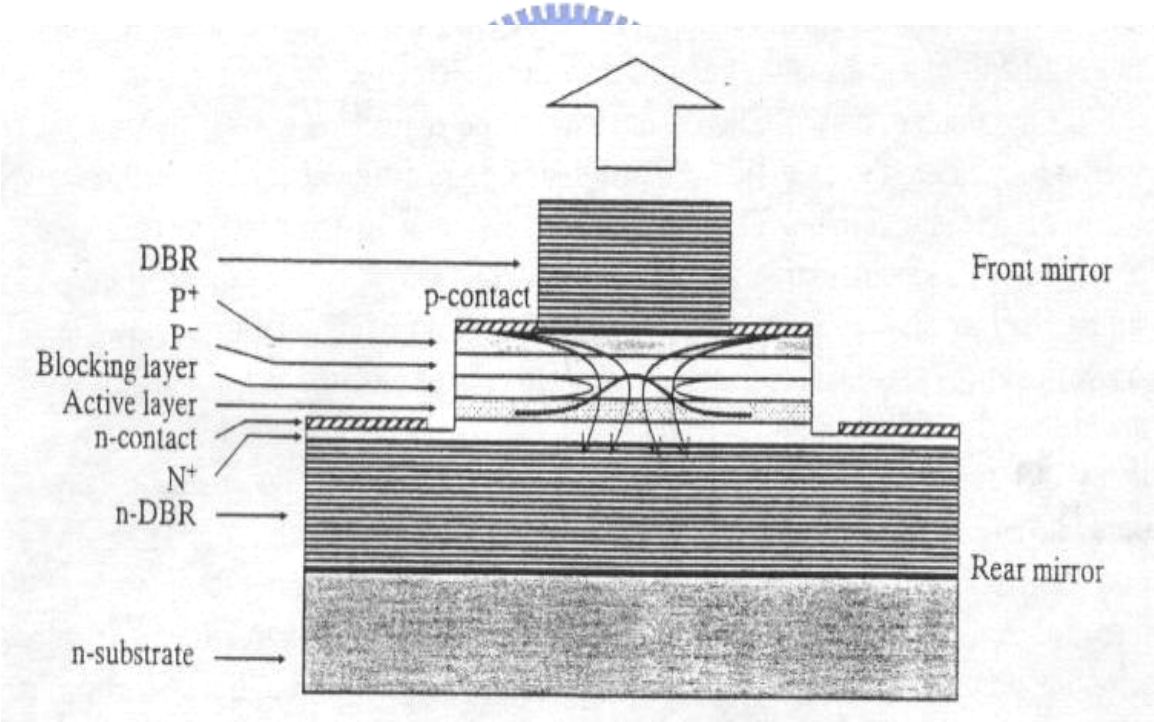

Figure 1-6 Schematic diagram of aorposted VCSEL (index-guided structure) with intracavity design.

(c) Buried heterostructure type:

Figure 1-7 shows a schematic buried heterostructure VCSEL, which is another type of index-guided structure [27]. As it is shown, the entire core region of VCSEL is immersed inside a current blocking region with careful selection of refractive index to cut off higher transverse modes. This blocking region provides enough transverse confinement of optical field and injection current, which improves the single-mode operation at high injection level. The blocking region can be polyimide or an epitaxial regrowth of p-n junction to block the diffusion of injection current outside the core region when the laser is forward-biased [28]. However, the fabrication process, which requires etching and regrowth of the blocking region, may not be suitable for mass production, and the production cost of such a device can be high.

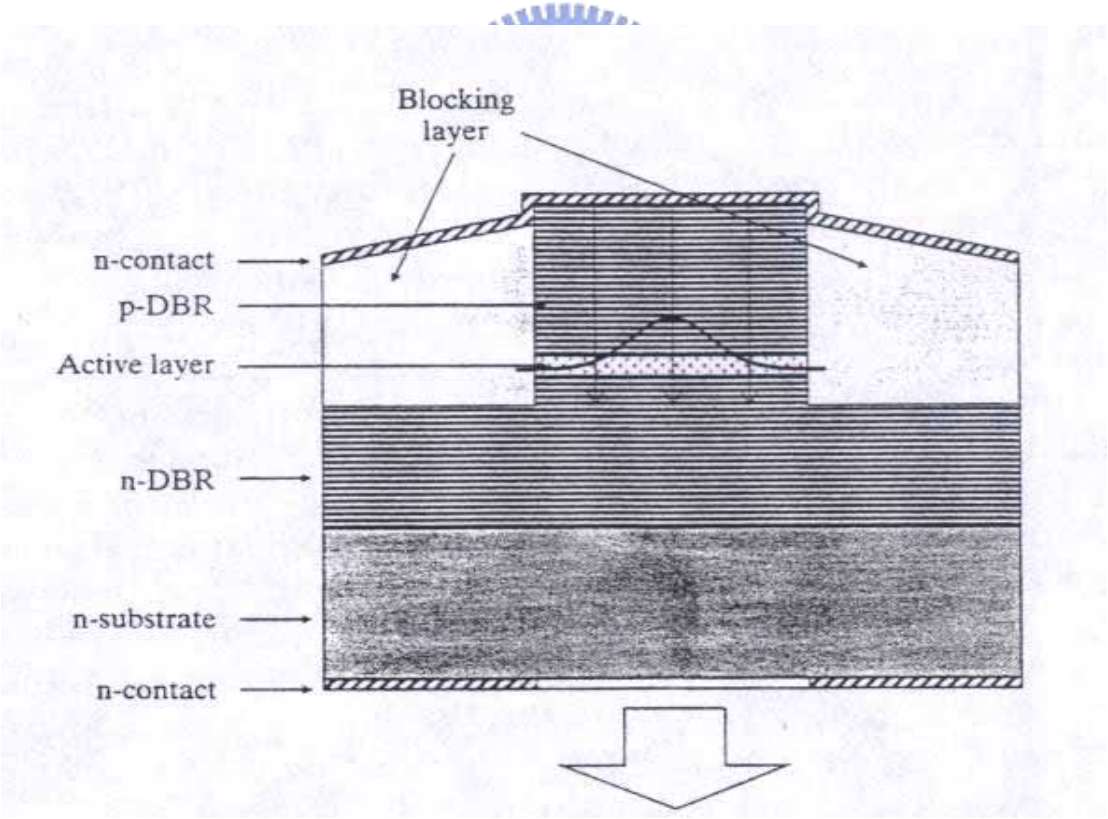

Figure 1-7 Schematic diagram of a buried heterostructure VCSEL (index-guided structure) with injection carrier concentration strongly confined uniformly inside the active region.

(d) Antiguiding type:

Figure 1-8(a) shows configuration of antiguided structure [29], which may be possible to realize high-power single-mode VCSELs. As shown in Figure 1-8(a), a low-temperature (LT) layer with enhanced resistivity is grown on top of the p-layer to confine the injected carrier concentration. An undoped cap layer is grown on top of the LT layer using molecular beam epitaxy (MBE). Hence, a circular recess can be formed in top of the cap layer using photolithography. The corresponding effective refractive index along the transverse direction of the active region is also shown in Figure 1-8(b). It is noted that the antiguided structure is experienced by the transverse mode along the active layer as the LT and cap layers increase the effective refractive index of the aperture. In this structure, the aperture diameter can be as large as 6 μm

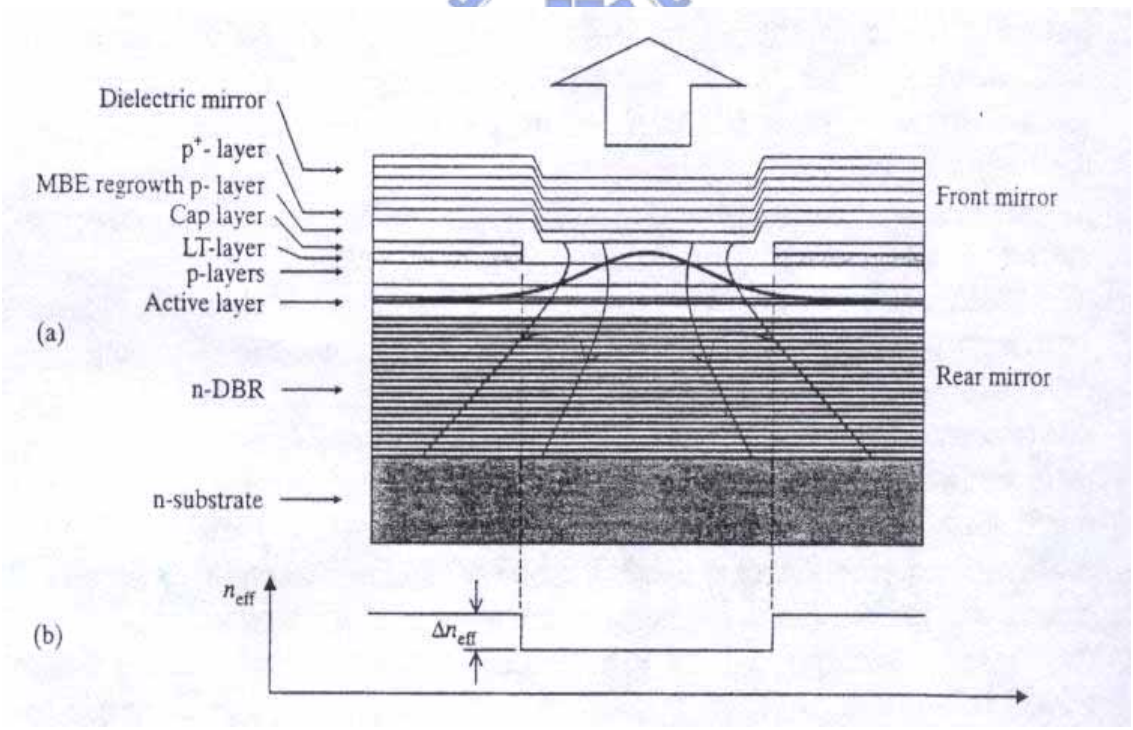

Figure 1-8 (a) Schematic diagram of an antiguided VCSEL; (b) the corresponding profile of effective refractive index n_{eff} and change of effective refractive index Δn_{eff} along the transverse direction of the laser cavity.

to suppress the excitation of high-order transverse modes at high injection level. However, the drawback of this structure is the inevitable high-threshold current due to strong radiation loss.

(e) Selective oxidation type:

Selective oxide-confined VCSELs are the often seen commercialized VCSELs with index-guided structure. Figure 1-9 shows a schematic structure of a VCSEL with commonly used single-oxide aperture. The VCSEL epitaxial wafer designed for selective oxidation needs to grow an AlGaAs layer with high Al content at the desired locations of the current apertures. For performing lateral oxidation of the high Al content layer, a mesa structure must to be formed by etching so as to expose the sidewall. Placing the mesa structure in a steam environment at temperatures of 350^{o}C to 500 ^{o}C converts the AlGaAs to an insulating oxide layer and forming an oxide aperture above the active region. It is noted that the refractive index of the oxide region is lower than that of the original semiconductor layer [30]. Hence, the induced effective index difference between the cavity and the surrounding region containing the oxide layer can be controlled through the thickness of the oxide layer and its position relative to the optical cavity. As a result, the optical field along the transverse direction can be confined tightly by the oxide apertures. Furthermore, the oxide apertures are insulation layers forcing the injection current through the aperture, which enhance the wallplug efficiency. Therefore, oxide-confined VCSELs exhibit extremely low threshold current [31] and high wallplug efficiency [32]. It must be noted that the oxidization procedure for the oxide aperture is compatible with the monolithic growth of GaAs-based material systems so that the production cost of oxide aperture VCSELs can compete with that of the ion-implanted devices. As indicated in Figure 1-9, the problem of high electrical resistivity of n and p DBRs can deteriorate the performance of oxide aperture VCSELs. However, this problem can

be solved by using the design of intracavity contacted cavity. This can be realized by removing the blocking layer as shown in Figure 1-6 by an oxide aperture or sandwiching the active layer by two oxide apertures [33]. In this structure, the biased voltage of the VCSELs as well as power consumption at threshold can be further reduced.

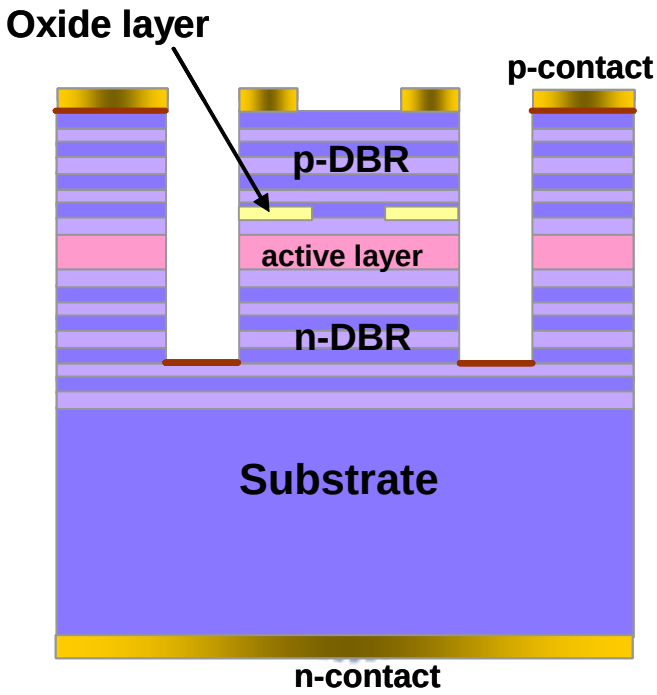

Figure 1-9 Schematic diagram of an index-guided VCSEL with single oxide aperture.

Although the selective oxide-confined VCSELs are commercialized devices, there are still two problems related to the design of oxide aperture VCSELs. The first one is the excitation of high-order transverse modes under high applied current. It is reported that using the tapered waveguide design as shown in Figure 1-10 can suppress the excitation of high-order transverse modes [34]. This is because the tapered region acts as a spatial filter to remove any high-order transverse modes generated inside the active layer. Therefore, single-mode operation can be maintained

in oxide-confined VCSELs at a wide range of injection levels. Another problem is the maximum output power of VCSELs is directly related to the surface area of the active region that amplified the transverse modes. Because of the small nature of the oxide aperture, the maximum output power of oxide-confined VCSELs is limited. It is possible to increase the diameter of the oxide aperture for higher output power, but the excitation of high-order transverse modes is inevitable even with the tapered waveguide design. In addition, the inclusion of the tapered waveguide in oxide-confined VCSELs is not preferred because of the increase in the complexity of the fabrication process as well as high production costs. Therefore, VCSELs only with selective oxidation are not an appropriate design for high-power operation.

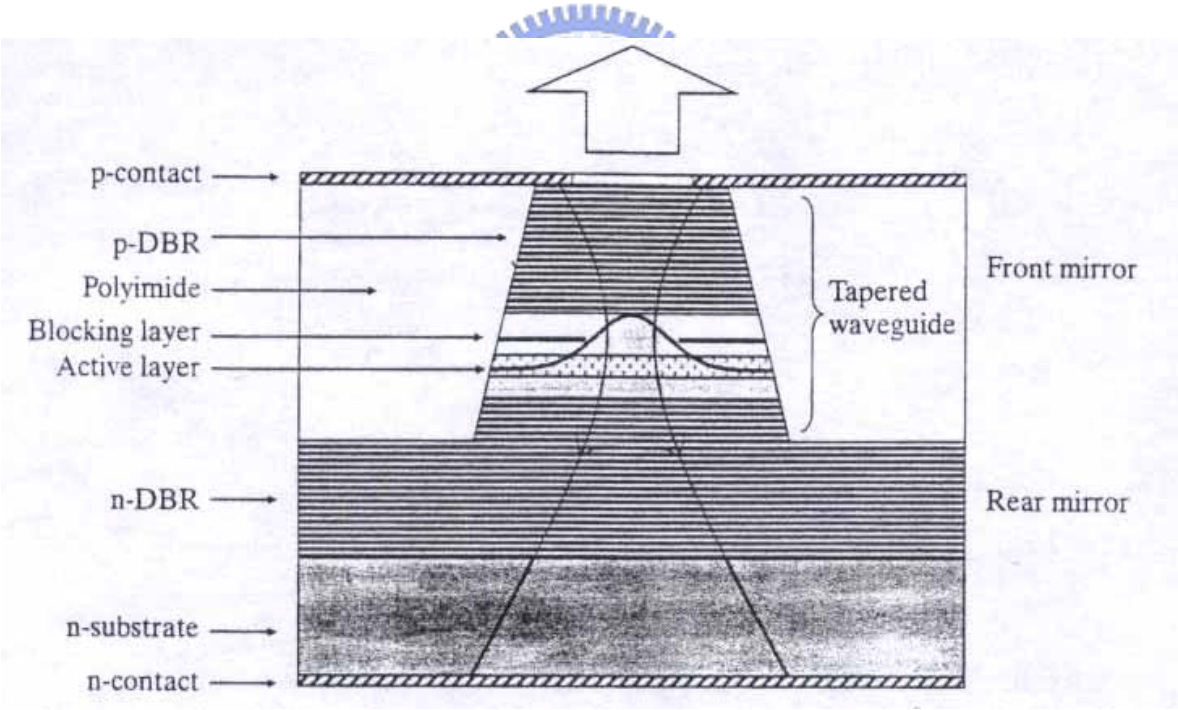

Figure 1-10 Schematic diagram of a tapered waveguide buried heterostructure VCSEL (index-guided structure).

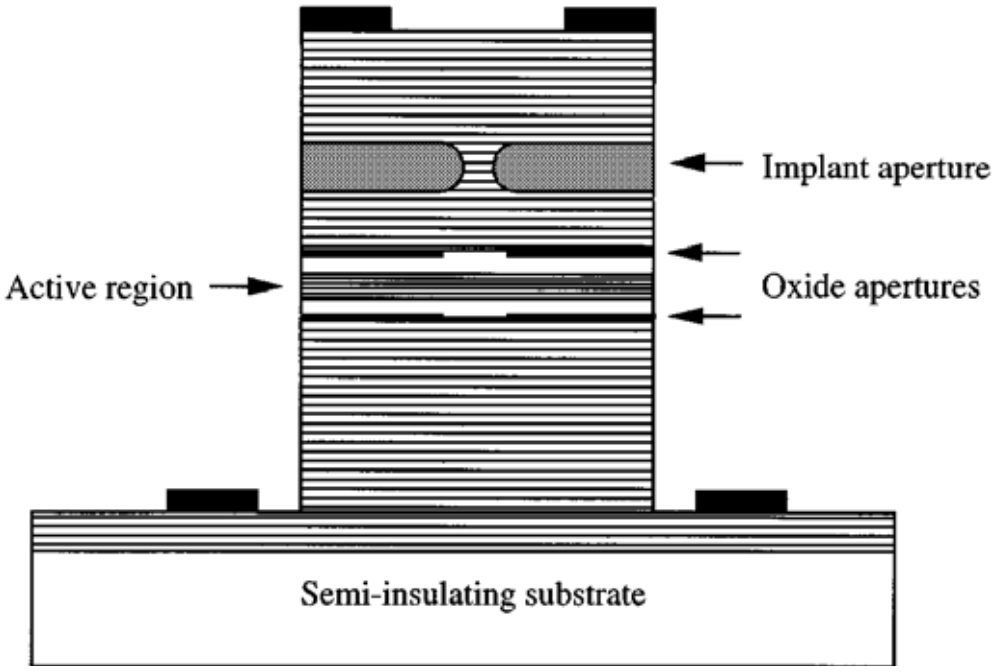

Figure 1-11 Schematic diagram of a hybrid-guided VCSEL using ion-implantation for gain-guiding and selective oxidation for index-guiding.

1-2-3 Hybrid-guiding mechanism

In order to obtain high-power output, the gain area of the device needs to be increased, which increases the number of transverse modes. Furthermore, the wavelength separation and differences in optical losses between these transverse modes decrease. In the limit of very large emission apertures, there are many transverse modes with wavelengths and losses equal to the plane-wave limits. Combining high-power and single-mode operation is therefore very difficult as we discuss in the previous paragraph. The popular design used to obtain single-mode operation VCSEL are antiguiding-structure concept (in section 1-2-2(b)) [26]. The main disadvantage of antiguiding structures is the fundamental mode also induces large radiation losses, and then increasing threshold and limiting maximum output power. Young et al proposed another approach using hybrid implant/oxide VCSELs

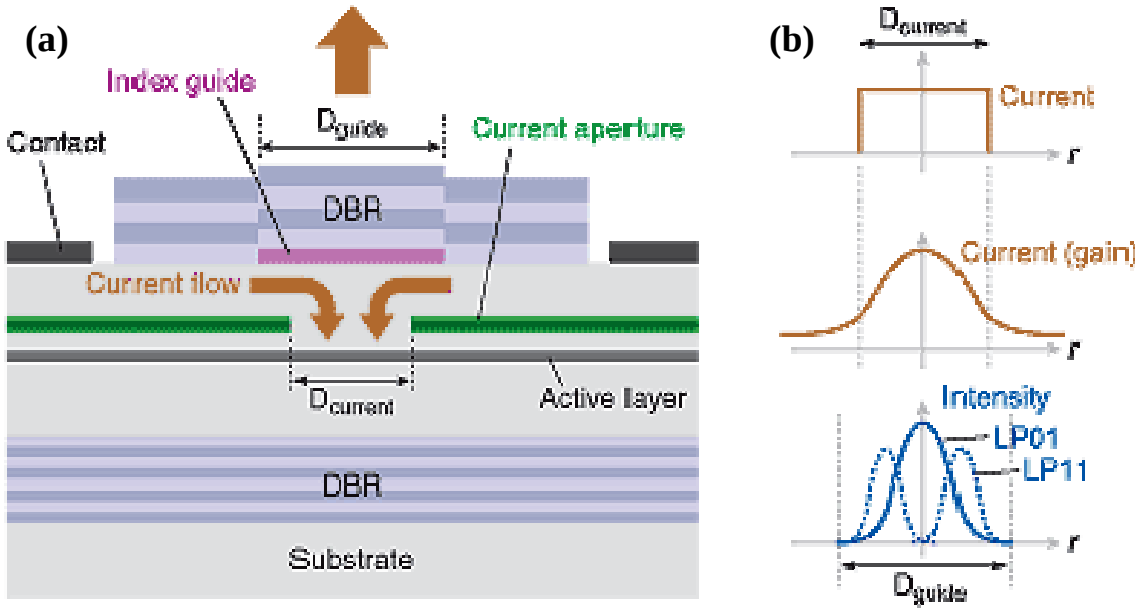

Figure 1-12 (a) The schematic structure of implant-apertured index-guided VCSEL (hybrid confinement), current confinement and photon confinement can be controlled independently. (b) The schematic of coupling relationship between transverse mode and gain spectrum.

that support single-mode operation [35]. This schematic structure of hybrid-guided approach is shown in Figure 1-11, which relies on modifying the overlap of the optical mode with the gain profile (also referred to as mode-selective gain) to generate high-power single-mode operation. However, the threshold current (I_{th}) of this VCSEL is rather high, at about 5.8 mA. Jean-Francois P. Seurin et al report this hybrid-confined structure as I^2-VCSEL (implant apertured index-guided VCSEL) and demonstrated the results in *Laser Focus World* [36]. The main advantage of the I^2-VCSEL is the independent control of the diameter of the etched gallium arsenide (GaAs) pillbox, which defines the index-guiding aperture, and the diameter of the ion implant, which defines the current aperture, by using different sets of masks. The structure is shown in Figure 1-12 (a). Photolithographic processing enables concise control of the diameters. Contrary to an oxide aperture, the implant aperture is

invisible to the optical beam. The current aperture can therefore be made smaller than the index-guide aperture to reduce the overlap of the higher-order modes with the gain profile while at the same time keeping a sufficient fundamental mode/gain overlap. The concept of decoupling the high-order mode with gain is shown in Figure 1-12 (b). As the index-guide diameter is increased, the mode diameters will also increase and the overlap with the gain profile will decrease. Because higher-order modes have a relatively larger amount of their power spreading off center than does the fundamental mode, they suffer more from this loss of overlap. Eventually, the modal threshold gains of higher-order modes will become too high and the fundamental mode will be the only one to lase.

1-3 Organization of this Dissertation

This study has focused on the design and investigation of several transverse confinement techniques. We try to improve the characteristics of the VCSEL with traditional gain guiding structure, develop new type of index-guiding technique and combine the merits of gain guiding and index guiding technique to obtain the high modulated speed VCSEL. The wafers using in this study are essentially GaAs-based VCSEL wafers especially most on 850nm GaAs VCSELs, because of the mature epitaxial growth techniques and easily purchasing the VCSEL wafers. In addition, we also develop new guiding technique—photoelectrochemical oxidation for GaN-based materials.

In Chapter 1, we discussed the original differences between EELs and VCSELs. Following reviewed the brief history of VCSEL development. Then we surveyed the commonly process techniques of VCSELs and the mechanisms of several reported VCSEL structures including gain-guiding, index-guiding and hybrid-guiding structures.

In Chapter 2, we studied the characteristics of the proton-implanted VCSEL, the

simplest fabricating technique of fabricating VCSEL devices. In order to improve the performances of the proton-implanted VCSEL, we reported by incorporation of a new p-contact scheme using a Ti and ITO transparent overcoating on the regular p-contact. The kink characteristics in L-I curve of the VCSEL with the Ti/ITO overcoating were improved with a reduction in the derivative kink factor of as large as 70% and the high-speed response of the overcoated device also shows a more open clear eye and lower jitter of 35 ps operating at 2.125 Gb/s under 10 mA bias and 9 dB extinction ratio compared to that without overcoating device.

In Chapter 3, we tried to find a new VCSEL structure with virtue of gain-guiding, simple planer process, and possessing index-guide. We utilize silicon implantation to replace proton implantation. The VCSELs exhibit kink-free current-light output performance with threshold currents about 2.2 mA, and the slope efficiencies about 0.45 W/A. The mode patterns of silicon-implanted VCSEL showed similar stable transverse mode patterns of oxide-confine one. This might result from the silicon-implantation induce disordering of the implanted regions, so that difference of refractive index existence between the implanted regions with original regions.

For high side mode suppression ratio (SMSR) single-mode VCSEL purpose for fiber communication, we suggested a hybrid-confined structure using oxygen implantation combine with selective oxide VCSEL in Chapter 4 and photonic crystal on proton-implanted VCSEL in Chapter 5. In Chapter 4, we focused the study on single transverse mode with high output-power and high modulation speed VCSEL. Oxygen implantation and selective oxide-confined for gain-guide and index-guide, respectively, were used in fabricating 850 nm GaAs VCSELs. The VCSELs with large emission aperture of 8 μm exhibit good performance with threshold currents of 1.5 mA, a single transverse mode emission within the full operational range and a maximum output power of 3.8 mW. Moreover, the single mode VCSELs also demonstrate superior high

speed performance up to 10 Gb/s.

Photonic crystal structures have attracted worldwide interest in recent years. Fabricating two-dimensional (2-D) photonic crystals on the surface of selective oxide-confined VCSELs had been investigated as a control method of lateral mode in the late years. In Chapter 5, we reported a different hybrid-confined structure by using 2-D photonic crystal and proton-implanted for gain-guide and index-guide, respectively. This approach showed single-output transverse mode with high side-mode suppression ratio (SMSR) over 40 dB. This is because of the superior optical field confinement of photonic crystal. These devices also exhibited ultra-low divergent angle about 7^{o}. This approach was also successfully applied on the long-wavelength 1.3 μm InAs quantum-dots VCSELs and the VCSELs also show the single-output transverse mode in whole operation range.

Chapter 6 concluded the studies in this dissertation. All of the developed techniques studied in this dissertation were promising applied on the long-wavelength VCSELs for the optical communication. Therefore, we put the discussion of applying to long-wavelength VCSELs as future work. In short-wavelength of blue and UV range using different material system, mostly nitride-based material, couldn't use wet selective-oxide technique to form oxide-confined region in the GaN-based structure devices. In recent year, photoelectrochemical (PEC) oxidation method with acid or base solution was investigated suitable forming native oxide film of GaN-based materials. We also develop PEC oxidation via H_2O for stable growing oxide film. We also applied the PEC oxidation on the p-GaN surface to improve light output of GaN-based LEDs. This oxide-confined method not applies on GaN-based VCSEL yet because the epitaxial structure of GaN-based VCSEL is hard to get. Hence, we put the development of PEC oxidation technique to the future work.

Reference

[1] S. F. Yu, "Analysis and design of vertical cavity surface emitting lasers", Wiley-Interscience, 2003, pp.18

[2] R. N. Hall, G. E. Fenner, J. D. Kingsley, T. J .Soltys and R. O. Carlson, "Coherent light emission from GaAs junctions," *Phys. Rev. Lett.*, vol. 9, pp. 366-268, 1962.

[3] M. I. Nathan, W. P. Dumke, G. Burns, F. H. Dill, Jr. and G. Lasher, "Stimulated emission of radiation from GaAs p-n junctions," *Appl. Phy. Lett.*, vol. 1, pp. 62-64, 1962.

[4] T. M. Quist, R. H. Rediker, R. J. Keyes, W. E. Krag, B. Lax, A. L. McWhorter and H. J. Zeiger, "Semiconductor maser of GaAs," *Appl. Phy. Lett.*, vol. 1, pp. 91-92, 1962.

[5] N. Holonyak, Jr. and S. F. Bevacqua, "Coherent (visible) light emission from $Ga(As_{1-x}P_x)$ junctions," *Appl. Phy. Lett.*, vol. 1, pp. 82-83, 1962.

[6] N. Holonyak, Jr., "The semiconductor laser : A thirty-five-year perspective," *Proc. IEEE*, vol. 85, No.11, pp. 1678-1693, 1997.

[7] H. Soda, K. Iga and Y. Suematsu, "GaInAs/InP surface emitting injection lasers", *Jpn. J. Appl. Phys.*, vol.18, pp. 2329, 1979.

[8] K. Iga, Sishikawa, S. Ohkouchi and T. Nishimura, "Room temperature pulsed oscillation of GaAlAs/GaAs surface-emitting injection laser", *App. Phys. Lett.*, vol. 45, pp. 348, 1984.

[9] F. Koyama, S. Kinoshita and K. Iga, "Room-temperature continuous wave lasing characteristics of GaAs vertical cavity surface-emitting lasers", *App. Phys. Lett.*, vol. 44, pp. 221, 1989.

[10] G. J. Fokken, W. L. Walters, L. E. Mattson and B. K. Gilbert, "Low cost, multi-GHz electrical packaging for serial optoelectronic links utilizing vertical cavity surface emitting lasers," *IEEE Trans. Adv. Pack.*, vol. 23, no. 1, pp.42-54, 2000.

[11] J. A. Hudging, S. F. Lim, G. S. Li, W. Yuen, K. Y. Lau and C. J. Chang-Hasnain, "Compact, integrated optical disk readout head using a novel bistable vertical cavity surface emitting lasers," *IEEE Photon. Technol. Lett.*, vol. 11, no. 2, pp. 245-247. 1999.

[12] J. Geske, V. Jayaraman, T. Goodwin, M. Culick, M. MacDougal, T. Goodmough,

D. Welch and J. Bower, “2.5 Gb/s transmission over 50 Km with a 1.3 μm vertical cavity surface emitting laser,” *IEEE Photon. Technol. Lett.*, vol. 12, no. 12, pp. 1707-1709, 2000.

[13] H. Kosaka, “Smart integration and packaging of 2D VCSEL’s of high speed parallel links,” *IEEE Select. Topics Quantum Electron.*, vol. 5, no. 2, pp. 184-192, 1999.

[14] K. Kasahara, “VSTEP based smart pixels,” IEEE J. Quantum Electron., Vol. 29, no. 2, pp. 757-768, 1993.

[15] H. E. Li and K. Iga Eds, “Vertical-cavity surface-emitting laser devices,” *Springer*, Chapter 1, pp.8, 2002.

[16] T. Uchida, T. Miyamoto, N. Yokouchi, Y. Inaba, F. Koyama and K. Iga, “CBE grown 1.5 lm GaInAsP–InP surface emitting lasers,” *IEEE J. Quant. Electron.*, vol. 29, pp. 1975, 1993.

[17] M. Kondow, T. Kitatani, S. Nakatsuka, M. C. Larson, K. Nakahara, Y. Yazawa, M. Okai and K. Uomi, “GaInNAs: a novel material for long-wavelength semiconductor lasers,” *IEEE J. Sel. Top.Quantum Electron.*, vol. 3, pp. 206-209, 1997.

[18] J. J. Dudley, D. I. Babic, R. Mirin, L. Yang, B. I. Miller, R. J. Ram, T. Reynolds, E. L. Hu and J. E. Bowers, “ Low threshold, wafer fused long wavelength vertical cavity lasers,” *Appl.Phys. Lett.*, vol. 64, pp. 1463, 1994.

[19] D. I. Babic, K. Streubel, R. P. Mirin, M. N. Margalit, E. L. Hu, J. E. Bowers, D. E. Mars, L. Yang and K. Carey, “Room-temperature continuous-wave operation of 1.54-μm vertical-cavity lasers,” *IEEE Photon. Technol. Lett.*, vol. 7, pp. 1225, 1995.

[20] S. F. Yu, “Analysis and design of vertical cavity surface emitting lasers”, Wiley-Interscience, pp.22, 2003.

[21] Y. J. Yang, T. C. Dziura, T. Bradin, S. C. Wang and R. Fernandez, “Continuous wave single transverse mode vertical cavity surface emitting lasers fabricated by Helium implantation and zinc diffusion,” *IEE Electron. Lett.*, vol. 28, no. 3, pp. 274-275, 1992.

[22] J. Boucart, C.Starck, F. Gaborit, A. Plais, N. Bouche, E. Derouin, L. Goldstein, C. Fortin, D. Carpentier, P. Salet, F. Brillouet and J. Jacquet, “1mW CW-RT monolithic VCSEL at 1.55μm,” *IEEE Photon. Technol. Lett.*, Vol. 11, pp.629-631,

no.6, 1999.

[23] Y. Qian, Z. H. Zhu, Y. H. Lo, D. L. Huffaker, D. G. Deppe, H. Q. Hou, B. E. Hammons, W. Lin and Y. K. Tu, "Low-threshold proton implanted 1.3μm vertical cavity top surface emitting lasers with dielectric and wafer bonded GaAs-AlAs bragg mirrors," *IEEE Photon. Technol. Lett.*, vol. 9, no.7, pp.866-868, 1997.

[24] H. Saito, K. Nishi, I. Ogura, S. Sugou and Y. Sugimoto, "Room temperature lasing operation of a quantum dot vertical cavity surface emitting lasers," *Appl. Phys. Lett.*, vol. 69, no. 21, pp. 3140-3142, 1996.

[25] P. Blixt, D. I. Babic, N. M. Margalit, K. Streubel and J. E. Bowers, "Multimode fiber transmission using room temperature double fused 1.54μm vertical cavity lasers," *IEEE Photon. Technol. Lett.*, vol. 8, no. 11, pp.1564-1567, 1996.

[26] J. W. Scott, B. J. Thibeault, D. B. Young, L. A. Coldren and F. H. Peters, "High efficiency submilliamp vertical cavity lasers with intracavity contacts," *IEEE Photon. Technol. Lett.*, vol. 6, no. 6, pp.678-680, 1994.

[27] Y. Kohama, Y. Ohiso, K. Tateno and T. Kurokawa, "0.85μm vertical cavity surface emitting laser diode arrays grown on p-type GaAs substrate," *IEEE Photon. Technol. Lett.*, vol. 9, no. 3, pp.280-282, 1997.

[28] K. D. Choquette, M. Hong, R. S. Freund, J. P. Mannaert, R. C. Wetzel and R. E. Leibenguth, "Vertical cavity surface emitting laser diodes fabricated by In Situ dry etching and molecular beam epitaxial regrowth," *IEEE Photon. Technol. Lett.*, vol. 5, no. 3, pp.284-287, 1993.

[29] T. –H. Oh, O. B. Shchekin and D. G. Deppe, "Single-mode operation in an antiguided vertical-cavity surface-emitting laser using a low-temperature grown AlGaAs dielectric aperture," *IEEE Photon. Technol. Lett.*, vol. 10, no. 8, pp. 1064-1066, 1998.

[30] J. M. Dallesasse, N. Holonyak, Jr., A. R. Sugg, T. A. Richard and N. El-Zein, "Hydrolyzation oxidation of $Al_xGa_{1-x}As$-AlAs-GaAs quantum well hetero-structures and superlattices," *Appl. Phys. Lett.*, vol. 57, pp. 2844-2846, 1990.

[31] G. M. Yang, M. MacDougal and P. D. Dupkus, "Ultralow threshold current vertical cavity surface emitting laser obtained with selective oxidation," *IEE Electron. Lett.*, vol. 31, pp. 886-888, 1995.

[32] P. W. Evans, J. J. Wierer and N. Holonyak, "Al_xGa-xAs native oxide based

distributed bragg reflectors for vertical cavity surface emitting lasers," *J. Appl. Phys.*, vol. 84, no. 10, pp. 5436-5440, 1998.

[33] M. H. MacDougal, J. Geske, C. K. Lin, A. E. Bond and P. D. Duplus, "Low resistance intracavity contacted oxide-aperture VCSELs," *IEEE Photon. Technol. Lett.*, vol. 10, no. 1, pp.9-11, 1998.

[34] P. Schnitzer, M. Grabberr, R. Jager, F. Mederer, R. Michalzik, D. Wiedenmann and K. J. Ebeling, "GaAs VCSEL's at λ=780 and 835 nm for short distance 2.5 Gb/s plastic optical fiber data links," *IEEE Photon. Technol. Lett.*, vol. 11, no. 7, pp. 767-769, 1999.

[35] E. W. Young, K. D. Choquette, S. L. Chuang, K. M. Geib, A. J. Fischer and A. A. Allerman, "Single-transverse-mode vertical-cavity lasers under continuous and pulsed operation," *IEEE Photon. Technol. Lett.*, vol. 13 pp. 927–929, 2001

[36] J.-F. P. Seurin, S. L. Chuang, L. M. F. Chirovsky, and K. D. Choquette, "Novel VCSEL designs deliver high single-mode output power," *Laser Focus World*, vol. 38, issue 5, 2002.

Chapter 2

Proton-implanted VCSEL with Transparent Contact

Using proton-implantation technique for gain-guiding of VCSEL devices is a simple and stable process for mass production of VCSELs. However, as described in section 1-2-1, proton-implanted VCSELs exhibit kink characteristics in light output power versus current (L-I) curve and could not be stable operated over 2.125 Gb/s. In this chapter, we demonstrated the enhancement in the performance of proton-implanted, gain-guided, GaAs VCSEL by incorporation of a new p-contact scheme using a Ti and ITO transparent overcoating on the regular p-contact. The kink characteristics in L-I curve of the VCSEL with the Ti/ITO overcoating were improved with a reduction in the derivative kink factor of as large as 70%. The high-speed response of the overcoated device also shows a more open clear eye and lower jitter of 35 ps operating at 2.125 Gb/s under 10 mA bias and 9 dB extinction ratio compared to the no overcoated device. Better current spreading and uniformity induced by the overcoating could be responsible for these performance improvements.

2-1 Literature survey

Currently, there are two main categories of mass production VCSELs namely oxide-confined VCSELs and proton-implanted VCSELs. The oxide-confined VCSELs have an oxided boundary surrounding the emitting aperture for index-guiding and current confinement resulting well defined transverse modes at low bias current [1, 2]. However, the oxide-confined VCSELs have a few technical issues. The oxidation procedure depends strongly on materials and processing parameters which could change

during the process making control of the aperture size relatively difficult. In addition, the strain and defects introduced by improper oxidation process might have some reliability problems [3]. Compared to the oxide-confined VCSELs, the proton-implanted VCSELs have a relatively simple fabrication process (planar process) and have been demonstrated with good reliability [4]. However, due to the gain-guided nature of the proton-implanted VCSELs, the kinks usually occur in light output power versus current (L-I) curve [5], and the laser power output jitter and noise also tend to limit the modulated speed around 1.25 Gb/s [4] that hardly meets the 2.125 Gb/s (2x Fiber channel) requirement. In VCSELs, the kinks in L-I curve were attributed to change of multi-transverse mode operation [5]. Some reports indicated the transverse mode structures depend on the driving current [9], and the injection current from the periphery of the top contact aperture into the active region tends to cause current crowding and non-uniform current spreading [10-13]. In the proton-implanted VCSELs, the evolution of transverse mode pattern would be strongly affected by the current crowding and non-uniform current spreading because of the lack of beam confinement by an index-guiding. Additionally, the metal aperture is smaller than the proton-implanted confinement aperture due to the contact concerned. Therefore, the output light which is localized in the periphery of the implant boundary resulted from the current crowding and non-uniform current spreading would be blocked by the metal contact and occurred the large kinks in L-I curve. Y. Liu *et al.* also indicated the non-uniformity and fluctuation in both injected carrier density and junction temperature could affect the frequency of lasing mode [14]. Consequently, the improvement of current spreading and reduction of current crowding in VCSELs could reduce the kinks and thus improve the device modulation speed especially in proton-implanted VCSEL.

Recently, there were reports of using transparent indium-tin-oxide (ITO) replaced regular Ti/Au or Ti/Pt/Au p-contact metal of the VCSELs to increase contact

transparency and showed that the ITO has good ohmic contact similar to the regular contact. These include the use of ITO [15, 16], Au-plated ITO [17] as the top contact and ITO as top ring contact [18]. However, the effects of these new contact schemes on the VCSEL performances such as kink characteristics of L-I curve and modulation response were not clearly mentioned. In this chapter, we report results of incorporation of a new p-contact scheme using Ti and ITO transparent overcoating on the regular p-contact of the implanted VCSEL that show substantial improvement in the kink characteristics and the modulation response of the proton- implanted VCSEL.

2-2 Experiment

The GaAs VCSEL wafer structure was grown on the n^+-GaAs substrate by a metal organic chemical vapor deposition system. The bottom distributed Bragg reflector (DBR) consists of n-type 30.5-period $Al_{0.12}Ga_{0.88}As$ / AlAs and the top DBR consists of 19.5-period p-type $Al_{0.12}Ga_{0.88}As$ / AlAs. The active region has an undoped three-quantum-well GaAs / $Al_{0.3}Ga_{0.7}As$, a lower linearly-graded undoped- $Al_xGa_{1-x}As$ ($x=0.6\rightarrow0.3$) waveguide layer and an upper linearly-graded undoped-$Al_xGa_{1-x}As$ ($x=0.3\rightarrow0.6$) waveguide layer. A heavily Carbon-doped p-type GaAs cap layer was grown to facilitate p-ohmic contact. Next a regular p-contact metallization of Ti (200 Å) / Au (1500 Å) were deposited by E-beam evaporator with a 15 μm diameter emission aperture and a contact pad size of 350×350 μm^2. Then Ge (200 Å) / Au (400 Å) / Ni (140 Å) / Au (1500 Å) layers were deposited as the n-ohmic contact, and annealed in a rapid thermal annealing system (RTA) at 380 ℃ under N_2 ambient for 30 second. The device was then subjected to the proton implantation with an energy of 200 KeV and a dosage of 1×10^{15} cm^{-2} with an aperture of 20 μm diameter. All the VCSELs were tested prior to the overcoating. The tested VCSELs were then overcoated with Ti/ITO transparent film on top of the regular Ti/Au p-contact by RF sputtering in Ar 12 sccm,

5×10^{-3} torr, at a base pressure of 1.6×10^{-6} torr and a deposition pressure of 3.3×10^{-4} torr. The thickness of Ti is 40 Å and ITO (In_2O_3-SnO_2) is 3200 Å. The thin Ti film was chosen because of its high transparency (~ 92% at 850 nm), low annealing temperature, good adhesive property and ohmic contact with GaAs. Subsequently, the device was annealed at 380 ℃ under N_2 ambient for 30 second to form ohmic contact. The dimension of the transparent overcoating is 300×300 μm^2 slightly smaller than the regular p-contact pad size for easy probing. The schematic of the fabricated VCSEL device is shown in Figure 2-1 and Figure 2-2 shows the process procedures.

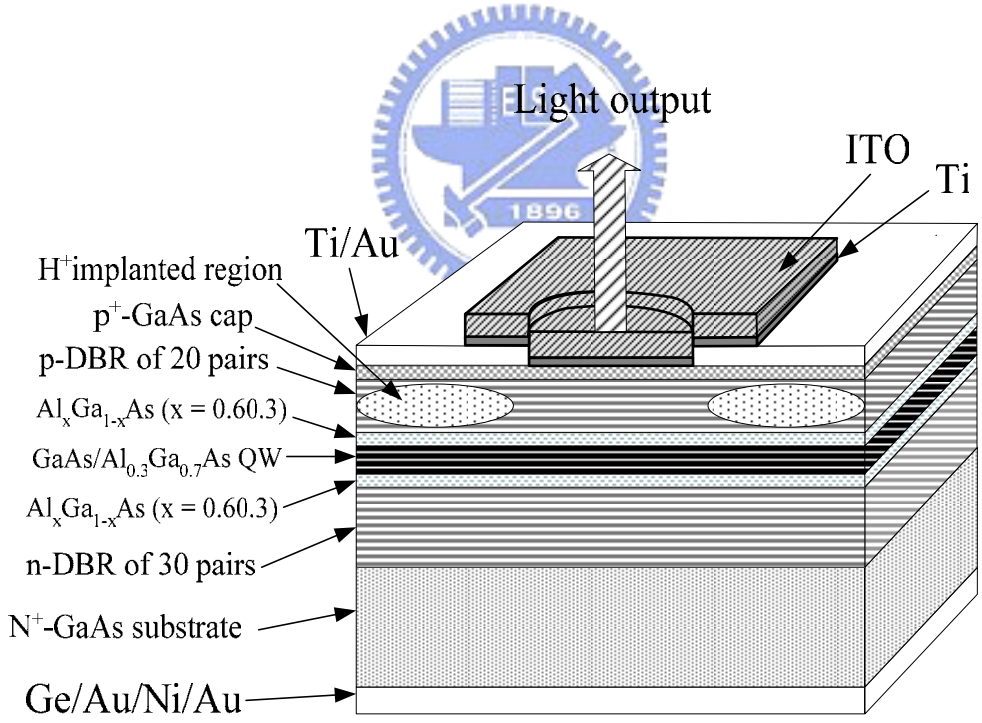

Figure 2-1 The schematic of the overcoated VCSEL device using Ti/ITO.

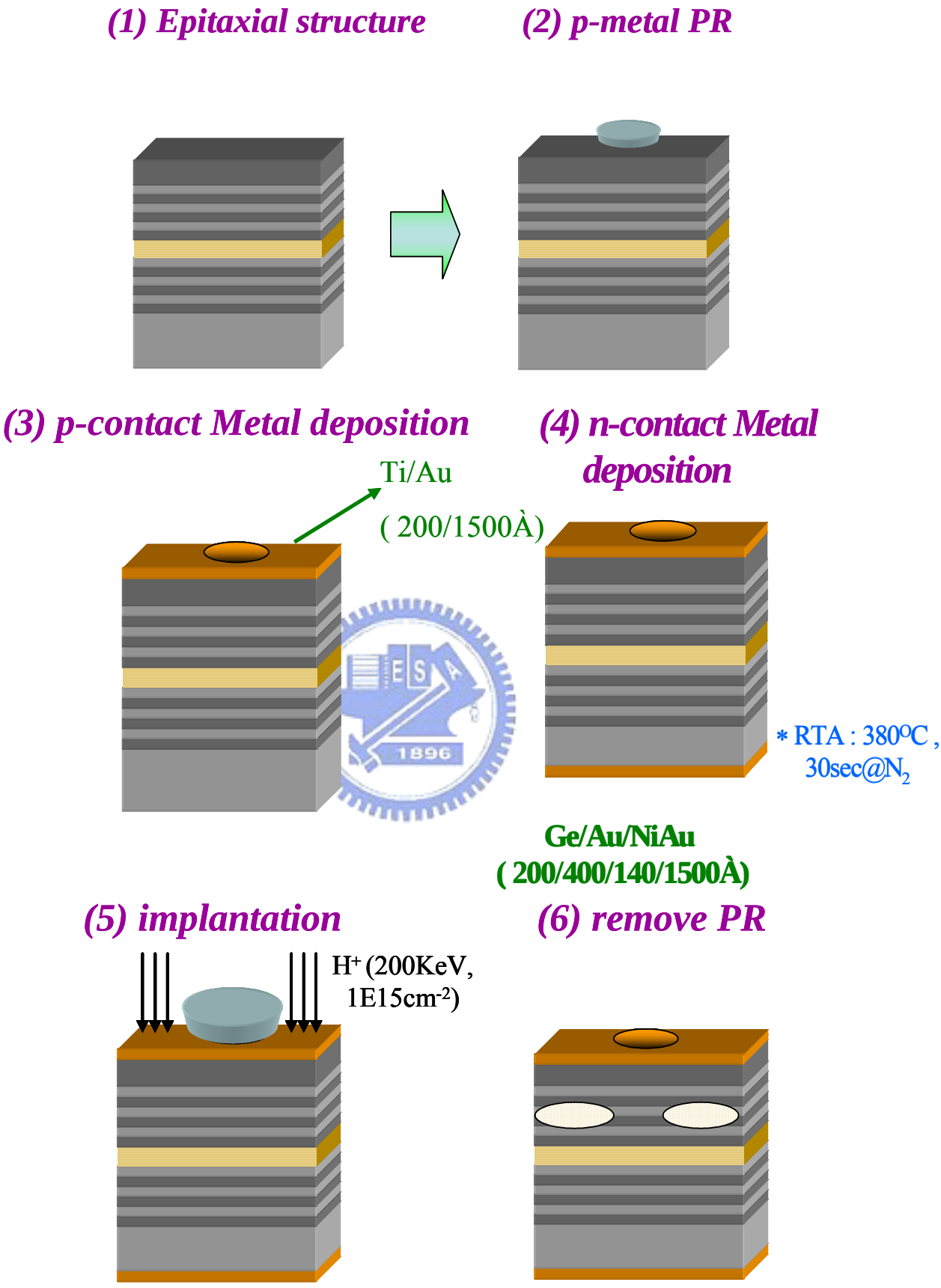

Figure 2-2 The process procedures of proton-implanted VCSEL with transparent contact.

2-3 Results and Discussions

Figure 2-3 shows the L-I-V characteristics of a typical VCSEL before and after the Ti/ITO overcoating. The maximum light output decrease slightly due to the slightly reduction in transparency from Ti/ITO overcoating. The series resistance of the overcoating VCSEL slightly increase which may be due to the additional Ti/ITO annealing process. However, the L-I curve of the overcoated VCSEL shows a substantial improvement in the kinks and the improvement of threshold current I_{th} (3.4 mA to 2.2 mA) compared with the uncoated VCSEL. It might be due to the improvement of uniform current spreading by the overcoated and the light output would not be blocked by the contact metal. The L-I curves of the overcoated VCSELs all show a substantial improvement in the kinks compared to the uncoated VCSELs. To quantify

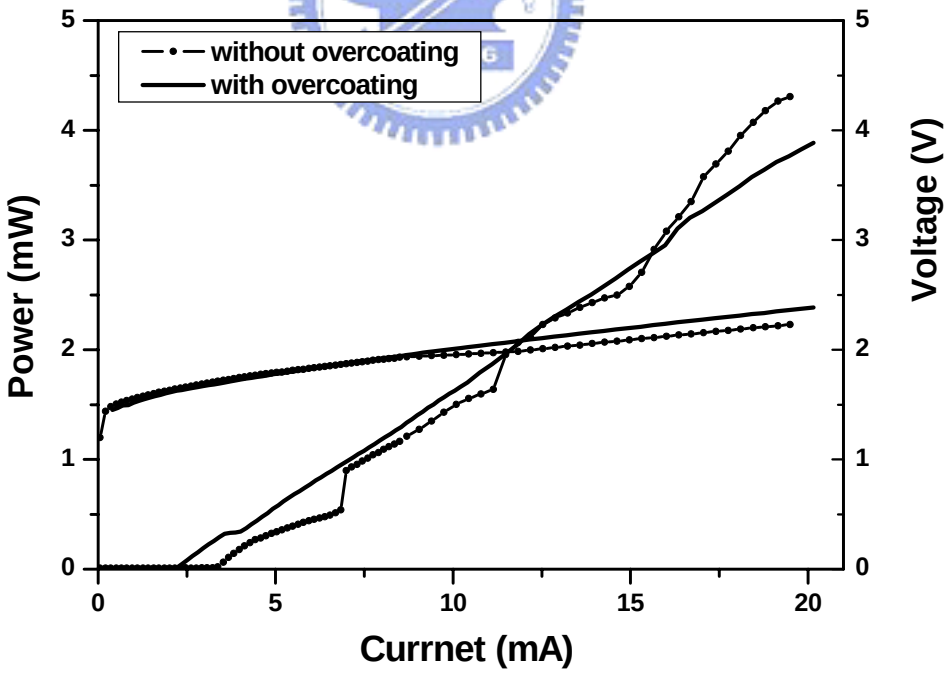

Figure 2-3 The L–I–V characteristics of a typical VCSEL with and without Ti/ITO transparent overcoating.

the kink characteristics in L-I curve, we define a Derivative Kink Factor (DKF) which measure the mean square deviation of the local slope from the average slope, normalized to the average slope of the L-I cure as show below:

$$Derivative\ \ Kink\ Factor = \frac{\left\langle \left(\partial L/\partial I - \left\langle \partial L/\partial I \right\rangle \right)^2 \right\rangle^{1/2}}{\left\langle \partial L/\partial I \right\rangle} \Bigg|_{L_{th}}^{L_{max}/2} \qquad (2\text{-}1)$$

where L is the light output power, I is the driving current, L_{max} is the maximum light output power, and L_{th} is the light output power at the threshold. To minimize the effect of thermal rollover at higher power output, the DKF is only evaluated from threshold up to $L_{max}/2$. From the L-I curves we evaluated DKF value of the VCSEL devices in the same wafer for current range from the threshold to 15 mA, and the DKF values distribute from 0.3 to 1 before the overcoating of Ti/ITO. After overcoating, the DKF values of the VCSELs distribute around 0.2±0.03. This result indicate the DKF values of the VCSELs are more unity and reduced around 33% ~ 70% after the Ti/ITO overcoating, clearly indicating the improvement in the kink characteristics and uniformity of the implanted VCSELs after the Ti/ITO overcoating.

To investigate kink reducing effect on high speed performance, large signal modulation response was checked. Figures 2-4 (a) and 2-4 (b) show the eye diagram of the typical VCSEL device before and after Ti/ITO overcoating respectively operating at 2.125 Gb/s with 10 mA bias and 9 dB extinction ratio. The uncoated VCSEL failed to pass the 2.125 Gb/s Eye-Mask and has a large jitter over 40 ps. While the overcoated VCSEL showed a wide open eye pattern, and easily passed the 2.125 Gb/s with a jitter of less than 35 ps. The result indicates the Ti/ITO overcoated VCSEL with lower DKF values has substantially improved in the device high-speed performance characteristic.

(a)

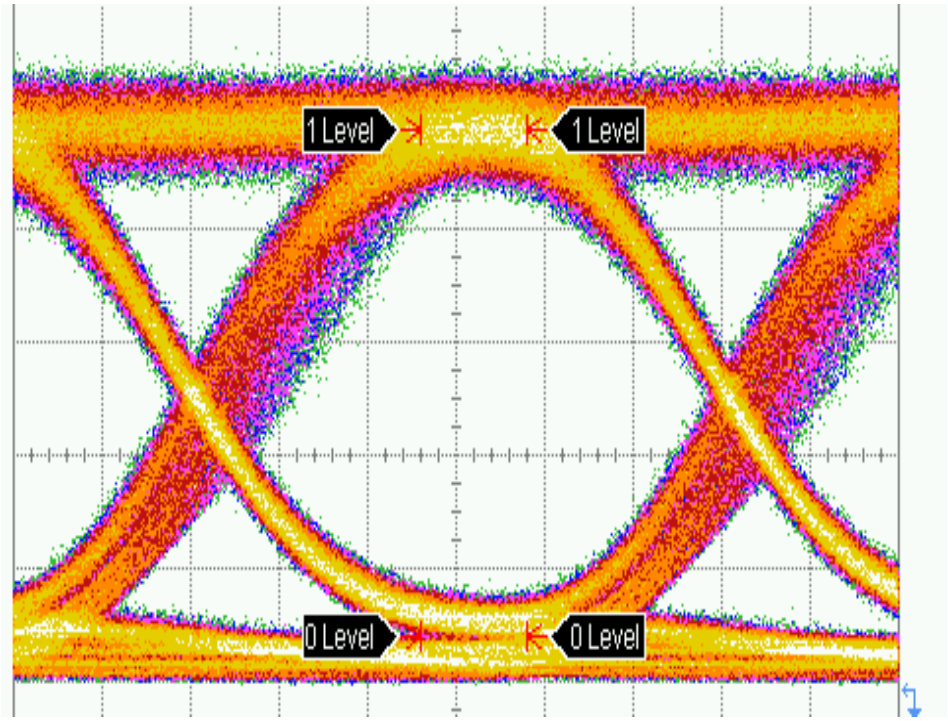

(b)

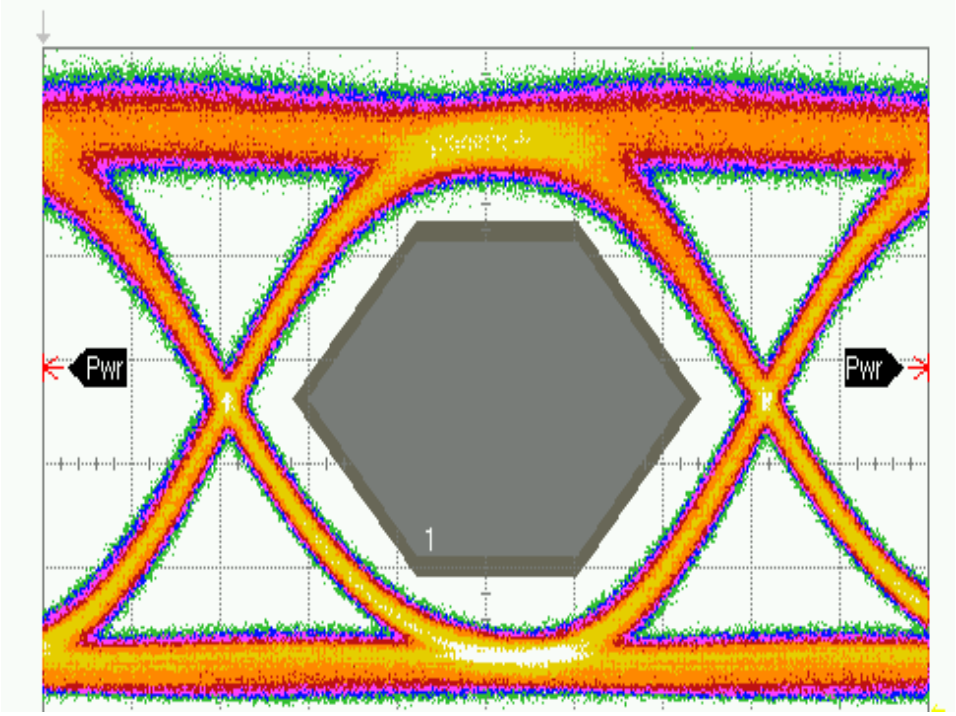

Figure 2-4 Eye diagrams of the typical VCSEL device (a) without and (b) with Ti/ITO transparent overcoating operating at 2.125 Gb/s with 10 mA bias and 9 dB extinction ratio. The horizontal scale is 40 ps/div.

The improvement in the kink characteristics and the modulation response of the Ti/ITO overcoated VCSEL maybe the result of better current injection uniformity and carrier spread induced by the overcoating. Since the change of light emission pattern correspond to the change of current injection density [6] into the VCSELs, Figure 2-5 (a) and 2-5 (b) compare the near-field optical microscope images of the emission patterns of the VCSEL before and after overcoating in the currents when the kinks occurred. Figure 2-5 (a) clear shows the switching between the different lasing mode patterns when large kinks took place in L-I curve and the large kinks occurred when the light output might partly blocked by metal contact. For comparison, emission patterns of the overcoated VCSEL were shown in Figure 2-5 which are more uniform and stable at the same current level. From the near-field images of uncoated and overcoated VCSELs, the overcoating layer did provide better uniformity in the current injection which could lead to the improvement in the kink characteristics in L-I curves and high speed response of the VCSELs.

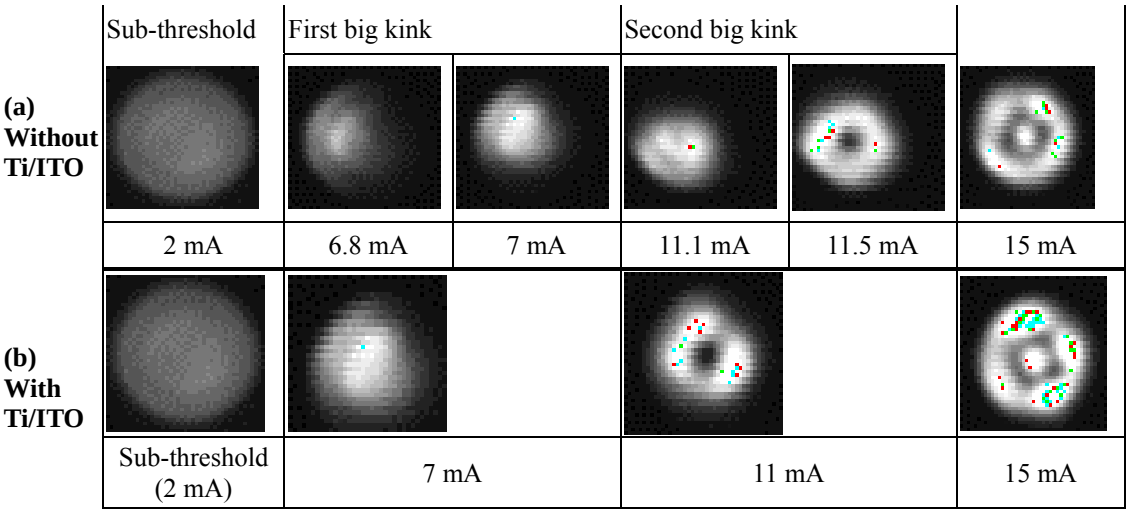

Figure 2-5 The near-filed emission patterns of the typical VCSEL device (a) without and (b) with Ti/ITO transparent overcoating at different injecting currents.

2-4 Summary

In this chapter, we demonstrated the enhancement in the performance of proton-implanted VCSEL by using a Ti/ITO overcoating on the regular p-contact. The kink characteristics of the VCSEL with the Ti/ITO overcoating show substantial improvement with as large as 70% reduction in the derivative kink factor. The high-speed response of the overcoated device shows better performance than the uncoated devices with clear eye with 35 ps jitter operating at 2.125 Gb/s with 10 mA bias and 9 dB extinction ratio. These improvements in the implanted VCSEL performance would be due to the better current spreading and uniformity induced by the overcoating. This overcoating technique should be applicable to the other types of VCSELs.

References

[1] C.W. Wilmsen, H. Temkin, and L.A. Coldren, eds., "Vertical-Cavity Surface-Emitting Lasers: Design, Fabrication, Characterization, and Applications," Cambridge University Press, 1999.

[2] K. L. Lear, A. Mai, K. D. Choquette, S. P. Kilcoyne, R. P. Schneider, Jr, and K. M. Geib, "High-frequency modulation of oxide-confined vertical cavity surface emitting lasers," *IEE Electron. Lett.*, vol. 32, pp.457, 1996.

[3] D. T. Mathes, R. Hull, K. Choquette, K. Geib, A. Allerman, J. Guenter, B. Hawkins and R. A. Hawthorne, in Proc. Vertical-Cavity Surface-Emitting Lasers VII, C. Lei and S. P. Kilcoyne, eds., *SPIE 2003*, vol. 4994, pp. 67-82, 2003.

[4] A. Tatum, A. Clark, J. K. Guenter, R. A. Hawthorne, and R. H. Johnson, "Commercialization of Honeywell's VCSEL technology," in Proc. Vertical-Cavity Surface-Emitting Lasers IV, K. D. Choquette and C. Lei, editors, *SPIE 2000*, vol. 3946, pp. 2-13, 2000.

[5] K. D. Choquette, S.P. Kilcoyne, K.L. Lear. R. P. Schneider, "Index guiding dependent Effects in Implant and oxide confined Vertical-cavity Lasers" *IEEE Photon. Technol. Lett.* vol. 8, pp. 740-742, 1996.

[6] Roy Lang, "Lateral transverse mode instability and its stabilization in stripe geometry injection lasers," *IEEE J. Quantum Electron.*, vol. 15, pp. 718-726, 1979.

[7] Tien-Pei Lee, Charles A. Burrus, JR., Pao-Lo Liu, William B. Sessa, and Ralph A. Logan, "An investigation of the frequency stability and temperature characteristics of 1.5μm coupled-cavity injection lasers," *IEEE J. Quantum Electron.*, vol. QE-20, pp. 374-384, 1984.

[8] G. R. Gray and R. Roy, "Bistability and mode hopping in a semiconductor laser," *J. Opt. Soc. Am.* B, vol. 8, pp. 632-638, 1991.

[9] C. J. Chang-Hasnain, J. P. Harbison, G. Hasnian, A. C. Von Lehmen, L. T. Florez and N. G. Stoffet, "Dynamic polarization, and transverse mode characteristics of vertical cavity surface emitting lasers," *IEEE J. Quantum Electron.*, vol. 27, pp. 1402-1409, 1991.

[10] N. K. Dutta, “Analysis of current spreading, carrier diffusion, and transverse mode guiding in surface emitting lasers,” *J. Appl. Phys.*, vol. 68, pp. 1961-1963, 1990.

[11] W. Nakwaski and M. Osinski, “Thermal properties of etched-well surface-emitting semiconductor lasers,” *IEEE J. Quantum Electron.*, vol. 27, pp. 1391-1401, 1991.

[12] H. Wada, D. I. Babic, M. Ishikawa, and J. E. Bowers, “Effects of nonuniform current injection in GaInAsP/InP vertical-cavity lasers,” *Appl. Phys. Lett.*, vol. 60, pp. 2974-2976, 1992.

[13] S. Sekiguchi, T. Miyamoto, T. Kimura, G. Okazaki, F. Koyama, and K. Iga, “Improvement of current injection uniformity and device resistance in long-wavelength vertical-cavity surface-emitting laser using a tunnel junction,” *Jap. J. Appl. Phys.*, vol. 39, Part 1, No. 7A, pp. 3997-4001, 2000.

[14] Y. Liu, W. C. Ng, B. Klein and K. Hess, “Effects of the spatial nonuniformity of optical transverse modes on the modulation response of vertical-cavity surface-emitting lasers,” *IEEE J. Quantum Electron.*, vol. 39, pp. 99-108, 2003.

[15] M. A. Matin, A. F. Jezierski, S. A. Bashar, D. E. Lacklison, T. M. Benson, T. S. Cheng, J. S. Robers, T. E. Sale, J. W. Orton, C. T. Foxon, and A. A. Rezazadeh, “Optically transparent indium-tin-oxide (ITO) ohmic contacts in the fabrication of vertical-cavity surface-emitting lasers”, *Electron. Lett.*, vol. 30, pp. 318-320, 1994.

[16] C. L. Chua, R. L. Tornton, D. W. Treat, V. K. Yang, and C. C. Dunnrowicz, “Indium tin oxide transparent electrodes for broad-area top-emitting vertical-cavity lasers fabricated using a single lithography step”, *Photon. Technol. Lett.* vol. 9, pp. 551-553, 1997.

[17] R. Thornton, Y. Zou, J. Tramontana, M. H. Crawford, R. P. Schneider, and K. D. Choquette, “Visible (670nm) vertical cavity surface emitting lasers with indium tin oxide transparent conducting top contacts”, in LEOS’95, San Francisco, CA, 1995, pp. 108-109, 1995.

[18] Wen-.Jang Jiang, Meng-Chyi Wu, Hsin-Chieh Yu, Chun-Yuan Huang, Chia-Pin Sung, Jim-Yong Chi, " The effect of indium tin oxide as an ohmic contact for the 850nm GaAs oxide-confined VCSELs,” *Solid-State Electron.*, vol. 46, pp. 1945-1948, 2002.

Chapter 3

Si^+-implanted VCSEL (Index-guided VCSEL)

In this Chapter, we report a novel implanted VCSELs utilizing silicon implantation induced disordering. The VCSELs exhibit kink-free current-light output performance with threshold currents about 2.2 mA, and the slope efficiencies about 0.45 W/A. The threshold current change with temperature is minimal and the slope efficiency drops less than about 30% when the substrate temperature is raised to 90 ^{o}C. The eye diagram of VCSEL operating at 2.125 Gb/s with 7 mA bias and 10 dB extinction ratio shows very clean eye with jitter less than 30 ps. We have accumulated life test data up to 5000 hours at 100 ^{o}C/20 mA with exceptional reliability and the wet high temperature operating life WHTOL, 85 ^{o}C/85 humidity) test biased at 8 mA has passed over 2000 hours.

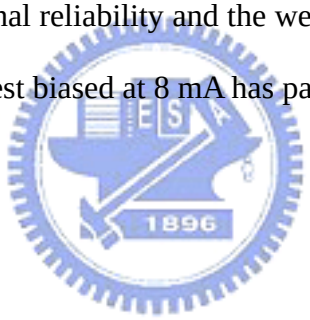

3-1 Literature survey

To date, only two types of commercial VCSELs are available: proton-implanted VCSEL and oxide-confined VCSEL. Proton-implanted VCSEL has been demonstrated with good reliability and decent modulation speed up to 1.25 Gb/s [1]. However, the kink in current versus light output (L-I) has been always an issue in the gain-guided proton-implanted VCSEL. [4] The jitter and noise performance of proton-implanted VCSEL made it difficult to achieve 2.5 Gb/s (OC-48) requirement. Compared to proton-implanted VCSEL, the oxide aperture in oxide-confined VCSEL provides precise boundaries near the active region for index-guiding which can give rise to well defined transverse modes at low bias current [2, 3]. Therefore, with lower threshold currents and enhanced noise properties, oxide-confined VCSEL can be used for 2.125

Gb/s and above applications. However, there are several manufacturing concerns for the oxide VCSEL. First, it is difficult to control the aperture sizes since the oxidation procedure depend strongly on numerous material and processing parameters which can easily and unpredictably changed. In addition, the strain and defects introduced by the oxide layer could cause potential reliability problem [5]. In this chapter, we report a new implanted VCSEL design that has the kink free L-I characteristics with an oxide-confined VCSEL-like performance and an implanted VCSEL-like reliability.

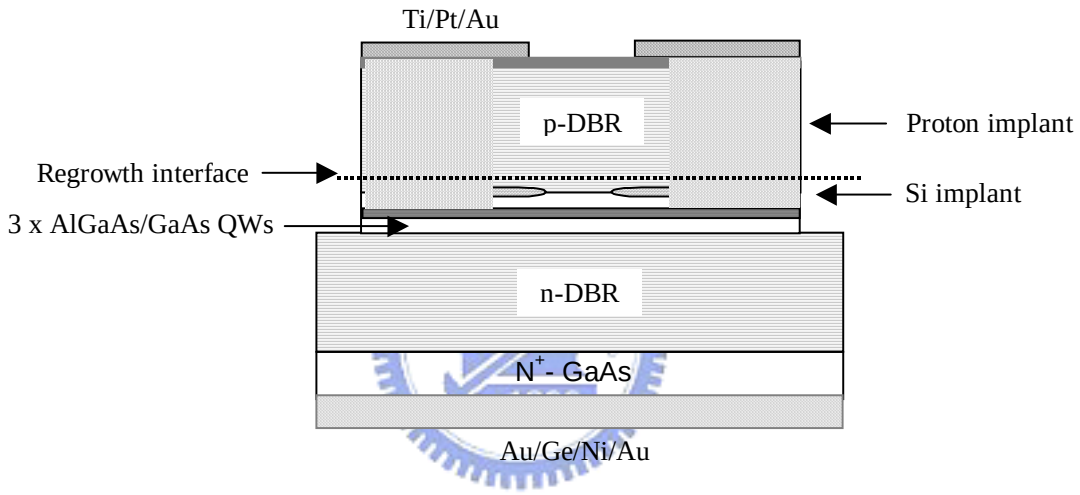

Figure 3-1 Schematic structure of a Si-implanted VCSEL. The Si^+-implanted aperture is 13×13 μm^2 and proton-implanted aperture is 30×30 μm^2.

3-2 Device structure and fabrication

The VCSEL structure contents of a n-type 35-period-$Al_{0.15}Ga_{0.85}As/Al_{0.9}Ga_{0.1}As$ distributed Bragg reflector (DBR), grown on *n*-GaAs (100) substrate by metal organic chemical vapor deposition (MOCVD) with the growth temperature 750 ^oC. Then, a three-quantum-well active region ($Al_{0.26}Ga_{0.74}As$/GaAs) was routinely grown, followed by the growth of 3-period $Al_{0.15}Ga_{0.85}As/Al_{0.9}Ga_{0.1}As$ *p*-type DBRs and a 5 nm thin

GaAs cap layer (to prevent oxidation of surface before re-growth). Then the 13×13 μm^2 emitting aperture was defined using silicon implantation. The implantation dose is 5×10^{14} cm^{-2} with the energy 90 KeV. The whole structure was finished by subsequent MOCVD re-growth of *p*-type 22-period-$Al_{0.15}Ga_{0.85}As$ $Al_{0.9}Ga_{0.1}As$ DBRs and cap layer. After re-growth, a mirror-like surface as obtained under microscope inspection

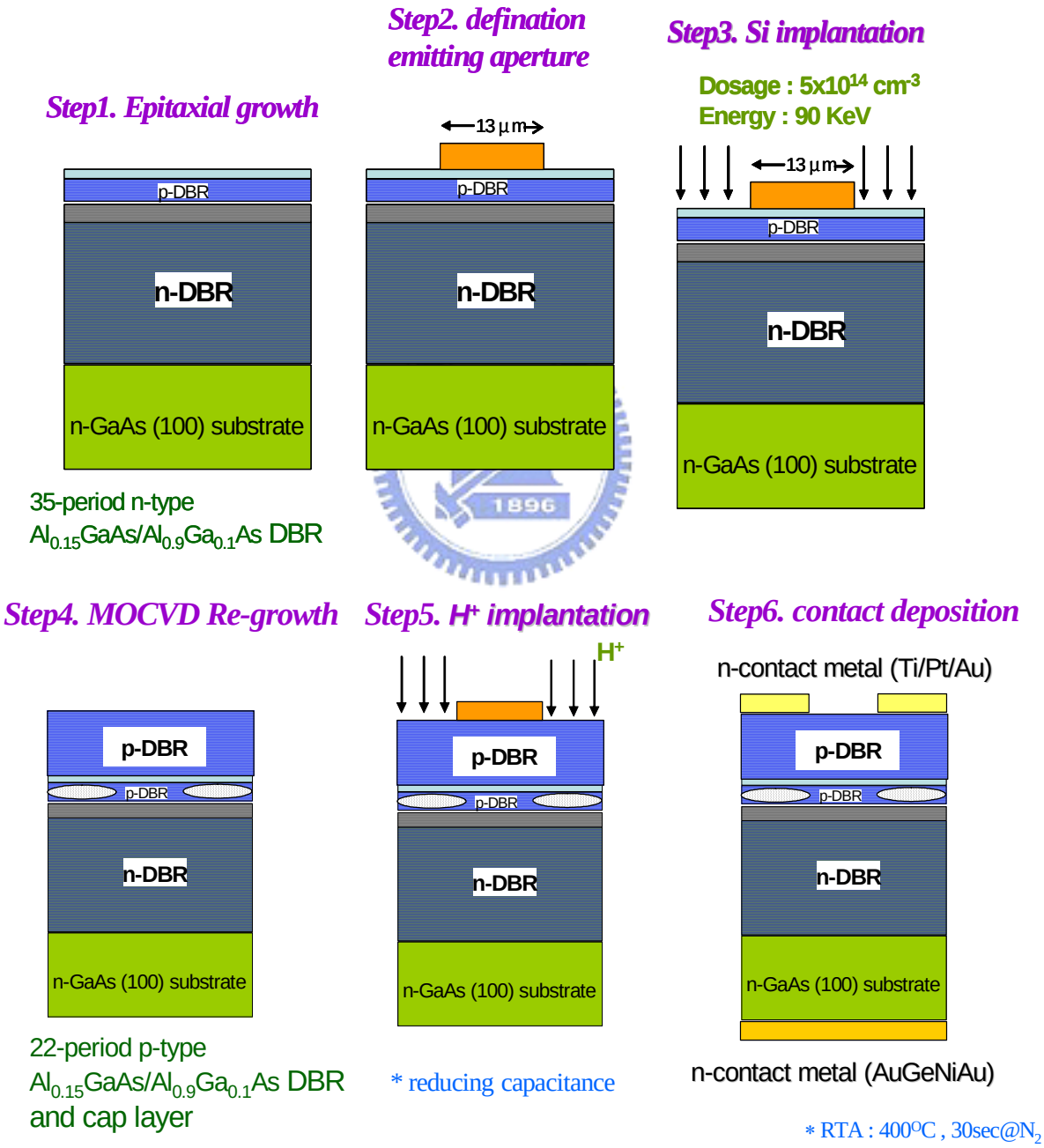

Figure 3-2 The schematic diagrams of fabricating processes

indicating good re-growth. Then the VCSELs were fabricated utilizing the routine processing – proton implantation to reduce capacitance, Ti/Pt/Au for p-metal and AuGe/Ni/Au for n-metal. The unique technique in this work is that during the MOCVD re-growth, the Si implantation region was annealed and induced disordering. The schematic of the fabricated VCSEL device is shown in Figure 3-1 and Figure 3-2 shows the schematic diagrams of fabricating processes.

3-3 VCSEL Performance

Figure 3-3 shows the typical Si-implanted VCSEL (a) light output, (b) voltage versus current (L-I-V) curves over temperature. The VCSEL exhibits kink-free current-

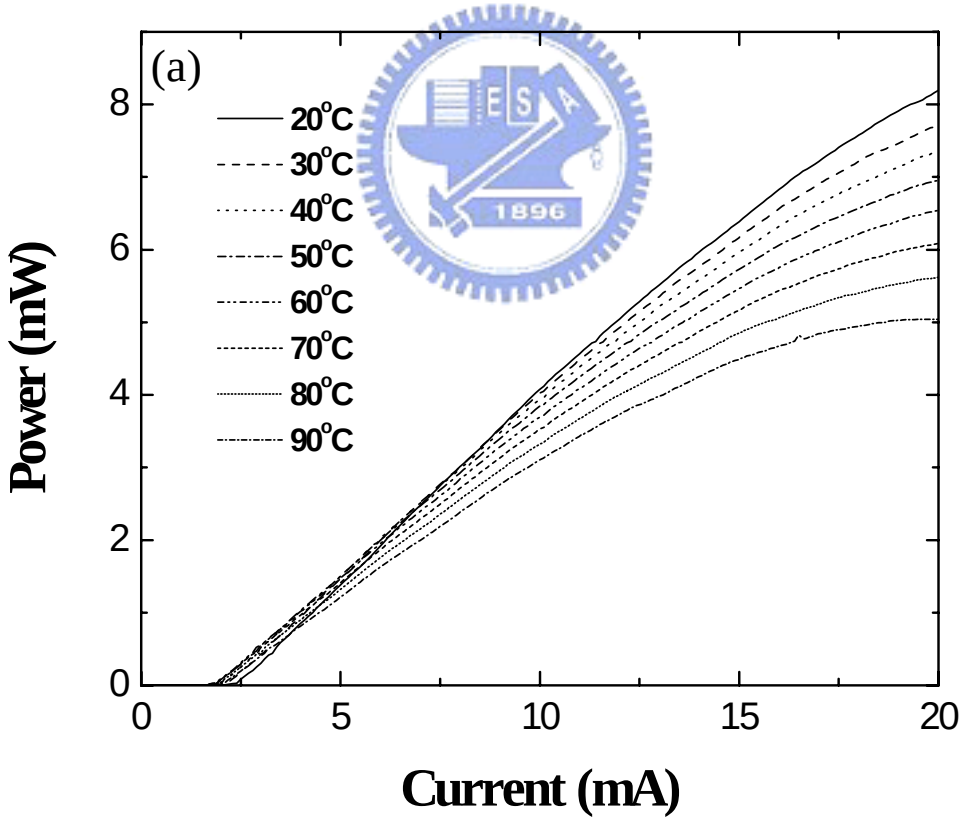

Figure 3-3 (a) Power versus current curves at 20 °C to 90 °C. The Si^+-implanted VCSELs exhibit kink-free current-light output performance with threshold currents ~2.4 mA, and the slope efficiencies ~ 0.45 W/A.

light output performance with threshold currents about 2.4 mA, and the slope efficiencies about 0.45 W/A. The threshold current change with temperature is less than 0.5 mA and the slope efficiency drops less than ~30% when the substrate temperature is raised from 25 ^{o}C to 90 ^{o}C. This is superior to the proton-implanted VCSEL with similar size and is comparable to that of oxide VCSEL. In addition, more than 90% series resistance of the VCSELs is within 40-45 Ohm indicating good re-growth interface.

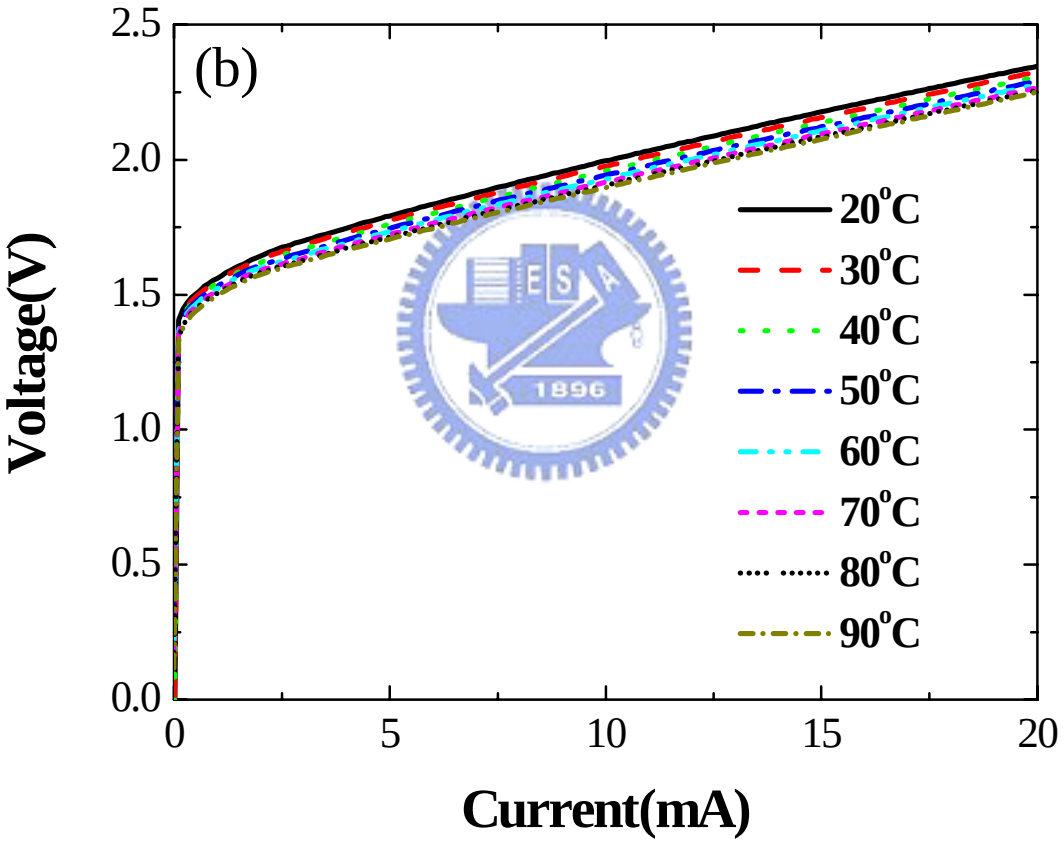

Figure 3-3 (b) Voltage versus current curves at 20 ^{o}C to 90 ^{o}C. The series resistance of more than 90% Si^{+}-implanted VCSELs is within 40-45 Ohm indicating good re-growth interface.

Figure 3-4 shows distributions for threshold current and slope efficiency of our VCSEL's sample test data (1262 chips in total). The sample test data is obtained from one out of 5×5 chips. The overall yield across a 3 inch wafer is over 90%. The narrow and normal distributions tell us the production performance of the Si-implanted VCSEL.

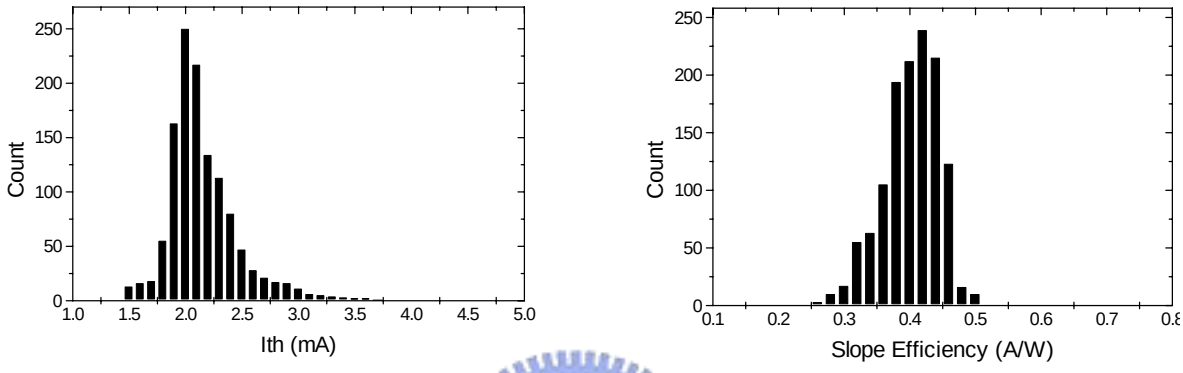

Figure 3-4 Distributions plot for threshold current and slope efficiency of Si^{+}-implanted VCSEL.

Spectral emission characterization consists of utilizing an optical spectrum analyzer (OSA) and Near-Field scanning optical microscopy. The output light from the VCSEL is collimated using a 100x objective. The beam is either redirected to a diffraction grating for near field analysis or coupled using 100x objective to multiple mode fiber and further fed to the OSA. Figure 3-5 shows the optical output power spectrum of a Si-implanted VCSEL driving at 5 mA ($1.4\times I_{th}$). The inset shows the spectrally resolved TEM_{00}, and TEM_{01*} (donut) intensity pattern. The near field patterns are similar as the patterns investigated in the selective oxide VCSEL with clear guiding patterns [6]. From the near field pattern of Si-implanted VCSEL, it suggests that silicon-implanted region does provide the good optical index-guiding. As a result, the Si-implanted VCSELs have much better kink characteristics compared to proton-implanted VCSELs.

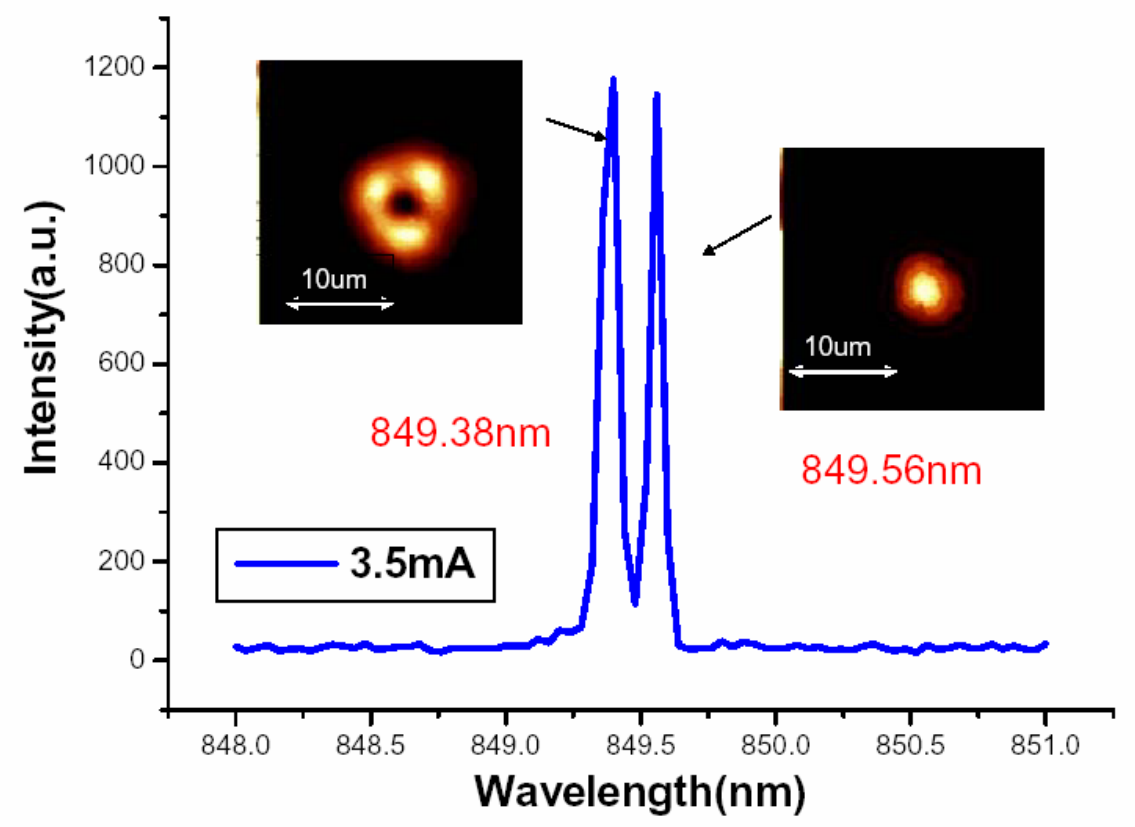

Figure 3-5 shows the optical output power spectrum of a Si^{+}-implanted VCSEL driving at 3.5 mA (1.45×I_{th}). Inset shows the spectrally resolved intensity pattern.

Figure 3-6 (a) shows the typical eye diagram of Si-implanted VCSEL on TO-46 operating at 2.125 Gb/s with 7 mA bias and 10 dB extinction ratio (ER) with P_{avg} ~ -5.3 dBm at 25 °C. The wide open eye pattern indicates good performance of our VCSEL. The 2.125 Gb/s Eye-Mask (with 20% margin) is passed with jitter (p-p) ~ 30 ps. Our VCSEL also show superior temperature performance. Figure 3-6 (b) demonstrated the eye-diagrams at 2.125 Gb/s at 85 °C of Si-implanted VCSEL. The 2.125 Gb/s Eye-Mask (with 20% margin) is passed with only a little noisy signal due to higher temperature operation. This confirms again the superior temperature performance of Si-implanted VCSEL.

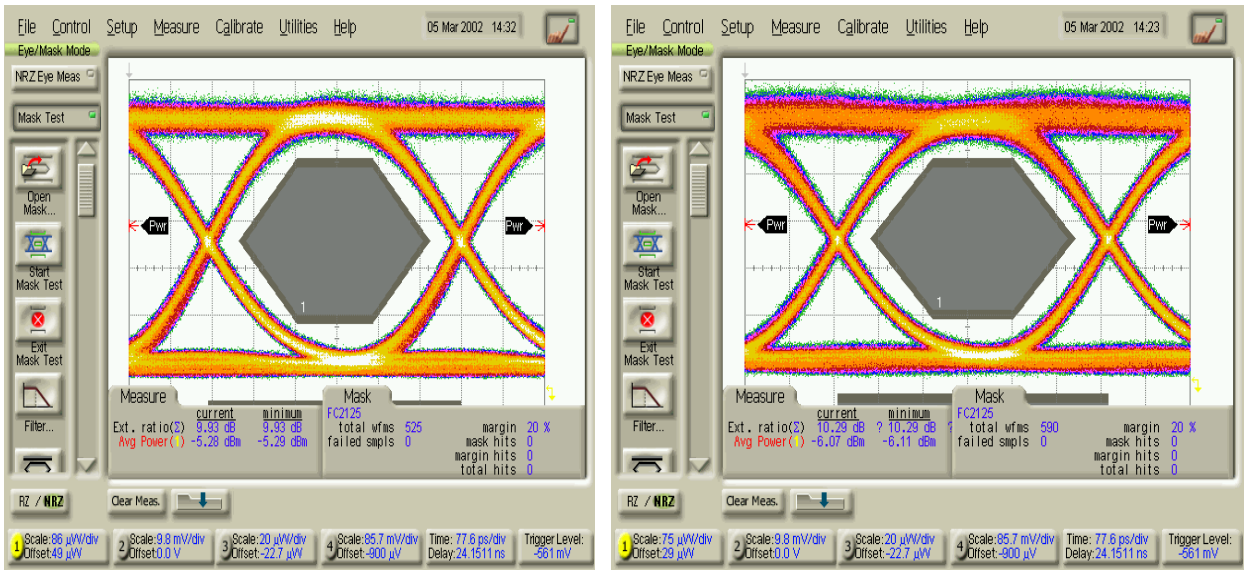

(a) **25 °C** -5.3 dBm 9.9 dB ER. (b) **85 °C** -6.1 dBm 10.3 dB ER.

Figure 3-6 Typical eye diagram of our VCSEL on TO-46 operating at 2.125 Gb/s (Fiber-Channel mask w. 20%-margin) with 7 mA bias and 9 dB extinction ratio at (a) 25 °C (b) 85 °C.

3-4 VCSEL reliability

The VCSELs reliability is a very important issue for many practical applications. We have accumulated life test data of our VCSELs up to 5000 hours at 100 ^{o}C/20 mA with exceptional reliability. In addition, our VCSEL chip is humidity proof and passed 2000-hour biased WHTOL (85 ^{o}C/85 humidity) test, a strongly desirable feature for parallel optics applications. As shown in Figure 3-7 is the I_{th} versus time scale for VCSEL chips under WHTOL test, none of them shows the abnormal behavior.

3-5 Summary

In conclusion, we report a novel implanted VCSEL process utilizing silicon implantation induced disordering. The VCSELs show good performance with kink-free

L-I characteristics, good temperature and high speed performance with wide open eye pattern. The Si-implanted VCSELs should be promise for the optoelectronic and other commercial applications in the coming days.

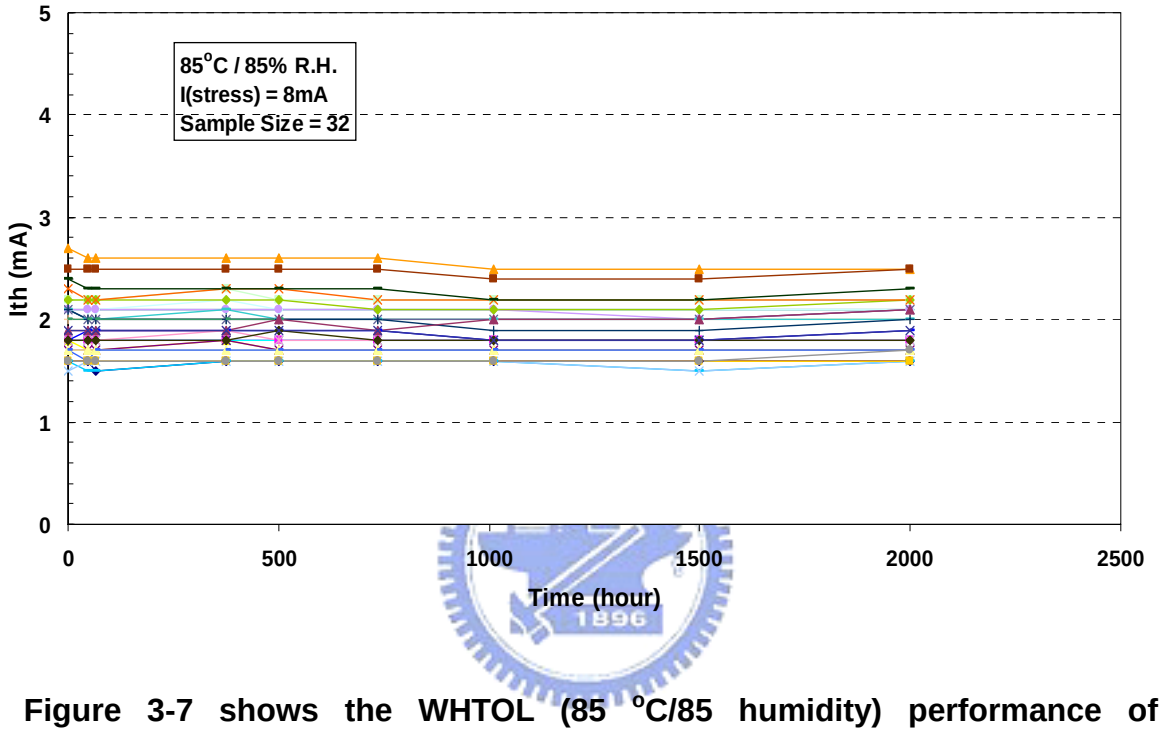

Figure 3-7 shows the WHTOL (85 °C/85 humidity) performance of Si^{+}-implanted VCSEL chips.

References

[1] A. Tatum, A. Clark, J. K. Guenter, R. A. Hawthorne, and R. H. Johnson, “Commercialization of Honeywell’s VCSEL technology,” in Proc. Vertical-Cavity Surface-Emitting Lasers IV, K. D. Choquette and C. Lei, editors, *SPIE 2000*, vol. 3946, pp. 2-13, 2000.

[2] C. W. Wilmsen, H. Temkin, and L. A. Coldren eds., “Vertical-Cavity Surface-Emitting Lasers: Design, Fabrication, Characterization, and Applications,” Cambridge University Press, 1999.

[3] K. L. Lear, A. Mai, K. D. Choquette, S. P. Kilcoyne, R. P. Schneider, Jr, and K. M. Geib, “High-frequency modulation of oxide-confined vertical cavity surface emitting lasers,” *IEE Electron. Lett.*, vol. 32, no.5, pp.457-458, 1996.

[4] K. D. Choquette, S. P. Kilcoyne, K. L. Lear. R. P. Schneider, “Index guiding dependent Effects in Implant and oxide confined Vertical-cavity Lasers,” *IEEE Photon. Technol. Lett.*, vol. 8, no.6, pp. 740 -742, 1996.

[5] K. L. Lear, S. P. Kilcoyne, R. P. Schneider, and J. A. Nevers, “Life-testing oxide confined VCSELs: too good to last? Fabrication, Testing, and Reliability of Semiconductor Lasers,” M. Fallahi and S.C. Wang, eds., *Proceedings of the SPIE*; vol. 2683, pp. 114-122, 1996.

[6] T. C. Lu, W. C. Hsu, Y. S. Chang, H. C. Kuo, and S. C. Wang, “Spectrally resolved spontaneous emission patterns of oxide-confined vertical-cavity surface-emitting lasers,” *J. Appl. Phys.*, vol.96, no. 11, pp.5992-5995, 2004.

Chapter 4

High speed oxygen-implanted VCSEL

VCSELs have become a standard applied technology in local area networks (LANs) from 1.25 Gb/s to 10Gb/s. High-power single transverse mode operation is preferred for many applications, including laser printing, optical storage and long-wavelength telecommunications, and especially for high data rate transmission in optical networks because of low dispersion effects and modal noise [l-3]. As one of the necessities, a simple highly effective coupling from single-mode VCSELs to single-mode fibers has already been demonstrated [4]. Besides the data transmission, there are more and more single-mode VCSELs applications emerging, such as gas sensing, spectroscopy, laser printing, optical storage, and longer distance communication [5]. Many of these applications require stable single-mode output powers of several milliwatts. But the VCSELs tend to lase with multimode as a result of the relative larger transverse dimensions, which support several transverse modes. By using antiguiding and hybrid-confined mechanism have chance to obtain the single-transverse-mode output as discussed in Section 1-2-2 and 1-2-3. We proposed two kinds of single-transverse-mode VCSEL structures utilizing hybrid-confined mechanism and will present in this chapter and next chapter.

In this chapter, high-speed single transverse mode 850 nm VCSELs with large emission aperture with a diameter of 8μm will reported. These VCSELs exhibit good performance with threshold currents of 1.5 mA, a single transverse mode emission within the full operational range and a maximum output power of 3.8 mW. The large aperture is advantageous to these VCSELs with a smaller dynamic resistance (60 Ω) than that of conventional single-mode VCSEL. These single mode VCSELs also

demonstrate superior high speed performance up to 10 Gb/s.

4-1 Literature survey

The most straightforward technique to obtain single-mode emission is simply reducing the aperture size of oxide-confined VCSEL until higher order modes are no longer supported by the waveguide [6], or prevented from lasing because of high diffraction losses. A single-mode power of 4.8 mW has been demonstrated by using oxide aperture with or less than 3.5 μm diameter [7]. This method suffers from several problems. Firstly, the small current confinement region limits the output power, and increases the differential resistance therefore limits the modulation bandwidth and degrades the high-speed performance. Furthermore, the lifetime of the oxide-confined VCSEL decreases proportionally as the diameter of the oxide aperture declines, even when the device is operated at a reduced current [8]. But the most important drawback lies in the oxide aperture size for single-mode operation is too small to be precisely controlled and reproduced. There are many other approaches developed for high order mode suppression [9]. A single-mode output power of 6.0 mW has been achieved by using proton-implantation with a monolithic coupled resonator VCSEL [10]. Another approach is to use an anti-resonant reflecting optical waveguide VCSEL, which has produced a single-mode output power of 7.1 mW [11]. The other similar approach has also been proposed earlier [12-14]. Other approaches of the fabricating single-mode VCSEL like suppressing the high-order mode in a multimode VCSEL by surface-relief etching [15, 16] can achieve single mode output. But these methods are a little bit complex and seem unsuitable for mass production. By carefully arranging the oxide aperture placement can help to improve single-mode operation [17-19]. Extending the cavity length can improve the single-mode operation ability [20]. E. W. Young et al. proposed hybrid implanted/oxide-confined VCSELs that support single-mode operation,

based on the concept of increasing the optical losses of higher-order modes as described in Section 1-2-3 [21]. However, the threshold current (I_{th}) of this VCSEL is rather high, at about 5.8 mA. This chapter presents our study about a low I_{th}, high-power single-mode VCSEL fabricated using oxygen (O^+) implantation, MOCVD re-growth and selective oxidation. Two types of apertures in this device were designed to reduce the overlap of the higher-order modes with the current-confined profile while at the same time keeping a sufficient fundamental mode/ current-confined overlap [22]. The current flow is confined by an oxygen-implanted aperture with a diameter of 8 μm and the optical mode is confined by an oxide aperture with a diameter of 10 μm. These VCSELs emit a single transverse mode within the full range of the operated current and can operate up 10 Gb/s.

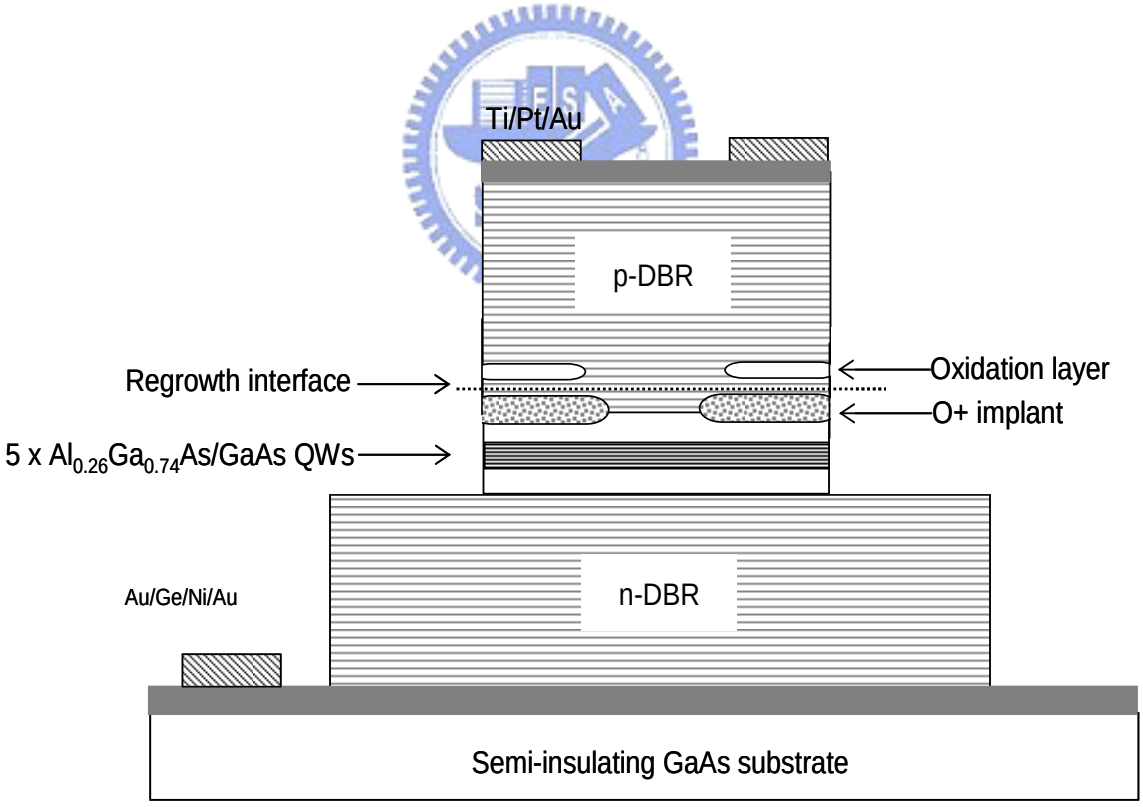

Figure 4-1 Schematic structure of single-mode VCSEL. The O^+-implanted aperture is 8 μm in diameter and the oxidation aperture is 10 μm in diameter.

4-2 Device structure and fabrication

Figure 4-1 schematically depicts cross-sectional O^+-implanted VCSEL structure. The epitaxial structure was grown by metal organic chemical vapor deposition (MOCVD) on a semi-insulated GaAs (100) at 6^o to (111A) substrate. Prior to O^+ implantation, the wafer structure consists of an n^+-GaAs (Si-doped) buffer layer and 39 pairs of *n*-type (Si-doped) $Al_{0.19}Ga_{0.81}As$ /$Al_{0.9}Ga_{0.1}As$ as bottom-distributed Bragg reflectors (DBRs), an $Al_{0.26}Ga_{0.74}As$/GaAs five period quantum-wells (QWs) active region in a one-wavelength cavity for 850-nm emission, and two pairs of p-type (C-doped) $Al_{0.19}Ga_{0.81}As/Al_{0.9}Ga_{0.1}As$ top-DBRs. Then, a 50 Å GaAs cap layer was grown at the null position of the optical field to avoid optical absorption; the GaAs layer was used to prevent oxidation of the surface before re-growth. O^+ was implanted (dosage of 2×10^{14} cm^{-2}) at 120 keV to define a current aperture with a diameter of 8 μm by photolithography, as indicated in Figures 4-2(a). The regrowth of 24 pairs of top-DBRs with a 30 nm $Al_{0.98}Ga_{0.02}As$ oxide layer which located at the third null node position. This position is one pair away from QW region compared to conventional VCSELs to reduce index guiding effect. During the regrowth period, the implanted layer became an effective insulator as current confined aperture because of the activation process. The processing sequence included six photomasks to fabricate oxide-confined polyimide-planarized VCSELs with coplanar wave-guide probe pads. This process was designed to minimize capacitance while keeping reasonably low resistance. Device fabrication began with the formation of cylindrical mesas 20 μm in diameter by etching the surrounding semiconductor to a depth of 5 μm into the bottom n-type mirror using a reactive ion etching (RIE) system as shown in Figure 4-2(b). The gas used in the ion source was Cl_2, and the gas that flowed on the sample was BCl_3. The samples were then selectively oxidized to form circular optical confined apertures with

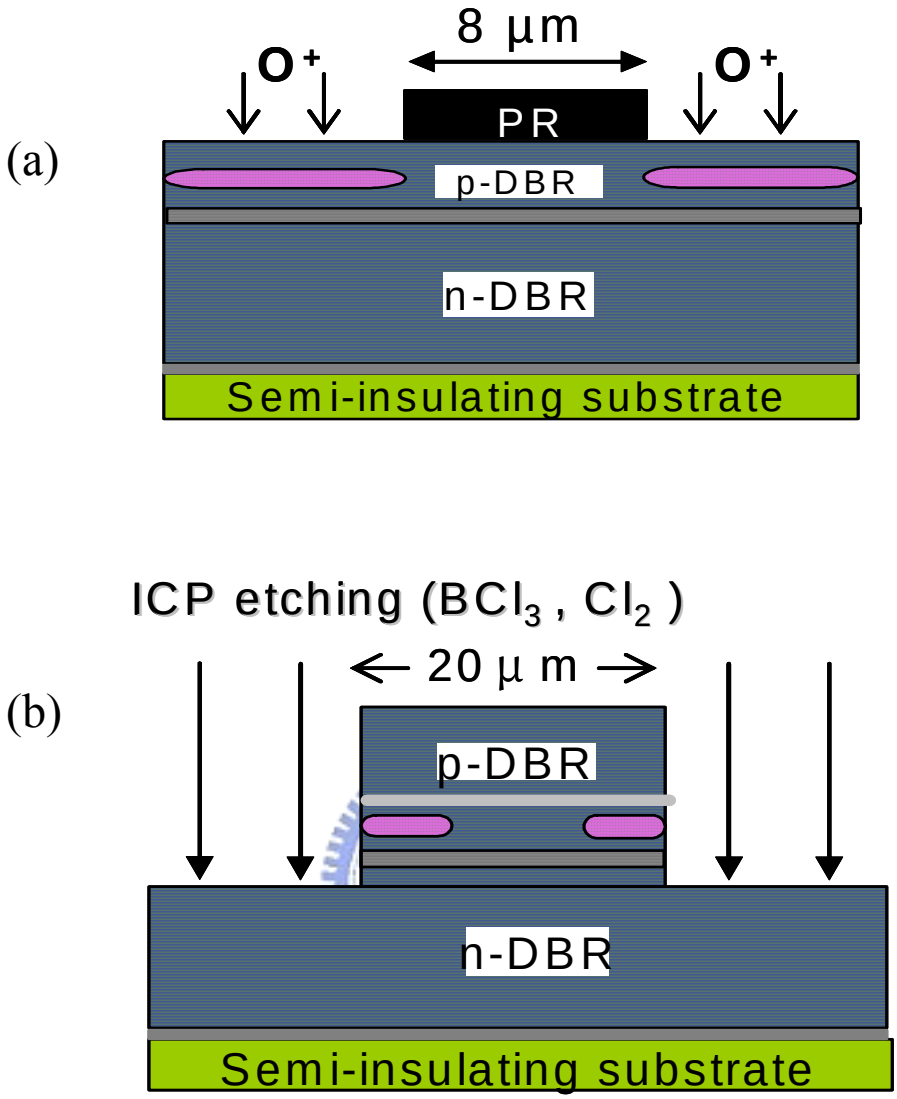

Figure 4-2 Device process flowchart. (a) The O^+-implanted aperture was defined by photolithography with diameter of 8 μm. (b) The surface relief pattern with a diameter of 20 μm was etched by chemically assisted RIE (Reactive Ion Etching).

a diameter of 10 μm. Following Si_3N_4 was deposited for passovation. Ti/Au was evaporated for the *p*-type contact ring, and AuGeNi/Au was evaporated onto the etched *n*–buffer layer etched bottom mirror to form the *p*-type contact which is connected to the semi-insulating substrate. Contacts were alloyed for 30 sec at 420 ^oC using RTA. After contact formation, photosensitive polyimide was spun on the sample for field

insulation and planarization. Ti/Au with thicknesses of 200/3000 Å were deposited for metal interconnects and coplanar waveguide probe-bond pads. Heat treatment after the metal deposition was utilized to improve metal-to-polyimide adhesion strength. For comparison, a conventional VCSEL was also processed with only oxide-confined aperture with a diameter of 8 μm. The same processes as above were performed but without O^+ implantation and regrowth process.

4-3 Results and Discussion

Figure 4-3(a) plots the continuous-wave (CW) power-current-voltage (L-I-V) curves and the spectral characteristics (insertion) of the O^+-implanted VCSELs. The VCSEL emits near 3.8 mW peak power at a 12.3 mA drive current and exhibits a low threshold current of 1.5 mA with a threshold voltage of 1.7 V and slope efficiencies of ~ 0.35 W/A. The insets of Figure 4-3(a) present the emission spectrum and the near-field pattern of the device at 10 mA. The figure reveals that only the fundamental mode is present over the full range of operational current. Over 90% of the series resistances of the VCSELs are 60-65 Ω. This range of resistance is almost the same as that for comparable conventional VCSELs (the L-I-V characteristics are shown in Figure 4-3(b)), but lower than for single-mode VCSELs with a small aperture, which typically have around 250 Ω of series resistance [23]. Additionally, the roll-over current is about 12 mA, which exceeds that of the single-mode VCSEL with a small aperture and so the proposed VCSELs should be more reliable [22]. Figure 4-3(b) plots the L-I-V characteristics of the comparable conventional VCSEL. The threshold current (I_{th}) of the VCSEL is around 1 mA with a threshold voltage of 1.5 V and the slope efficiency of ~ 0.4 W/A. The peak output power is 4.7 mW at a drive current of 12.3 mA. Although the O^+-implanted VCSELs have a lower peak power and a higher I_{th} than comparable conventional VCSELs, perhaps because of the regrowth interface and the losses of

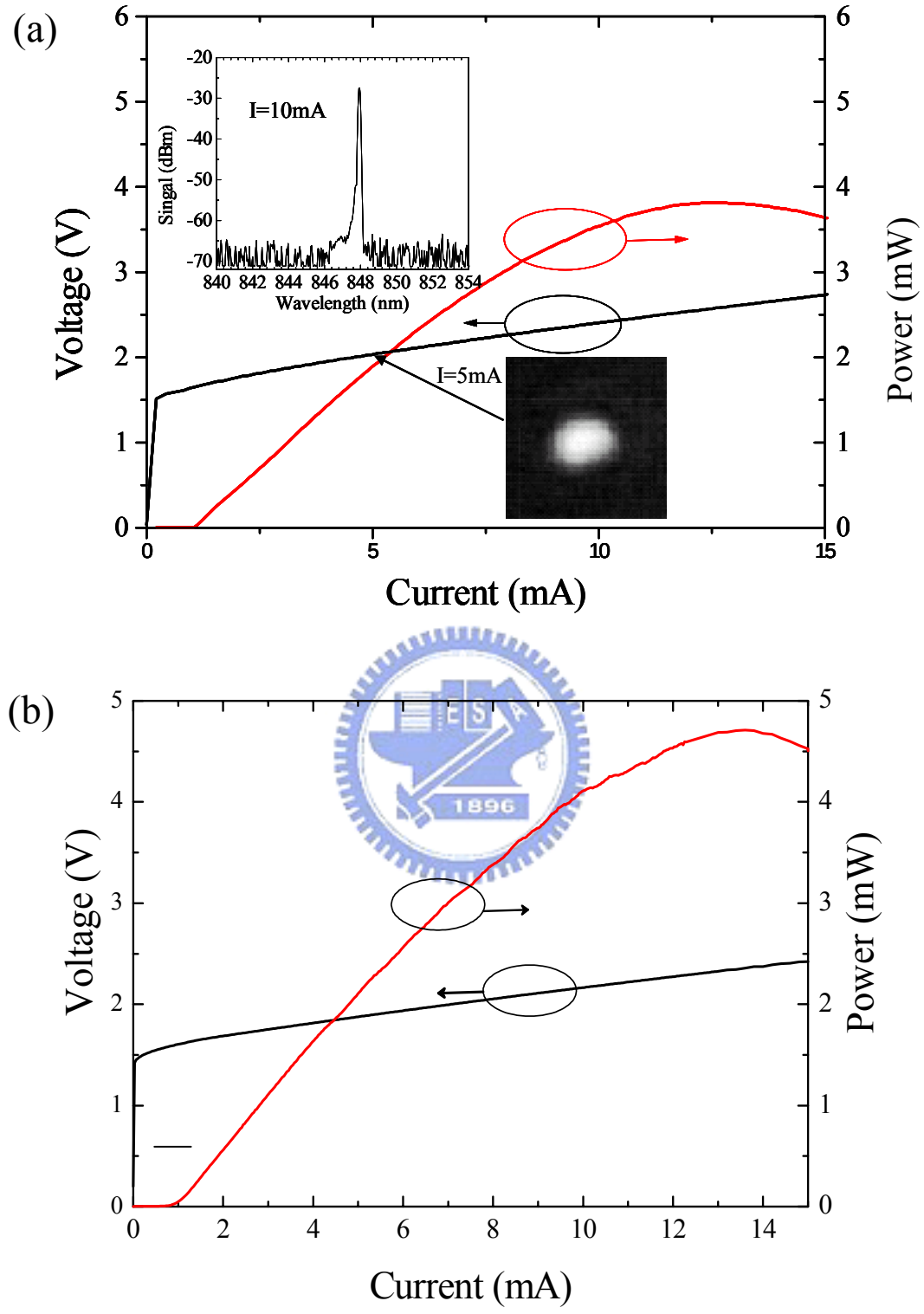

Figure 4-3 (a) L-I-V curves, spectral characteristics and the near-field pattern of the O^+-implanted VCSEL. The emission spectrum is obtained at 10 mA and the near-field pattern is obtained at 5 mA. They demonstrate that the O^+ implanted VCSEL has a fundamental mode only over the full operating range. (b) L-I-V curves of the comparable conventional VCSEL.

higher-order modes, the O^+-implanted VCSELs can operate in the fundamental single ode within the full operating range exhibiting a better high-speed modulation response than conventional VCSELs [24].

To measure the high-speed characteristic of the O^+-implanted and comparable conventional VCSELs under large signal modulation, microwave and light wave probes were used in conjunction with a 10 Gb/s (223-1 long pseudorandom bit sequence generated) by an pattern generator (MP1763 Anritsu). A 12.5 GHz New Focus photoreceiver with an OC-192 low pass Bessel Thompson filter was used for detection. The eye diagrams were obtained for back-to-back (BTB) transmission of VCSELs. Figures 4-4(a) and 4-4(b) demonstrate the eye patterns of O^+-implanted and comparable conventional VCSELs, respectively. Figure 4-4(a) shows the wide-open eye pattern, indicating good performance of the O^+-implanted single-mode VCSEL. The rise time (T_r) and the fall time (T_f) are estimated to be 28 ps and 38 ps, respectively, with jitter (p-p) =14 ps. The comparable conventional oxide-confined multiple-mode VCSEL yields a more noisy eye pattern, with jitter = 17 ps (see Figure 4-4(b)).

4-4 Summary

This study reports a new technique for fabricating a single-mode VCSEL with a large emission aperture with a diameter of 8 μm, using oxygen implantation, MOCVD re-growth and selective oxidation. The single-mode VCSELs have a low I_{th} of about 1.5 mA, a high output power of 3.8 mW. Although this approach involves re-growth, it provides the single transverse mode with large aperture with a low I_{th} and the high output power. These single mode VCSELs also demonstrate superior high speed performance up to 10 Gb/s. The authors believe that the concept can be applied be applicable to fabricate long-wavelength single-mode VCSELs.

(a)

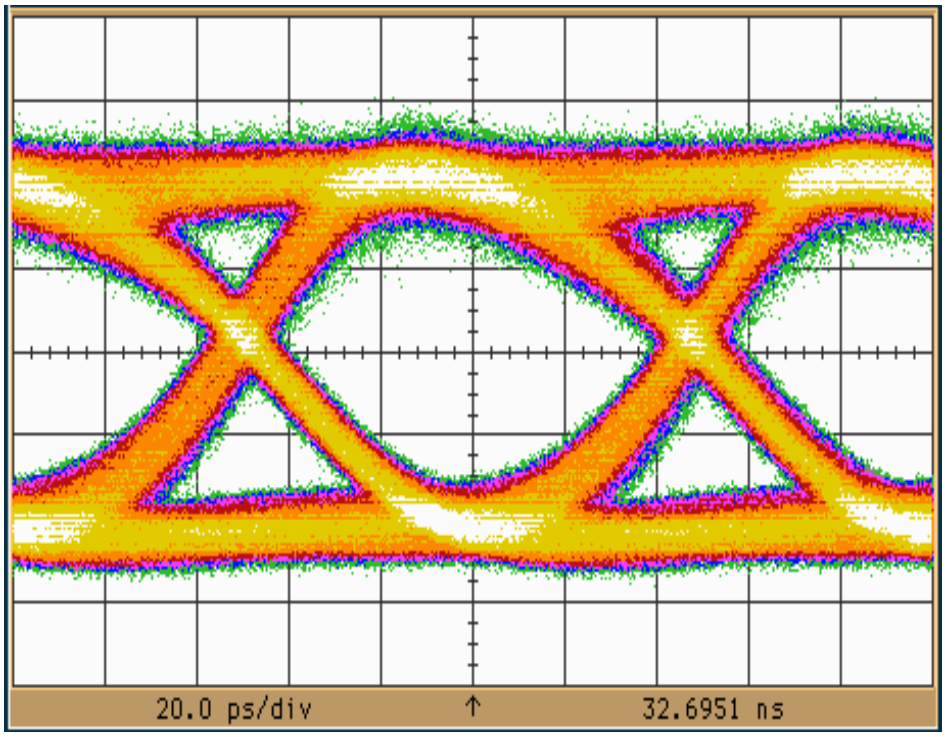

(b)

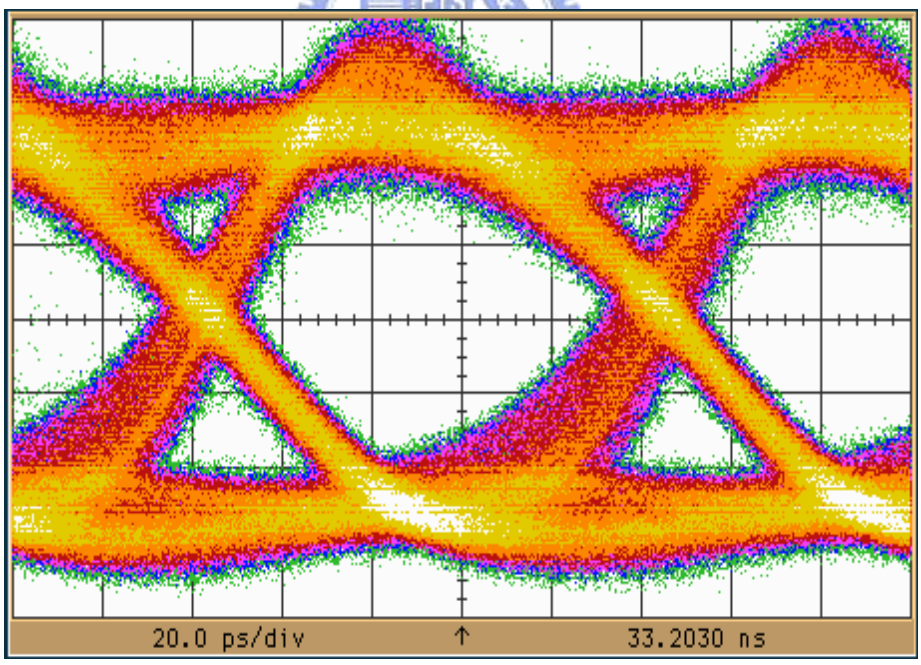

Figure 4-4 Characteristic eye diagram of (a) large-aperture single-mode VCSEL with diameter of 8 μm; (b) conventional multi-mode VCSELs with diameter of 8 μm, transmitted at 10 Gb/s with a bias of 5 mA and an extinct ratio of 6 dB.

References

[1] U. Fiedler, G. Reiner, P. Schnitzer, and K.J. Ebeling, "Top surface-emitting vertical-cavity laser diode for 10 Gbit/s data transmission," *IEEE Photon. Technol. Lett.*, vol. 8, pp. 746-748, June 1996.

[2] D. Wiedenmann, R. King, C. Jung, R. Jäger, R. Michalzik, P. Schnitzer, M. Kicherer, and K. J. Ebeling, "Design and Analysis of Single-Mode Oxidized VCSEL's for High-Speed Optical Interconnects," *IEEE J. Select. Topics Quantum Electron.*, vol. 5, pp. 503-511, 1999.

[3] T. H. Hsueh, H. C. Kuo, F. I. Lai, L. H. Laih, and S. C. Wang, "High-speed characteristics of large-area single-transverse-mode vertical-cavity surface-emitting lasers," *Electron. Lett.*, vol. 39, pp. 1519-1520, 2003.

[4] K. Tai, G. Hasnain, J. D. Wynn, R. J. Fischer, Y. H. Wang, B. Weir, J. Gamelin, and A. Y. Cho, "90% coupling of top surface emitting GaAs/AlGaAs quantum well laser output into 8 μm diameter core silica fiber," *Electron. Lett.*, vol. 26, *no.* 19, pp. 1628-1629, 1990.

[5] K. D. Choquette, "Technology status and opportunities of VCSELs," *Proc. 14th Indium Phosphide and Related Materials Conf.*, 2002, pp.295-297.

[6] B. Weigl, M. Grabherr, R. Michalzik, G. Reiner, and K. J. Ebeling, "High-Power Single-Mode Selectively Oxidized Vertical-Cavity Surface-Emitting Lasers," *IEEE Photon. Technol. Lett.*, vol. 8, pp. 971-973, June 1996.

[7] C. Jung, R. Jager, M. Grabherr, P. Schnitzer, R. Michalzik, B. Weigl, S. Muller, and K. J. Ebeling, "4.8 mW singlemode oxide confined top-surface emitting vertical-cavity laser diodes," *Electron. Lett.*, vol. 33, pp. 1790-1791, 1997.

[8] Bobby M. Hawkins, Robert A. Hawthorne III, James K. Guenter, Jim A. Tatum, and J. R. Biard, presented at ECTC 2002.

[9] H. J. Unold, S. W. Z. Mahmoud, R. Jäger, M. Golling, M. Kicherer, F. Mederer, M. C. Riedl, T. Knödl, M. Miller, R. Michalzik, and K. J. Ebeling, "Single-mode VCSELs," *Proc. SPIE*, vol. 4649, pp. 218-229, 2002.

[10] A. J. Fischer, W. W. Chow, D. K. Serkland, A. A. Allerman, K. M. Geib, and K. D. Choquette, "Multi-section vertical-cavity laser diode for high power single-mode operation," *Proc. Conf. Lasers and Electro-Optics'01*, p. 106, 2001.

[11] D. Zhou and L. J. Mawst, "High-power single-mode antiresonant reflecting optical waveguide-type vertical-cavity surface-emitting lasers," *IEEE J. Quantum Electron.*, vol. 38, pp. 1599-1606, 2002.

[12] Y. A. Wu, C. J. Chang-Hasnain, and R. Nabiev, "Transverse Mode Selection with a Passive Antiguide Region in Vertical Cavity Surface Emitting Lasers," *IEEE Photon. Technol. Lett.*, vol. 6, pp. 924-926, 1994.

[13] Y. A. Wu, G. S. Li, R. F. Nabiev, K. D. Choquette, C. Caneau, and C. J. Chang-Hasnain, "Single mode, passive antiguide vertical cavity surface emitting laser," *IEEE J. Select. Topics Quantum Electron.*, vol. 1, p. 629, June 1995.

[14] Y. A. Wu, G. S. Li, W. Yuen, C. Caneau, and C. J. Chang-Hasnain, "High-Yield Processing and Single-Mode Operation of Passive Antiguide Region Vertical-Cavity Lasers," *IEEE J. Select. Topics Quantum Electron.*, vol. 3, pp. 429-434, 1997.

[15] H. Martinsson, J. A. Vukusic, M. Grabherr, R. Michalzik, R. Jager, K. J. Ebeling, and A. Larsson, *IEEE Photon. Technol. Lett.*, vol. 11, pp. 1536–1538, Dec. 1999.

[16] D. Wiedenmann, R. King, C. Jung, R. Jäger, P. Schnitzer, R. Michalzik, and K. J. Ebeling, *IEEE J. Quantum Electron.*, vol. 5, pp. 503–511, May/June 1999.

[17] M. Grabherr, R. Jäger, R. Michalzik, B. Weigl, G. Reiner, and K. J. Ebeling, "Efficient Single-Mode Oxide-Confined GaAs VCSEL's Emitting in the 850-nm Wavelength Regime," *IEEE Photon. Technol. Lett.*, vol. 9, pp. 1304-1306, 1997.

[18] A. E. Bond, P. D. Dapkus, and J. D. O'Brien, "Design of Low-Loss Single-Mode Vertical-Cavity Surface-Emitting Lasers," *IEEE J. Select. Topics Quantum Electron.*, vol. 5, pp. 574-581, 1999.

[19] H. Deng, J. J. Dudley, S. Lim, C. Lei, "Transverse mode control in large area oxide-confined vertical cavity surface emitting lasers," *Proc. Conf. Lasers and Electro-Optics 99*, p. 486, 1999.

[20] H. J. Unold, S. W. Z. Mahmoud, R. Jager,M. Kicherer,M. C. Riedl, and K. J. Ebeling, “Improving single-mode VCSEL performance by introducing a long monolithic cavity,” *IEEE Photon. Technol. Lett.*, vol. 12, pp. 939-941, 2000.

[21] E. W. Young, K. D. Choquette, S. L. Chuang, K. M. Geib, A. J. Fischer, and A. A. Allerman, “Single-transverse-mode vertical-cavity lasers under continuous and pulsed operation,” *IEEE Photon. Technol. Lett.*, vol.13, pp. 927–929, Sep. 2001.

[22] Jean-Francois P. Seurin, Shun Lien Chuang, Leo M. F. Chirovsky, and Kent D. Choquette, *Laser Focus World*, vol. 38, Issue: 5, May. 2002.

[23] Noriyuki Yokouchi, Norihiro Iwai andAkihiko Kasukawa, presented at Photonic West 2003, vol. 4994, pp. 189-196.

[24] Å. Haglund, J. S. Gustavsson, J. Vukusic, P. Modh, and A. Larsson, “Single fundamental-mode output power exceeding 6 mW from VCSELs with a shallow surface relief,” *IEEE Photon. Technol. Lett.*, vol.16, pp. 368–370, Feb. 2004.

Chapter 5

Proton-implanted VCSELs with photonic crystal

After the first proposal of photonic crystals by John [1] and Yablonovich [2], photonic crystal devices have been intensely investigated in recent years owing to their potential to form dense highly integrated optical circuits. Photonic crystals are artificial dielectric materials which modulate the refractive index on a scale of the wavelength. Similar to the formation of energy bands in the periodic potential of the crystal lattice, optical bands and bandgaps emerge in photonic crystal structure. Light propagation is suppressed in the gaps between the bands. These properties enable the control of light propagation and generation on a very small scale. Furthermore, the similarity of the fundamental equations allows one to transfer a number of concepts from solid state physics, such as defects, doping, bloch states, etc. to optical systems.

Because of the superior index-guiding property, photonic crystals are also worldwide applied on modal control in photo-electronic devices. In this chapter, a photonic crystal on proton-implanted VCSELs for fiber-optic applications is demonstrated in this paper. Ultra-low threshold current about 1.25 mA, single fundamental mode (SMSR > 40 dB) under continuous-wave (CW) output power of over 1 mW, with a pulsed output power of exceeding 2 mW has been achieved in the 850 nm range.

5-1 Literature survey and Background

Recently, a two-dimensional (2-D) photonic crystal structure formed on a VCSEL surface has been investigated as a control method of lateral mode. D. S. Song et al. first applied 2-D photonic crystal on oxide-confined VCSEL, and the schematic

structure was shown in Figure 5-1 [3]. This concept was from the endless single-mode from photonic crystal fibers [4]. By introducing the single defect photonic crystal to the VCSEL, a waveguide is expected to be formed around the central defect region where the effective index is larger than the surrounding region. The effective index model [5, 6] is used in this structure to understand the VCSEL with lateral structural variation. According to the effective index model, in ref. [3], the number of guided mode of an oxide-confined VCSEL is determined by V value, which has the form [6]

$$V^2 \equiv (h_{core}^2 - h_{clad}^2)d^2 \approx \langle \varepsilon \rangle (k_{clad,z}^2 - k_{core,z}^2)d^2 \qquad (5\text{-}1)$$

where $k_{core,z}$, $k_{clad,z}$, are longitudinal resonance wave vectors of core and cladding

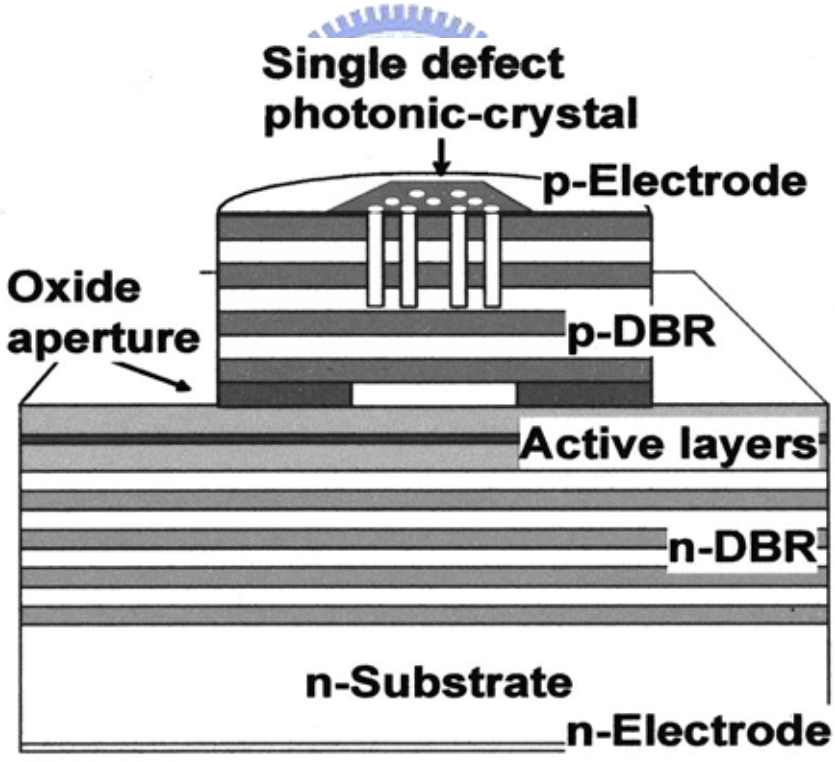

Figure 5-1 Schematic of the 850 nm PC-VCSEL. Note that the first generation PC-VCSEL structure has no oxide current aperture. The oxide aperture is added to the second generation devices for current confinement.

region, respectively, and h_{core} , h_{clad} are transverse wave vector in the medium. d is a diameter of the core. The $\langle \varepsilon \rangle$ represents the dielectric constant weighted by the longitudinal standing wave. For the photonic crystal VCSEL shown in Figure 5-1, the resonance wavelengths would be different for the central core region and the surrounding region. This situation is approximated as a simple step-index waveguide as shown in Figure 5-2. With the aid of this model, the difference of effective indices in the two regions can be estimated by measuring the resonant wavelengths in the core and surrounding regions. The overall effects of the etch diameter, and pitch of the holes show up experimentally as the shift of the resonant wavelength. This may be written compactly as

$$\Delta n_{eff,core-clad} / n_{eff,core} \approx \Delta\lambda_{core-clad} / \lambda_{core} \qquad (5\text{-}2)$$

Fabricating photonic crystals on selective oxide VCSEL, single-mode output with higher output power were realized from larger aperture [3, 7-8]. However,

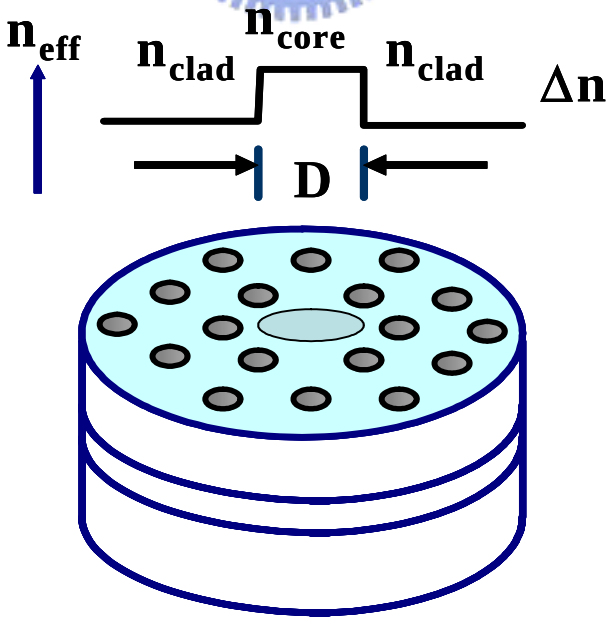

Figure 5-2 The Schematic of lateral effective index variation provided by the photonic crystal.

those photonic crystal PC-VCSELs exhibit relatively high threshold current (I_{th}) due to large oxide confined apertures. In this chapter, we focus study on mode controlling characteristics of photonic crystal and design a low I_{th}, high-power, single-lateral-mode operation VCSEL by employing proton implantation and photonic crystal index-guiding mechanism.

5-2 Experiment

The epitaxial layers of the PC-VCSELs wafer structure were grown on the n^+-GaAs substrate by a metal organic chemical vapor deposition (MOCVD) system. The bottom distributed Bragg reflector (DBR) consists of a 30.5-pair *n*-type (Si-doped) quarter-wave stack of $Al_{0.12}Ga_{0.88}As$/AlAs. The top DBR consists of 22-period p-doped (carbon-doped) $Al_{0.12}Ga_{0.88}As$/AlA quarter-wave stack. Above that, a heavily-doped p-type GaAs contact layer. The graded-index separate-confinement heterostructure (GRINSCH) GaAs/AlGaAs active region has an undoped three-quantum-well (3 QWs) GaAs/$Al_{0.3}Ga_{0.7}As$, a lower linearly-graded undoped $Al_xGa_{1-x}As$ ($x = 0.6 \rightarrow 0.3$) waveguide layer and an upper linearly-graded undoped-$Al_xGa_{1-x}As$ ($x=0.3 \rightarrow 0.6$) waveguide layer. The proton (H^+)-implanted VCSEL was fabricated before combination with photonic crystal holes. was then Firstly, the *p*-contact ring with an inner diameter of 24 to 46 μm was deposited on the top of *p*-contact layer and n-contact was deposited on the bottom of n^+-GaAs substrate. The device was annealed in thermal annealing system at 430 ℃ under N_2 ambient for 30 sec. The current confinement of the device, with a diameter of 10 μm, was then defined by proton implantation. The implantation energy was 270 KeV, with a dosage of 6×10^{14} cm^{-2}. After that, hexagonal lattice patterns of photonic crystal with a single- or seven-point defect were defined within

the p-contact ring using photo-lithography and etched through the *p*-type DBR by using reactive ion etch (RIE). The lateral index around a single defect can be controlled by the hole diameter (α) -to-lattice constant (Λ) ratio and etching depth [8]. The ratios for fabricating are referred to ref. [3] and [8].

The relation of the normalize lattice constant and V_{eff} were calculated by software of Rsoft-BandSOLVE and shown in Figure 5-3. The ratios (α/Λ) are changed from 0.2 to 0.7 and the defects are 1 and 7 point defects. γ is an etching depth dependence factor. By using the γ-factor, the effective index ($n_{eff,clad}$) of the VCSEL structure can be written as $n_{eff,clad} = n_{eff,core} - \gamma \Delta n_{eff,core}$. γ varies from 0 to 1 depending on the etching depth and structure. In our structure, the etching depth of the holes is about 17 pairs and the γ is 0.06. As shown in Figure 5-3, when the ratios (α/Λ) change from 0.2 to 0.7 with one point defect, the V_{eff} parameter all

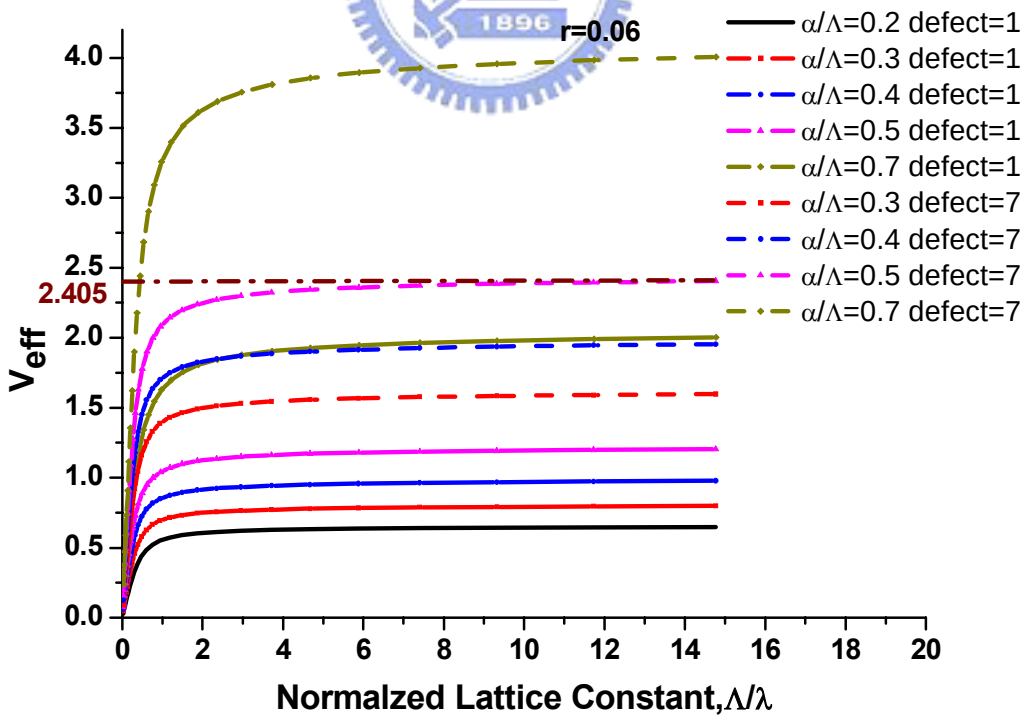

Figure 5-3 V_{eff} parameters for γ=0.06, which correspond to etching depths of 17 pairs, are calculated.

under single-mode guiding condition of 2.405. For 7 point defects, the ratios (α/Λ) below 0.5 are all suitable single-mode guiding condition, but when the ratio (α/Λ) is larger than 0.5, the guiding condition is multi-mode. Therefore, we designed the lattice constant Λ is 5 μm in the PC-VCSEL and the etching depth of the holes is about 17 pairs of the top DBR. The device structure is shown in Figure 5-4. By using two types of apertures in this device, we decouple the effects of the current confinement from the optical confinement. The H^+ implant aperture of 10 μm is used to confine the current flow, while the single- or seven-point defect (≥ 10 μm in diameter) photonic crystal is used to confine the optical mode. The mechanism of In order to clarify the effect of photonic crystal index-guiding layer, a VCSEL with H^+ implant aperture (10 μm in diameter without photonic crystal) was also fabricated for comparison.

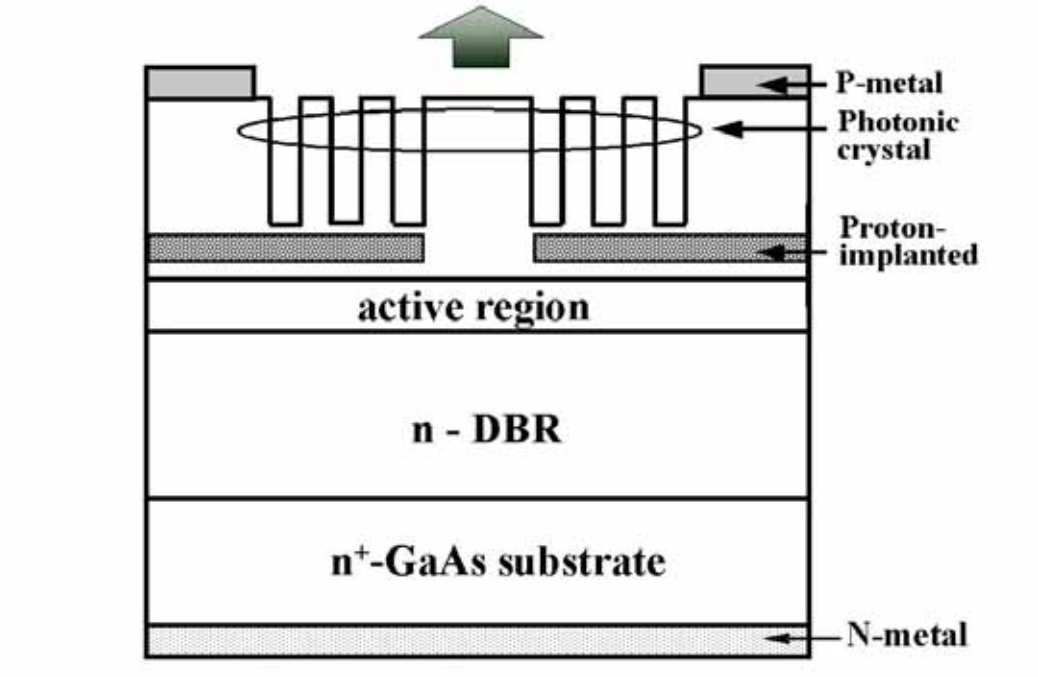

Figure 5-4 Schematic of PC-VCSEL. The hole depth of PC is 17 pairs out of 22 pairs of top DBR been etched off. The proton implantation position is 3 pairs of DBR layers above active region

5-3 Results and Discussions

Figure 5-5 shows CW light-current-voltage (L-I-V) output and near-field image operated at 0.1 mA (inset) of the PC-VCSEL. The VCSEL emits over 1 mW peak power and exhibits single modes throughout the current range of operation. The threshold current (I_{th}) of the PC-VCSEL is 1.25 mA and the slop efficiency is approximately 0.18 W/A. The I-V characteristic exhibits higher series resistance of the PC-VCSEL which should be mainly due to proton implantation through the p-ohmic contact of the device and the region of current flow was damaged by photonic crystal holes. The output power could be improved by reducing the series resistance of the PC-VCSEL.

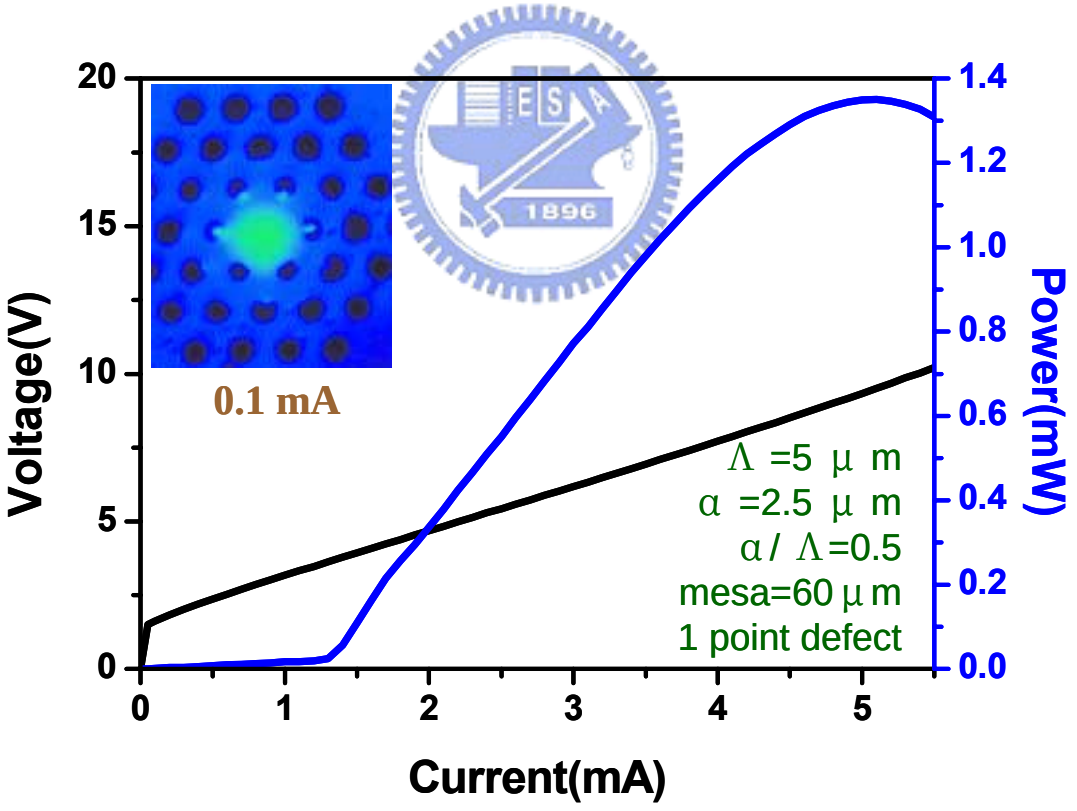

Figure 5-5 CW L-I-V characteristics and near-field image (inset) of a PC-VCSEL. The ratio (α/Λ) is 0.5 and the lattice constant Λ is 5 μm.

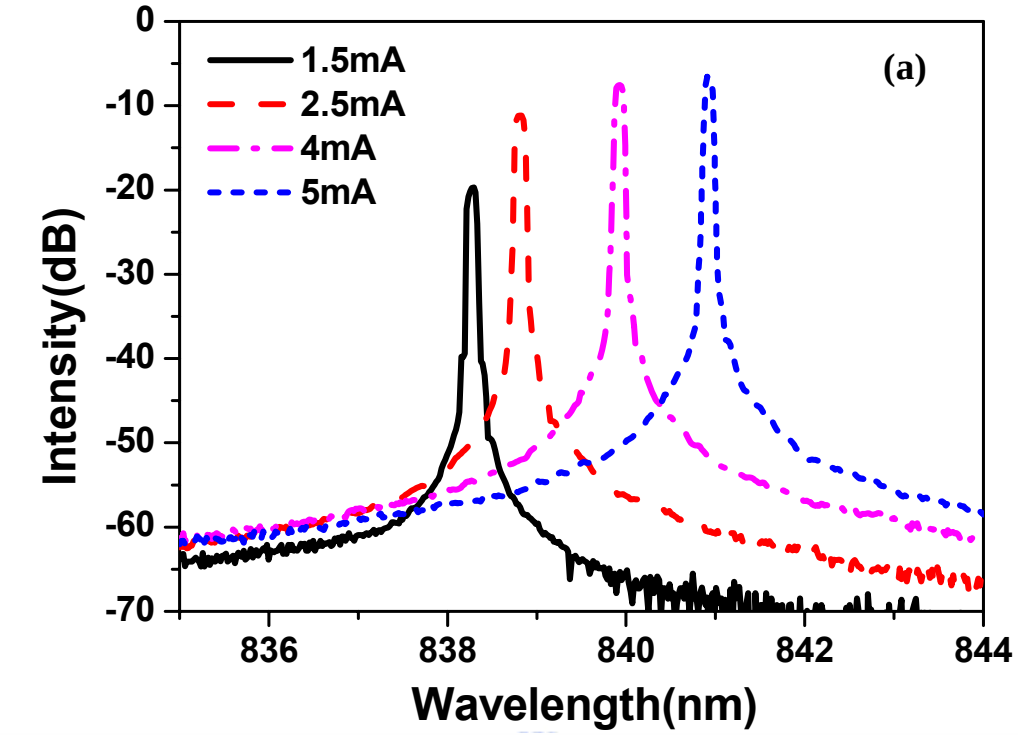

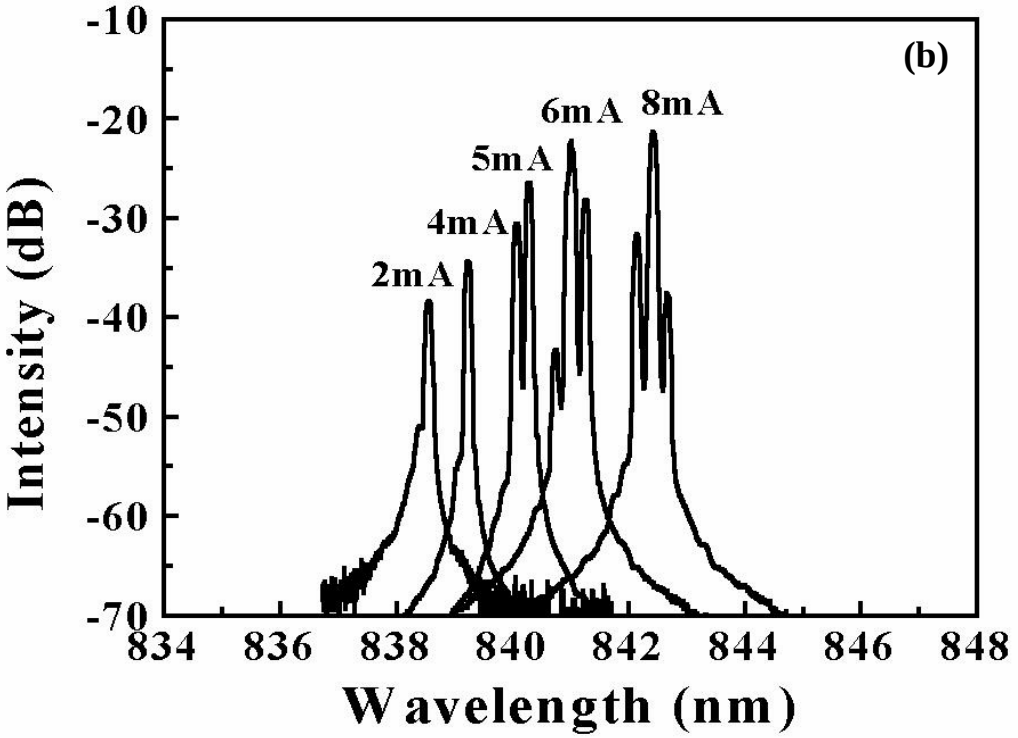

Figure 5-6 Spectra of the proton-implanted (a) photonic crystal VCSEL with ratio (α/Λ) is 0.5 and the lattice constant Λ is 5 μm and (b) VCSEL without photonic crystal holes.

Lasing spectra of the PC-VCSEL is shown in Figure 5-6 (a), confirming single-mode operation within overall operation current. The PC-VCSEL reveals side mode suppression ratio (SMSR) > 40dB throughout the current range. For comparison, a lasing spectra of proton implanted VCSEL without photonic crystal holes shows multiple mode operation as the driving current increased above 4.25 mA (Figure 5-6 (b)). As the driving current increases, even higher order transverse mode emerges. The pulsed L-I characteristics of the PC-VCSEL is also measured and the maximum output power is exceeding 2 mW (not shown here). Temperature-dependent measurements are underway to verify the non-linearity characteristics. Figure 5-7 shows the lasing spectrum of seven-point defects condition and exhibits the single-mode output.

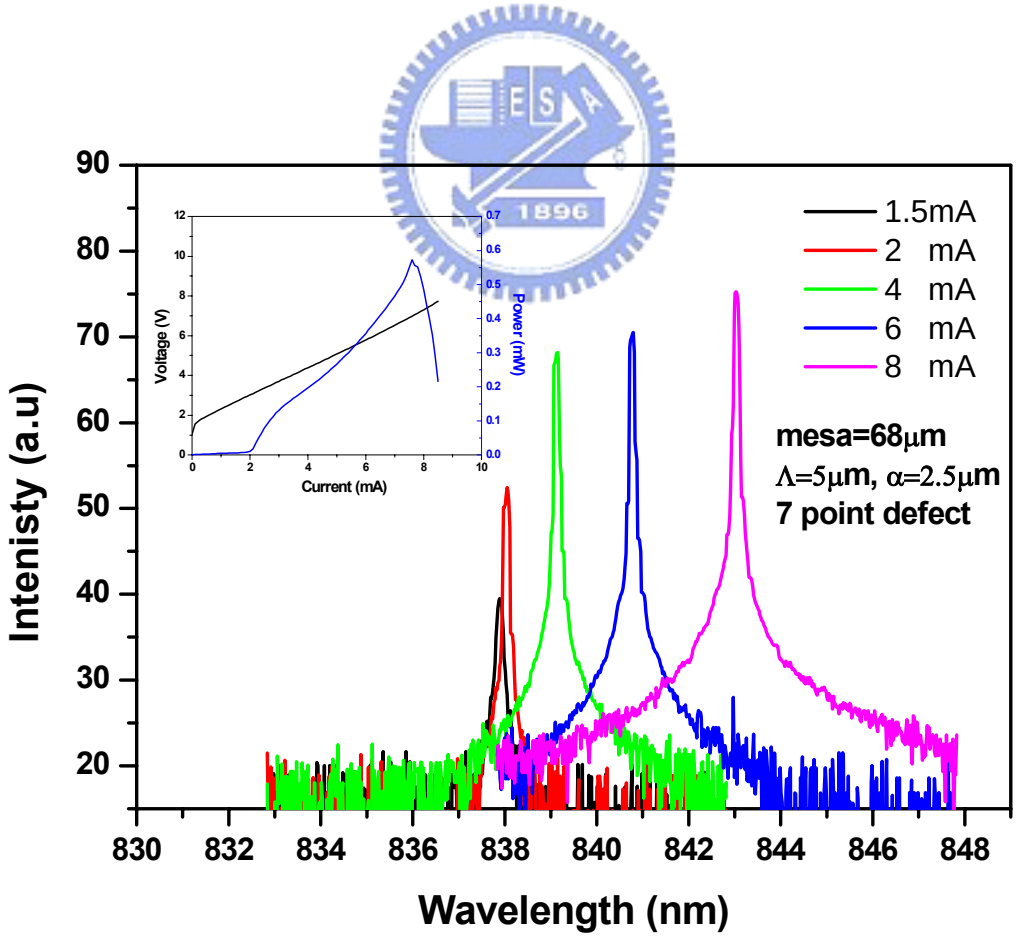

Figure 5-7 Spectra of the proton-implanted VCSEL with photonic crystal of seven-point defects. The ratio (α/Λ) is 0.5, and the lattice constant Λ is 5 μm. The mesa of this device is 68 μm.

The divergent angles of far-field pattern of proton-implanted VCSEL with and without photonic crystal on it are measured for comparison and shown in Figure 5-8. As shown in Figure 5-8 (a), the divergent angles of the proton-implanted multi-mode VCSEL were increase with the increasing operation current and the divergent angles are over 29°. But for proton-implanted VCSEL with photonic crystal as shown in Figure 5-8 (b), the divergent angles are around 7.7°, and are persistent even when the applied current is increased. The divergent angle is smaller than the conventional oxide-confined single-mode VCSEL and exhibit superior guiding effect of photonic crystal.

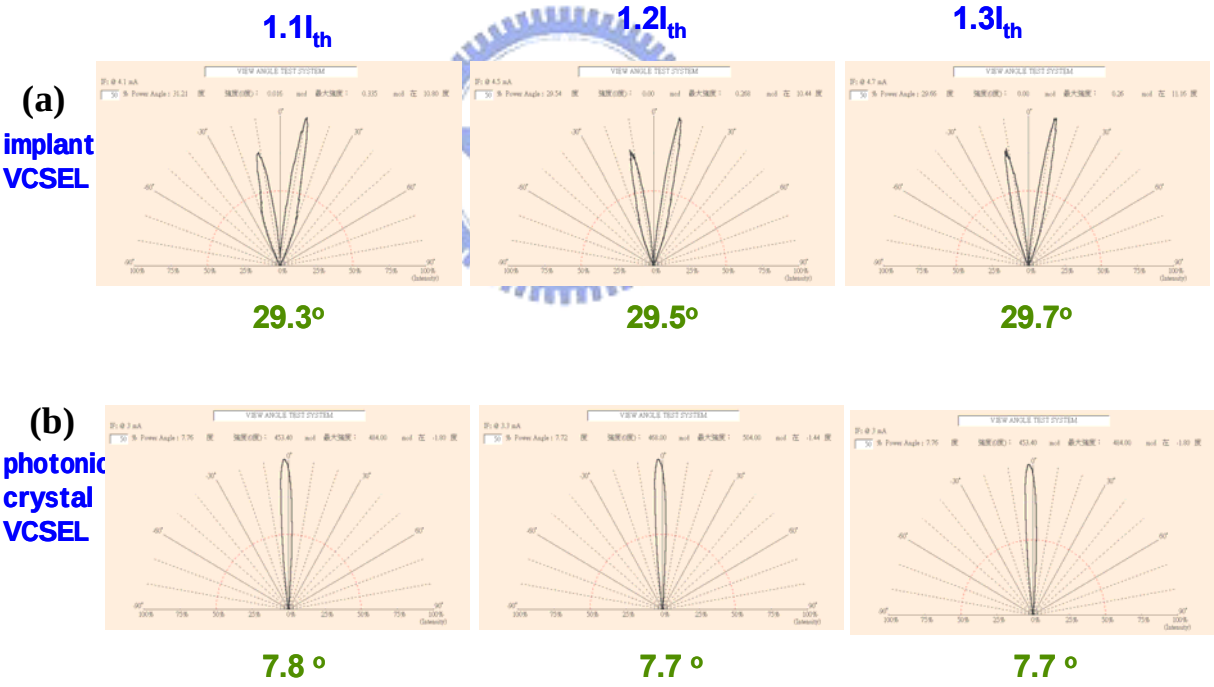

Figure 5-8 Divergent angles of the proton-implanted VCSEL (a) without and (b) with photonic crystal.

5-4 Summary

We report a high power (> 1 mW) single mode PC-VCSEL with SMSR > 40 dB throughout the operation current range. This PC-VCSEL with aperture about 10 μm poses ultra-low threshold current about 1.25mA. The present results indicate that a VCSEL using proton implantation for current confinement and photonic crystal for optical confinement is a reliable approach to achieve high power single-mode operation of VCSEL. The superior guiding effect of photonic crystal results in the small divergent angle of the VCSEL devices, and make the devices could easy to couple to single-mode fiber or could increase the density of storage. This concept was also first successfully applied on the 1.3 μm InAs quantum-dots VCSEL and obtained the single-transverse-mode output with SMSR over 40dB [9], which shown the reliable applied on the long-wavelength structure or other commercial applications in the future.

Reference

[1] S. John, "Strong localization of photons in certain disordered dielectric superlattices," *Phys. Rev. Lett*., vol. 58, pp. 2486-2489, 1987.

[2] E. Yablonovitch, "Inhibited spontaneous emission in solid-state physics and elelctronics," *Phys. Rev. Lett.* vol. 58, pp. 2059-2062, 1987.

[3] Dae-Sung Song, Se-Heon Kim, Hong-Gyu Park, Chang-Kyu Kim and Yong-Hee Lee, "Single-fundamental-mode photonic-crystal vertical-cavity surface-emitting lasers" *Appl. Phys. Lett.*, vol. 80, No.21, pp. 3901, 2002.

[4] J. C. Knight, T. A. Birks, P. St.J. Russell, D. M. Atkin, "All-silica single-mode optical fiber with photonic crystal cladding:errata," *Opt. Lett.* vol. 22, pp. 484-485, 1997.

[5] G. Ronald Hadley, "Effective index model for vertical-cavity surface-emitting lasers," *Opt. Lett*. vol. 20, pp.1483-1485, 1995.

[6] D. K. Serkland, G. R. Hadley, K. D. Choquette, K. M. Geib, and A. A. Allerman, "Modal frequencies of vertical-cavity lasers determined by an effective-index model" *Appl. Phys. Lett.*, vol. 77, pp. 22-24, 2000.

[7] D. Berkedal, N. Gregersen, S. Bischoff, M. Madsen, F. Romsted, J. Oestergarrd, "Large-area single-mode photonic bandgap VCSELs," *Proc. Optical Fiber Communications Conf.*, Atlanta, GA, USA, 2003, pp. 83–85, 2003.

[8] N. Yokouchi, , A. J. Danner and K. D. Choquette, "Etching depth dependence of the effective refractive index in two-dimensional photonic-crystal-patterned vertical-cavity surface-emitting laser structures," *Appl. Phys. Lett.*, vol. 82, pp. 1344-1346, 2003

[9] H. P. Yang, et al., "Single mode InAs quantum-dot photonic-crystal VCSELs," acctepted to be published in Elect. Lett., 2005. (paper ELL-2005-2518)

Chapter 6

Conclusions and Future Works

6-1 Conclusions

In this dissertation, we have studied the processing technology and characteristics improvement of vertical-cavity surface-emitting lasers (VCSELs). We have proposed several various transverse guiding mechanisms and improved the performances of traditional gain-guided VCSELs, achieved single-transverse output mode and the devices can be operated up to 10 Gb/s.

In Chapter 2, we studied the characteristics of the proton-implanted 850 nm GaAs VCSEL, the simplest fabricating technique of fabricating VCSEL devices and we proposed a new p-contact scheme incorporation of a Ti and ITO transparent overcoating on the regular p-contact to improve the performances of the proton-implanted VCSEL. The VCSEL with Ti/ITO transparent overcoating showed better performances than VCSEL without overcoating. The kink characteristics in L-I curve of the VCSEL with the Ti/ITO overcoating were improved with a reduction in the derivative kink factor of as large as 70% and the high-speed response of the overcoated device also shows a more open clear eye and lower jitter of 35 ps operating at 2.125 Gb/s under 10 mA bias and 9 dB extinction ratio compared to the no overcoated device.

In Chapter 3, we tried to find a new VCSEL structure with virtue of gain-guiding, simple planer process, and possessing index-guide. We utilize silicon implantation to replace proton implantation. The VCSELs with aperture of 13×13 μm^2 exhibit kink-free current-light output performance with threshold currents about 2.2 mA, and the slope efficiencies are about 0.45 W/A. The wide open 2.125 Gb/s eye pattern of the silicon-implanted VCSEL indicates good performance of these VCSELs. The mode

patterns of silicon-implanted VCSEL showed similar stable transverse mode patterns of oxide-confine one, which might result from the silicon-implantation induce disordering of the implanted regions, so that difference of refractive index existence between the implanted regions with original regions.

In Chapter 4, we focused the study on single transverse mode with high output-power and high modulation speed VCSEL. We propose another hybrid-guided structure by using oxygen implantation and selective oxide-confined for gain-guide and index-guide, respectively on fabricating 850 nm GaAs VCSELs. The VCSELs with large emission aperture of 8 μm exhibit good performance with threshold currents of 1.5 mA, a single transverse mode emission within the full operational range and a maximum output power of 3.8 mW. Moreover, the single mode VCSELs demonstrate superior high speed performance up to 10 Gb/s.

By cooperating photonic crystal on gain-guided proton-implanted VCSELs, we achieved high side mode suppression ratio (SMSR) single-mode VCSELs in Chapter 5. In this hybrid-guided VCSEL, the 2-D photonic crystal and proton-implanted structures are for gain-guide and index-guide, respectively. The superior optical field confinement of photonic crystal resulted in single-output transverse mode output of the VCSELs with high side-mode suppression ratio (SMSR) over 40 dB. The output aperture of 10 μm defined by proton-implantation is larger than traditional oxide-confined VCSELs, so the photonic-crystal VCSELs possess potential for higher output power than traditional VCSELs. These devices also exhibited ultra-low divergent angle about 7^{o}. We also apply this technique on the long-wavelength 1.3 μm InAs quantum-dots VCSELs and the VCSELs also show the single-output transverse mode in whole operation range.

6-2 Future work

All of the developed techniques studied in this dissertation were performed on GaAs-based material. Therefore, the process techniques should be suitable to apply on the long-wavelength GaAs-based VCSELs for the optical communication. But in short-wavelength range, it is hard to nature growth oxide by wet thermal oxidation methods. Recently, many researchers make efforts in developing the oxidation of GaN-based material, and reported a usable technique utilizing Photoelectrochemical (PEC) reaction to produce nature growing oxide in GaN-based material [1-5]. But its property and stability are steel under investigating. In order to develop the process of GaN-based VCSEL, we also develop PEC oxidation system, and there is still much room need to be effort and for improvement. Consequently, we will discuss the future work in two parts, Long-wavelength VCSEL, and GaN-based material.

6-2-1 Long-wavelength VCSEL

It is known that intrinsic material absorption for silica fiber is smallest in 1.3 to 1.6 μm wavelength window. Hence to develop long-wavelength VCSEL for low loss, and high speed data communication attracts worldwide interesting. There are two types of materials are often used, one is InP-based material and another is GaAs-based materials including InGaAsN, InAs quantum-dats, InGaAs, and InGaAsN:Sb etc. for gain media. In the VCSEL process techniques what we studied in this dissertation could all suitable for fabricating high-speed long-wavelength VCSELs. Gain-guided mechanism is independent of material so it could perform on these two kinds of long-wavelength VCSELs and the transparent overcoating could improve the performance of these devices as we discuss in chapter 2. The Si^{+}-implantation index-guiding mechanism could also be performed on both two

types of long-wavelength VCSELs cause the independent with materials. We also performed the photonic crystal on the proton-implanted 1.3 μm InAs quantum-dots VCSELs, so the photonic crystal technology has already been proven that this technique can be applied to the long-wavelength VCSEL and improve the single-mode operation ability significantly. But the resistance of the photonic crystal VCSEL is higher than the normal commercial VCSELs. Utilizing transparent overcoating might decrease the resistance and would improve the high-speed performance. Other process technique as oxygen-implantation cooperating with selective oxidation might just suitable in growing high Al content layer in the epi-wafer, but it no doubt could be applied on GaAs-based long-wavelength VCSELs. In the recent years, the growth techniques of long-wavelength materials and structure were dramatically improved. We believe all the techniques studied in this dissertation could be applied on the long-wavelength VCSELs and expand the capability of fiber-optics communication in the near future.

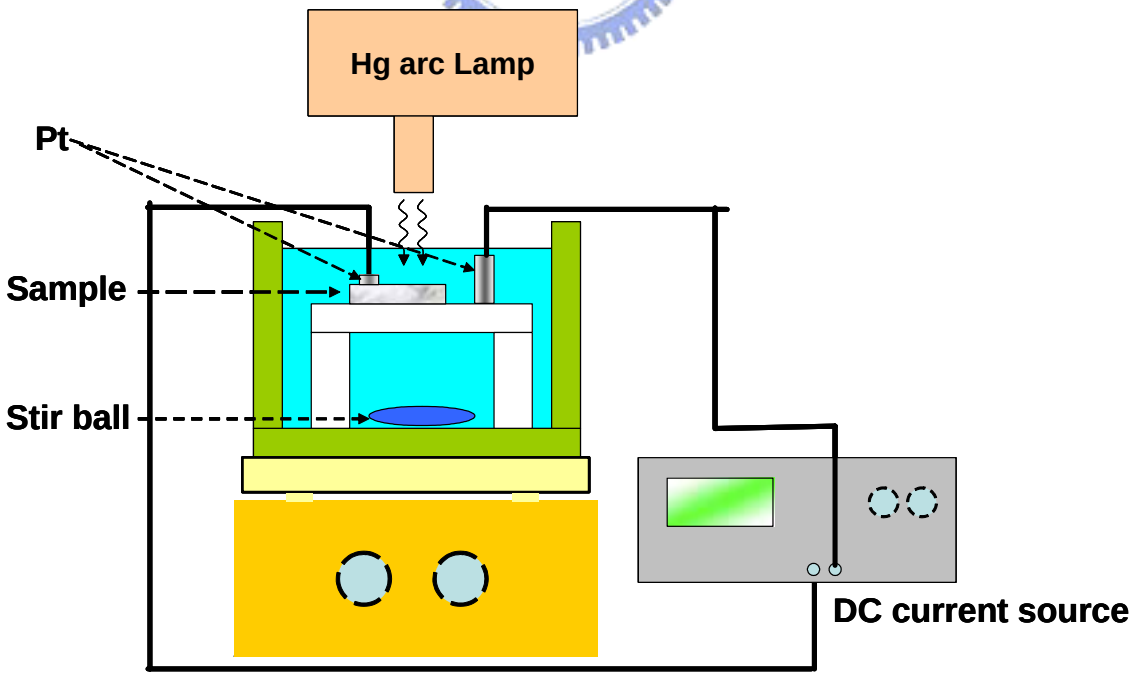

Figure 6-1 Schematic of photoelectrochemical oxidation setup.

6-2-2 Oxidation developed in GaN-based material

In short-wavelength of blue and UV range using GaN-based material system, we develop PEC oxidation via H_2O for stable growing oxide film. The setup of PEC is shown in Figure 6-1. The UV light source is Hg and applied energy for electro-hole pair generating. In our PEC setup, the solution we used to transfer GaN into Ga_2O_3 is water to avoid the etching agent [5]. The detail conditions of PEC oxidation were not shown in here [6]. We tried to apply the PEC oxidation on the *p*-GaN surface to improve light output of GaN-based LEDs [7]. The comparison of L-I characteristic of conventional LED and PEC-oxide LED are shown in Figure 6-2, and exhibits that the light output of the PEC-oxide LED was much higher than the conventional LED (about 2.5 mW) under 20 mA current injection. The light output of the oxided LEDs during 30 min. and 45 min. PEC process were increased about 16% and 37% respectively compared with the conventional LED drived at 20 mA. This enhancement might result from the roughness of interface between oxide and surface of *p*-GaN. Moreover, the oxide film on the top surface of the LED would also provide an efficient surface passivation effect for the devices [1]. In conclusion, PEC oxidation applied on the GaN-based materials was established, and we believe that the PEC oxidation could apply on fabricating GaN-based VCSEL. Although several kinds of transverse confinement mechanisms are studied in GaAs-based materials, the basic concepts of confining mechanism and experiment would turn into useful information in fabricating LW-VCSELs and blue/UV VCSELs in the future.

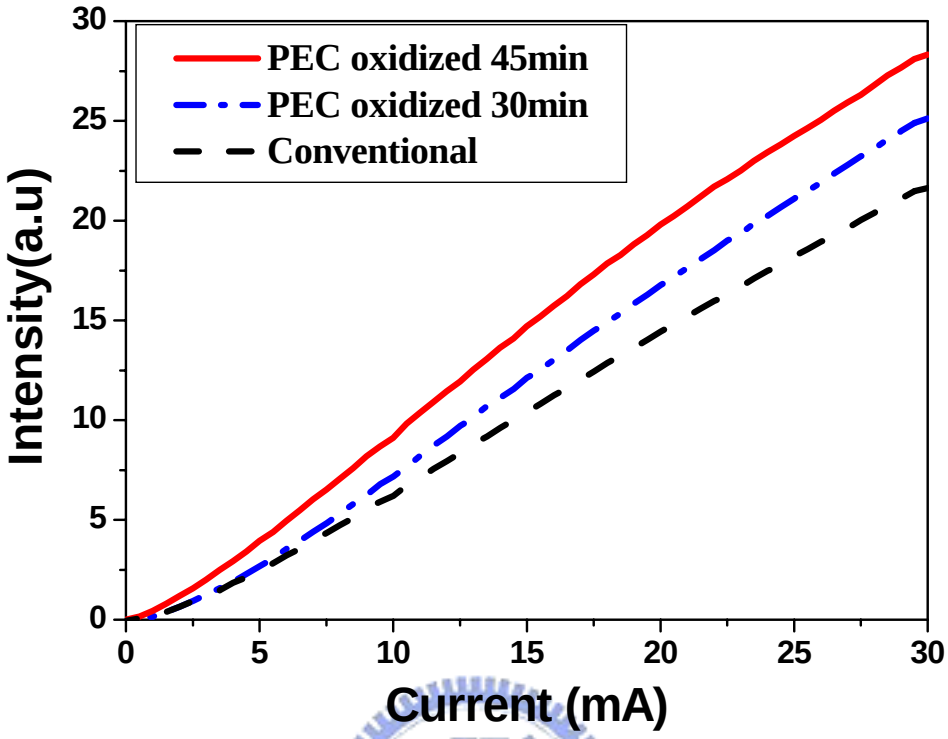

Figure 6-2 L-I characteristics of conventional and PEC oxided GaN-based LEDs.

Reference

[1] L.-H. Peng, C.-H. Liao, and Y.-C. Hsu, C.-S. Jong, C.-N. Huang, J.-K. Ho, C.-C. Chiu, and C.-Y. Chen, "Photoenhanced wet oxidation of gallium nitride," *Appl. Phys. Lett.*, vol. 76, No. 4, pp.511-513, 2000.

[2] T. Rotter, D. Mistele, J. Stemmer, F. Fedler, J. Aderhold, and J. Graul, V. Schwegler, C. Kirchner, and M. Kamp and M. Heuken, " Photoinduced oxide film formation on n-type GaN surfaces using alkaline solutions," *Appl. Phys. Lett.*, vol. 76, No. 26, pp.3923-3925, 2000.

[3] D. J. Fu, T. W. Kang, Sh. U. Yuldashev, N. H. Kim, S. H. Park, J. S. Yun and K. S. Chung, "Effect of photoelectrochemical oxidation on properties of GaN epilayersgrown by molecular beam epitaxy," *Appl. Phys. Lett.*, vol. 78, No. 9, pp.1309-1311, 2001.

[4] Dejun Fu, Shavakat U. Yuldashev, Nam Hwa Kim, Young Sun Ryu, Jae Sung Yun, Seung Ho Park, Tae Won Kang and Kwan Soo Chung, "A study of photoelectrochemical Oxidation of GaN Epilayers by Extrinsic Photoconductivity," *Jpn. J. Appl. Phys.*, vol. 40, pp. L10-L12, 2001.

[5] J. W. Seo, C. S. Oh, H. S. Jeong, J. W. Yang, K. Y. Lim, C. J. Yoon, and H. J. Lee, "Bias-assisted photoelectrochemical oxidation of n-GaN in H_2O," *Appl. Phys. Lett.*, vol. 81, No. 6, pp.1029-1031, 2002.

[6] W. Y. Chen, "Study of Oxidation Process of GaN Light Emitting Diode," Master thesis, June, 2004.

[7] Fang-I Lai, W. Y. Chen, C. C. Kao, C. F. Lin, H. C. Kuo, and S. C. Wang, "Enhancement of Light-output of GaN-based Light-emitting Diodes by Bias-assisted Photoelectrochemical oxidation of *p*-GaN in H_2O," *IQECand CLEO-PR* 2005.

Vita

PERSONAL DATA			
Name	Fang-I Lai	**Sex**	Female
Date of birthday	October 4, 1975		
Phone	+886-3-5712121ext. 52962		
Institution	Department of Photonics and Institute of Electro-Optical Engineering, National Chiao-Tung University		
Address	1001 Ta Hsueh Road, Hsinchu, Taiwan, 30050, ROC		
E-mail address	fangi.eo88g@nctu.edu.tw		

EDUCATION		
2001.9- Now	Ph. D.	Dep. of Photonics and Institute of Electro-Optical Eng., National Chiao-Tung Univ., Taiwan
1999.9-2001.6	M. S.	Dep. of Photonics and Institute of Electro-Optical Eng., National Chiao-Tung Univ., Taiwan
	Thesis:	*Study of P-type Ohmic Contact and Laser Lift-off Technique for GaN*
1994.9-1998.6	B. S.	Department of Physics, Thughai Univ., Taiwan

WORK EXPERIENCE

1. 1998.7-1999.6 Intern (practice teacher).
2. 2005.5-2005.8 Visiting researcher of Tokyo Institute of Technology

FIELDS OF SPECIALTY:

1. Process of VCSEL
2. Optical and electrical characterization of VCSEL
3. Optical Characterization of Ⅲ-Ⅴ Nitride materials

Title of Ph.D. dissertation:

Study of Process Techniques of Vertical Cavity Surface Emitting Lasers

Publication list

Journal paper:

1. **Fang-I Lai**, Hao-Chung Kuo, Ya-Hsien Chang, Min-Ying Tsai, Chia-Pu Chu, Shou-Yi Kuo, Shing-Chung Wang, N. Tansu, Jeng-Ya Yeh and Luke J. Mawst, "Temperature-Dependent Photoluminescence of Highly Strained InGaAsN/GaAs Quantum Wells (λ=1.28-1.45μm) with GaAsP Strain-Compensated Layers" *Japanese Journal of Applied Physics*, Vol. 44, No. 8, pp. (2005)

2. Y. H. Chang, H. C. Kuo, **Fang-I Lai**, K. F. Tzeng, H. C. Yu, C. P. Sung, H. P. Yang and S. C. Wang, "High Speed (>13GHz) Modulation of 850nm Vertical Cavity Surface Emitting Lasers (VCSELs) with Tapered Oxide Confined Layer", accepted at IEE Optoelectronics.

3. Yi-An Chang, **Fang-I Lai**, Hsin-Chieh Yu, Hao-Chung Kuo, Li-Wen Laih, Chun-Lung Yu, and Shing-Chung Wang," High temperature stability 850-nm $In_{0.15}Al_{0.08}Ga_{0.77}As/Al_{0.3}Ga_{0.7}As$ VCSEL with single $Al_{0.75}Ga_{0.25}As$ current blocking layer", *Japanese Journal of Applied Physics Part II*, Vol. 44, No. 28, 2005, pp.L901-L902.

4. Ya-Hsien Chang, Tau-Hung Hsueh, **Fang-I Lai**, Chun-Wei Chang, Chang-Chin Yu, Hung-Wen Huang, Chia-Feng Lin, Hao-Chung Kuo and Shing-Chung Wang, "Fabrication and Micro-Photoluminescence Investigation of Mg-Doped Gallium Nitride Nanorods" *Jpn. J. Appl. Phys.* Vol. 44 (2005) Part 1, No. 4B, pp. 2657-2660.

5. Jung-Tang Chu, Hung-Wen Huang, Chih-Chiang Kao, Wen-Deng Liang, **Fang-I Lai**, Chen-Fu Chu, Hao-Chung Kuo and Shing-Chung Wang, "Fabrication of Large-Area GaN-Based Light-Emitting Diodes on Cu Substrate" *Jpn. J. Appl. Phys.* Vol. 44 (2005) Part 1, No. 4B, pp.2509-2511 (2005)

6. H. P. D. Yang, **Fang-I Lai**, Y. H. Chang, H. C. Kuo, H. C. Yu, C. P. Sung, S. C. Wang, S. Y. Lin, J. Y. Chi, "Single mode (SMSR > 40 dB) proton-implanted photonic crystal vertical-cavity surface-emitting lasers" *IEE Electronics Letters,* Vol.41 No. 6, pp. 326-328 (2005)

7. T. H. Hsueh, H. W. Huang, **F. I. Lai**, J. K. Sheu, Y. H. Chang, H. C. Kuo and S. C. Wang, "Photoluminescence from $In_{0.3}Ga_{0.7}N$/GaN multiple-quantum-well nanorods" *Nanotechnology*, Vol. 16, No. 4 (2005) 448-450

8. H. C. Kuo, Y. H. Chang, H. H. Yao, Y. A. Chang, **Fan-I Lai**, M. Y. Tsai and S. C. Wang, "High-Speed Modulation of InGaAs:Sb-GaAs-GaAsP Quantum Well

Vertical-Cavity Surface-Emitting Lasers with 1.27-μm Emission Wavelength," *IEEE Photonics Technology Letters* vol.17, No. 3, March, pp.528, 2005.

9. Hao-Chung Kuo, Ya-Hsien Chang, Yi-An Chang, **Fang-I Lai**, Jung-Tang Chu, Min-Ying Tsai, and Shing-Chung Wang, "Single mode 1.27-μm InGaAs:Sb-GaAs-GaAsP Quantum Well Vertical Cavity Surface Emitting Lasers" *IEEE Journal of Selected Topics in Quantum Electronics (JSTQE),* vol. 11, NO. 1, Jan/Feb, pp.121, 2005.

10. Ya-Hsien Chang, H. C. Kuo, **Fang-I Lai**, Yi-An Chang, C. Y. Lu, L. H. Laih, and S. C. Wang, "Fabrication and Characteristics of High-Speed Oxide-Confined VCSELs Using InGaAsP–InGaP Strain-Compensated MQWs" *IEEE J. of Light Wave Technologies*, Vol. 22, Issue12 , Dec. 2004,pp.2828-2833.

11. **Fang-I Lai**, Ya-Hsien Chang, T.H. Hsueh, H.W. Huang, L.H. Laih, H.C. Kuo, S.C. Wang, Tai-Cheng Guung, "Improvement of kink characteristics and high speed performance of implanted VCSEL with a top transparent overcoating" *Material Sciences &Engineering B-Solid State Mater. Adv. Technol.*, Vol. 113/3, pp. 203-206, Nov., (2004).

12. **Fang-I Lai**, Tao-Hung Hsueh, Ya-Hsien Chang, Hao-Chung Kuo, S C Wang, Li-Hong Laih, C P Song, H P Yang, "10 Gb/s single-mode vertical-cavity surface-emitting laser with large aperture and oxygen implantation," *Semiconductor Science and Technology*, 19 (8): L86 2004

13. Y H Chang, **Fang-I Lai**, C Y Lu, H C Kuo, H C Yu, C P Sung, H P Yang, S C Wang, "High-speed (>10 Gbps) 850 nm oxide-confined vertical cavity surface emitting lasers (VCSELs) with a planar process and reduced parasitic capacitance," *Semiconductor Science and Technology*, 19 (7): L74-L77 2004.

14. Hsin-Chieh Yu, Shoou-Jinn Chang, Yan-Kuin Su, Chia-Pin Sung, Hong-Pin Yang, Chun-Yuan Huang, Yu-Wei Lin, Jin-Mei Wang, **Fang-I Lai** and Hao-Chung Kuo, "Improvement of high-speed oxide-confined vertical-cavity surface-emitting lasers," *Japanese Journal of Applied Physics* part1-regular paper short notes & review papers 43 (4B): 1947-1950 APR 2004.

15. Chen-Fu Chu, **Fang-I Lai**, Jung-Tang Chu, Chang-Chin Yu, Chia-Feng Lin, H. C. Kuo, and S. C. Wang "Study of GaN light-emitting diodes fabricated by laser lift-off technique**."** *Journal of Applied Physics* (J. Appl. Phys.)(2004), vol. 95, pp. 3916-3922.

16. Tao-Hung Hsueh, Hao-Chung Kuo, **Fang-I Lai**, Li-Hong Laih, and S. C. Wang,

"High Speed Characteristics of Large-Area Single-Transverse-Mode Vertical-Cavity Surface-Emitting Lasers." *Electronics Letter*s (Electron. Lett.) (2003), vol. 39, no. 21, pp.1519-1521.

17. H. C. Kuo, Y. S. Chang, **F. Y. Lai**, T. H. Hseuh, L. T. Chu, L. H. Laih, and S. C. Wang, "High Speed Performance of 850nm Silicon-Implanted AlGaAs/GaAs Vertical Cavity Emitting Lasers" *Solid-State Electronics* (2004), vol. 48, pp. 483-485.

18. **Fang-I Lai**, Tao-Hung Hsueh, Ya-Hsien Chang, Wen-Chun Shu, Li-Hung Lai, H. C. Kuo, and S. C. Wang, "Performance of 850nm AlGaAs/GaAs Implanted VCSELs Utilizing Silicon Implantation Induced Disordering." *Solid-State Electronics* (Solid-State Electron.) (2003), vol. 47, pp. 1805.

19. H. C. Kuo, Y. S. Chang, **F. Y. Lai**, T. H. Hsueh, L. H. Laih and S. C. Wang, "High-Speed Modulation of 850nm InGaAsP/InGaP Strain-Compensated VCSELs." *Electronics Letters* (2003), vol. 39, no. 14, pp. 1051-1053.

20. Chen-Fu Chu, C. C. Yu, Y. K. Wang, J. Y. Tsai, **F. I. Lai**, and S. C. Wang "Low-resistance ohmic contacts on p-type GaN using Ni/Pd/Au metallization," *Appl. Phys. Lett.* vol. **77**, 3423 (2000)

21. "Effects of doping concentration and annealing temperature on structural and optical properties of highly-oriented Al-doped ZnO films", Shou-Yi Kuo, Wei-Chun Chen, **Fang–I Lai**, Chin-Pao Cheng, Hao-Chung Kuo, Shing-Chung Wang and Wen-Feng Hsieh, submitted to Journal of Crystal Growth (revised).

22. Y. H. Chang, H. C. Kuo, **Fang-I Lai**, Y. A. Chang, H. C. Yu, H. P. Yang, C. P. Sung, and S. C. Wang," Relative intensity noise of vertical-cavity surface-emitting lasers (VCSELs) with polarization-selective feedback" submit to *IEEE Photonics Technology Letters*

Conference paper:

International:

1. **Fang-I Lai**, W. Y. Chen, C. C. Kao, H. C. Kuo, S. C. Wang, "Light-output Enhanced of GaN-based Light-emitting Diodes by Photoelectro-chemical oxidation in H_2O", *International Conference on Solid State Devices and Materials (SSDM)*, Kobe, Japan (2005).
2. Shou-Yi Kuo, **Fang-I Lai**, Wei-Chun Chen, Chin-Pao Cheng, Hao-Chung Kuo and Shing-Chung Wang, "Ultraviolet Lasing of Sol-Gel Derived Zinc Oxide Polycrystalline Films", *International Conference on Solid State Devices and Materials (SSDM)*, Kobe, Japan (2005).
3. **Fang-I Lai**, Y. H. Chang, H. P. Yang, H. C. Yu, H. C. Kuo, S. C. Wang, "Single Mode Output (SMSR > 40 dB) Utilizing Photonic Crystal on Proton-Implanted Vertical-Cavity Surface-Emitting Lasers", *CLEO/Pacific Rim 2005*.
4. **Fang-I Lai**, W. Y. Chen, C. C. Kao, C. F. Lin, H. C. Kuo, and S. C. Wang, "Enhancement of Light-output of GaN-based Light-emitting Diodes by Bias-assisted Photoelectrochemical oxidation of p-GaN in H_2O", *CLEO/Pacific Rim 2005*.
5. Shou-Yi Kuo, Wei-Chun Chen, **Fang–I Lai**, Chin-Pao Cheng, Hao-Chung Kuo, Shing-Chung Wang, "Observation of Ultraviolet lasing from polycrystalline ZnO Films", CLEO-PR 2005, Tokyo Japan.
6. S. Y. Kuo, C. C. Kei, C. K. Chao, C. N. Hsiao, **F. –I Lai**, H. C. Kuo, W. F. Hsieh, S. C. Wang, "Catalyst-free GaN nanorods grown by metalorganic molecular beam epitaxy", IEEE-NANO 2005, Nagoya Japan.
7. Shou-Yi Kuo, Wei-Jium Chen, Chini-Pao Cheng, **Fang-I Lai**, H.C. Kuo, S.C. Wang, W.F. Hsieh, "Effects of Doping Concentration and Annealing Temperature on Structural and Optical Properties of Highly-oriented Al-doped ZnO Films", 3rd International Conference on Materials for Advanced Technologies (ICMAT 2005) and 9th International Conference on Advanced Materials (ICAM 2005), Singapore.
8. H. –P. D. Yang, **F. I. Lai**, H. C. Yu, Y. H. Chang, H. C. Kuo, C. P. Sung, S. Y. Lin, and J. Y. Chi, "Mode Control of Photonic Crystal Vertical-Cavity Surface-Emitting Lasers," IEDMS (*The 2004 International Electron Devices and Materials Symposia*), C. 4.1, Dec. 20-23,2004, Hsinchu, Taiwan.
9. H. P. Yang, C. P. Sung, H. C. Yu, Y. K. Su, Y. H. Chang, **F. I. Lai**, K. F. Tzeng, H. C. Kuo, "Planarized 850nm oxide-implanted Vertical Cavity Surface Emitting Lasers (VCSELs) with High Speed Modulation Bandwidth over 13GHz,"

IEDMS (*The 2004 International Electron Devices and Materials Symposia*), B. P. 11, Dec. 20-23,2004, Hsinchu, Taiwan

10. Y. H. Chang, H. C. Hsueh, **F. I Lai**, W. Y. Chang, C. C. Yu, W. H. Huang, C. F. Lin, H. C. Kuo, S. C. Wang," Observation of large spectral blue-shift in photoluminescence spectra of Mg-doped gallium nitride Nanorods", *International Conference on Solid State Devices and Materials (SSDM)*, Tokyo, Japan (2004).

11. Ya-Hsien Chang , Hao-Chung Kuo , **Fang-I Lai** , Yi-A Chang , Po-Tsung Lee , Shing-Chung Wang," Fabrication of high speed sngle mode 1.27 um InGaAs:Sb-GaAsP Quantum Wells Vertical Cavity Surface Emitting Laser", *International Conference on Solid State Devices and Materials (SSDM)*, Tokyo, Japan (2004) to be published Japanese Journal of Applied Physics.

12. **Fang-I Lai**, Jung-Tang Chu, Chen-Fu Chu, Wen-Deng Liang, Hao-Chung Kuo, Shing-Chung Wang," Fabrication of large-area GaN Vertical Light Emitting Diodes on copper substrates by laser lift-off ", *International Conference on Solid State Devices and Materials (SSDM)*, Tokyo, Japan (2004).

13. **F. I Lai**, C. F. Chu, J. T. Chu, C. C. Yu, C. F. Lin, H. C. Kuo, and S. C. Wang, "Improvement of high power and high current operation of GaN lught emitting diodes by laser lift-off technique," *IEEE Lasers and Electro-Optics CLEO* 2004, CWA29 (2004).

14. T. H. Hsueh, Y. H. Chang, **F. I Lai**, H. W. Hung, M. C. Ou-yang, C. W. Chang, H. C. Kuo, and S. C. Wang, "Fabrication and emission characteristic of InGaN/GaN multiple quantum wells nanorods," *IEEE Lasers and Electro-Optics CLEO* 2004, IWA20.

15. Hsueh, T.H.; Chang, Y.S.; **Lai, F.**; Huang, H.W.; Ou-yang, C.; Chang, C.W.; Kuo, H.C.; Wang, S.C.; Sheu, J.Y., "Fabrication and emission characteristic of InGaN/GaN multiple quantum wells nanorods" *IEEE International Quantum Electronics Conference*, 2004. (IQEC), May 16-21, 2004 Page(s):520 - 521

16. H. C. Kuo, C. F. Chu, J. T. Chu, **Fang-I Lai**, C. C. Yu, C. F. Lin, and S. C. Wang " Fabrication of p-side down GaN Vertical Light Emitting Diodes on Copper Substrates by Laser Lift-off" *ISBLLED* (2004)

17. **Fang-I Lai**, L. H. Laih, H. C. Kuo, and S. C. Wang, "Improvement of Kink Characteristic of Proton Implanted VCSEL with ITO Overcoating" *Photonics West 2004*.

18. Y. S. Chang, H.C. Kuo, **F. I. Lai**, Y. A. Chang, L. H. Laih and S. C. Wang, " Improvement of high speed performance for 10-Gb/s 850 nm VCSELs," *SPIE Photonic West*, Conference 5364, paper 5364-10, Jan. 2004 (EI)

19. **Fang-I Lai**, Li-Hong Laih, T. H. Hsueh, S. P. Tseng, H. C. Kuo, and S. C. Wang, "Performances and Reliability of 850nm VCSELs with Various Offset in Gain Peaak and Fabry-Perot Dip" *CLEO/Pacific Rim 2003*, vol. 2, pp. 511.

20. **Fang-I Lai**, L. H. Laih, Y. S. Chang, T. H. Shei, H. C. Kuo, and S. C. Wang, "Enhancement of Proton-Implanted GaAs VCSEL Performance by Transparent Overcoating" *CLEO/Pacific Rim 2003*, vol. 1, pp. 229.

21. H.C. Kuo, T.C. Lu, Y.S. Chang, **F.Y. Lai**, G.C. Kan, L.H. Laih, S.C. Wang, "Growth and characterization of 850nm InGaAsP/InGaP strain-compensated VCSELs by MOCVD" *CLEO/Pacific Rim 2003*, vol. 1, pp. 164.

22. H.C. Kuo, W.C. Shu, T.C. Lu, Ya-hsien Chang, **Fang-I Lai**, Li-Hung Lai, S.C.Wang, "Characterization of 850nm AlGaAs/GaAs Implant Vertical Cavity Emitting Lasers Utilizing Silicon Implantation Induced Disordering" *CLEO/Pacific Rim 2003*, vol. 2 pp. 512 - 512

23. H. C. Kuo, Y. S. Chang, T. H. Hseuh, **F. Y. Lai** and S. C. Wang, "Development of High Speed 850nm VCSEL for OC-192 Application" *The Electrochemical Society 2003*.

24. Tao-Hung Hsueh, Hao-Chung Kuo, **Fang-I Lai**, Li-Hong Laih, and S. C. Wang, "High Speed Modulation of Large-Area Single-Transverse-Mode Vertical-Cavity Surface-Emitting Lasers" *CLEO 2003*.